

1 **Wheat Pm4 resistance to powdery mildew is controlled by alternative splice variants**
2 **encoding chimeric proteins**

3

4 Javier Sánchez-Martín^{1*}, Victoria Widrig¹, Gerhard Herren¹, Thomas Wicker¹, Helen Zbinden¹, Julien
5 Gronnier¹, Laurin Spörri^{1,2}, Coraline R. Praz^{1,3}, Matthias Heuberger¹, Markus C. Kolodziej¹, Jonatan
6 Isaksson¹, Burkhard Steuernagel⁴, Miroslava Karfiátová⁵, Jaroslav Doležel⁵, Cyril Zipfel^{1,6}, Beat
7 Keller^{1*}

8

9 ¹Department of Plant and Microbial Biology and Based-Zurich Plant Science Center, University of
10 Zurich, Zollikerstrasse 107, 8008 Zurich, Switzerland

11 ²Present address, Department of Zoology, Stockholm University, Svante Arrhenius väg 18b, 11418
12 Stockholm, Sweden

13 ³Present address, Unité de Recherche Résistance Induite et BioProtection des Plantes, UFR
14 Sciences Exactes et Naturelles, SFR Condorcet FR CNRS 3417, Université de Reims-Champagne-
15 Ardenne, 51687 Reims Cedex 2, France

16 ⁴John Innes Centre, Norwich Research Park, Norwich, NR4 7UH, UK

17 ⁵Institute of Experimental Botany of the Czech Academy of Sciences, Centre of the Region Haná for
18 Biotechnological and Agricultural Research, Šlechtitelů 31, 779 00 Olomouc, Czech Republic

19 ⁶The Sainsbury Laboratory, University of East Anglia, Norwich Research Park, NR4 7UH, Norwich,
20 UK

21 *Corresponding authors

22 Correspondence and requests for materials should be addressed to J.S-M. and B.K.

23 E-mail: javier.sanchezmartin@botinst.uzh.ch, bkeller@botinst.uzh.ch,

24

25 **Abstract**

26 Crop breeding for resistance to pathogens largely relies on genes encoding receptors that
27 confer race-specific immunity. Here we report the identification of the wheat *Pm4* race-
28 specific resistance gene to powdery mildew. *Pm4* encodes a putative chimeric protein of a
29 serine-threonine kinase and multiple C2-domains and transmembrane regions, a unique
30 domain architecture among known resistance proteins. *Pm4* undergoes constitutive
31 alternative splicing generating two isoforms with different protein domain topologies that are
32 both essential for resistance function. Both isoforms interact and localize to the
33 endoplasmatic reticulum (ER) when co-expressed. *Pm4* reveals additional diversity of
34 immune receptor architecture to be explored for breeding and suggests an ER-based
35 molecular mechanism of *Pm4*-mediated race-specific resistance.

36

37 Bread wheat (*Triticum aestivum*) sustains more than one third of humankind¹. Around 5% of
38 the total yield losses caused by wheat pathogens and pests is attributable to *Blumeria*
39 *graminis* f. sp. *tritici* (*Bgt*), the causal agent of wheat powdery mildew². Host resistance is
40 crucial for controlling the disease and reducing pesticide dependency³. Race-specific
41 resistance is the basis of host resistance in many wheat genotypes, where resistance (*R*)
42 genes confer strong and mostly complete immunity to some but not all races of a pathogen
43 species. The molecular identification of genetic components of *R*-mediated resistance
44 contributes to improve disease resistance by tracking *R* genes with markers and by stacking
45 them⁴. Moreover, resistance durability benefits from broader *R* gene pools, allowing more
46 effective gene combination schemes⁵, by, for instance, combining different molecular modes
47 of resistance⁶.

48 Many of the molecularly identified *R* genes in crops encode nucleotide-binding domain and
49 leucine-rich repeat-containing (NLR) proteins that are intracellular immune receptors that
50 recognize cytoplasmic pathogen-derived effectors^{7,8}. Some wheat immune receptors active
51 against rust pathogens have non-canonical architectures resulting from the fusion of
52 additional domains to the NLR protein (NLR-ID): the wheat stripe rust genes *Yr5*, *Yr7* and
53 *YrSP9* encode proteins with an N-terminal zinc-finger BED domain and the *YrU1*¹⁰ gene
54 encodes a protein with N-terminal ankyrin-repeat and C-terminal WRKY domains. Although
55 functionally not well characterized¹¹, these integrated domains are believed to act as decoys
56 of virulence effector targets to detect the pathogen, and ultimately, activate immune
57 signalling^{12,13}.

58 In addition to NLR or NLR-ID receptors, proteins localizing in the plasma membrane such as
59 the Cf receptor-like proteins in tomato against the *Cladosporium fulvum* pathogen have also
60 been shown to be products of race-specific *R* genes¹⁴. Furthermore, the wheat *Stb6* gene
61 encodes a wall-associated receptor kinase (WAK)-like protein¹⁵ conferring race-specific
62 resistance against the fungus *Zymoseptoria tritici* by detecting the presence of a matching
63 apoplastic effector^{16,17}. Finally, tandem kinase-pseudokinases (TKP) have emerged as a new

64 protein family involved in plant immunity¹⁸ and include barley and wheat rust resistance
65 genes *Rpg1*¹⁹, *Yr15*¹⁸ and *Sr60*²⁰ as well as the wheat powdery mildew resistance gene
66 *Pm24*²¹. The diversity of molecular mechanisms resulting in gene-for-gene specificity
67 observed in wheat-pathogen interactions makes the diverse wheat germplasm a promising
68 genetic resource for the identification of novel molecular mechanisms resulting in plant
69 immunity.

70 We report on cloning the wheat *Pm4* race-specific resistance gene to powdery mildew,
71 originally introgressed from tetraploid *T. carthlicum*²². Constitutive alternative splicing of *Pm4*
72 generates two isoforms, both required for resistance, with different domain architectures
73 forming an ER-associated complex revealing an additional and unique molecular basis for
74 race-specific resistance mechanism in a major crop.

75

76 **Results**

77 **The *Pm4* gene provides race-specific resistance to a wide range of *Bgt* isolates**

78 The near-isogenic genetic background of Fed-*Pm4a*²³ and Fed-*Pm4b*²² wheat lines allowed
79 the assessment of the resistance spectra of these two *Pm4* alleles. Mildew resistance testing
80 revealed a largely overlapping, yet distinct resistance spectrum (Supplementary Table 1).
81 Both alleles conferred complete resistance to 37 (34.6%) *Bgt* isolates, mostly from China,
82 Israel and Switzerland, whereas 28 (26.1%) of the *Bgt* isolates were virulent on both alleles
83 (Extended Data Fig. 1a and Supplementary Table 1). The remaining 42 (39.3%) *Bgt* isolates
84 showed different reactions on *Pm4a* and *Pm4b*, confirming the race-specific nature of the
85 two resistance alleles (Extended Data Fig. 1b and Supplementary Table 1). We evaluated by
86 microscopy the resistance reaction of Fed-*Pm4a* and Fed-*Pm4b* lines challenged with a
87 *Pm4a/b*-avirulent isolate (*Bgt96224*) and compared it with Fed-*Pm2* near-isogenic line (NIL)
88 with the *Pm2* gene²⁴. *Pm2* encodes a canonical NLR receptor that also confers resistance to
89 *Bgt96224*. All three genotypes share cv. Federation as recurrent parent, which has no known
90 *Pm* genes and is susceptible to *Bgt96224*. At 2 dpi, hypersensitive cell death (HR) was

91 visible in *Pm4a/b* NILs at significantly lower levels than in the *Pm2*-containing line (HR 15%
92 Fed-*Pm4a* and 14% Fed-*Pm4b* compared to 28% Fed-*Pm2*). At 6 dpi, almost no fungal
93 microcolonies were observed in both the *Pm4a* (1%), nor the *Pm4b* (0%) genotype
94 compared to the *Pm2*-containing line (26%). Interestingly, *Pm4*-containing lines showed
95 significantly higher levels of pre-penetration resistance compared to the *Pm2* line at 2 and 6
96 dpi (87% Fed-*Pm4a* and 88% Fed-*Pm4b* compared to 49% Fed-*Pm2*) (Fig. 1a). We
97 conclude that both *Pm4* alleles confer rapidly acting resistance mostly at the pre-penetration
98 level but also resulting in some cell death.

99 **Molecular identification and characterization of a *Pm4b* candidate gene**

100 We identified and confirmed 18 EMS-derived *pm4b* mutants of the *Pm4b*-containing wheat
101 genotype Fed-*Pm4b*²². All these mutants were susceptible to the *Pm4alb*-avirulent *Bgt96224*
102 isolate (Supplementary Table 2). Chromosome 2A carrying *Pm4b* was flow-sorted from eight
103 mutants and from the parental genotype (Fig. 1b) and sequenced for gene identification
104 using the MutChromSeq²⁴ approach. After identification of variations in the mutant
105 chromosomes using a Fed-*Pm4b* *de novo* assembly, contig_18057 was the only candidate
106 contig for *Pm4b*. In addition, all of the independent mutations falling within a predicted ORF
107 based on the annotation of the *Ae. tauschii* *Pm4b* homologue AET2Gv21296200. Given the
108 multiple splicing variants predicted in AET2Gv21296200, we first clarified the genomic
109 structure and splicing pattern of the *Pm4b* gene by aligning cDNA products derived from RT-
110 PCR reactions primed with gene-specific primers located on predicted exons 1, 6 and 7, as
111 well as 5' and 3' RACE products to the contig_18057 genomic sequence (Fig. 1c).
112 Sequence analysis confirmed that the *Pm4b* gene consists of seven exons, of which the six
113 and seven exons are alternatively spliced in a mutually exclusive way giving rise to two
114 alternative transcripts, denoted *Pm4b_V1* and *Pm4b_V2* (Fig. 1c). The two transcripts were
115 also detected in the *Pm4a*-containing line Fed-*Pm4a*. Importantly, *Pm4*-like alternative gene
116 splicing was observed in RNA-seq expression data for the barley *Pm4* orthologue
117 HORVU.MOREX.r2.2HG0181350, hereinafter referred as to *Hv2HG0181350*, where two

118 *Pm4_V1*- and *Pm4_V2*-like transcripts translated into two intact ORFs (GenBank:
119 GFJN01021221.1, GFJN01021222.1). Based on the splicing variant *Pm4b_V2*, seven of the
120 flow-sorted *pm4b* mutants contained non-synonymous amino acid exchanges, whereas a
121 premature termination codon was introduced in the eight mutant *pm4b_m495*, possibly
122 resulting in a non-functional protein (Fig. 1c,d and Supplemental Table 2). We confirmed by
123 PCR amplification and Sanger sequencing the mutations identified by MutChromSeq.
124 Further pivotal confirmation of the gene identity was obtained by Sanger sequencing of ten
125 additional *pm4b* mutants as well as 14 *pm4a* mutants, which all revealed mutations in the
126 candidate gene. Most mutations were G/C-to-A/T transitions as expected after EMS
127 mutagenesis and caused nonsense (n=4) or missense (n=23) mutations (Fig. 1d and
128 Supplemental Table 2; note that *pm4b_m244* has two point mutations). All these mutants
129 were susceptible to the *Pm4alb*-avirulent *Bgt96224* and *Bgt94202* isolates. Motivated by the
130 alternative splicing (AS) exhibited by the *Pm4b* gene, we focused on mutants affected in
131 exon six (*pm4b_m7*, *pm4b_m89*, *pm4b_m510*) and seven (*pm4b_m180*, *pm4b_m244*,
132 *pm4b_m256*). All these critical mutants did not exhibit significantly different expression levels
133 for splicing variants *Pm4b_V1* nor *Pm4b_V2* compared to the *Pm4b* wild type genotype after
134 mock- and *Bgt96224*-infection at 48 hai (Fig. 1c and Extended Data Fig. 2). Therefore, the
135 loss of resistance was not due to downregulation of *Pm4* transcripts. The *Pm4_V1* ORF
136 encodes a protein of 560 amino acids, while the *Pm4_V2* ORF encodes a predicted protein
137 of 747 amino acids. As mutations in the mutually exclusive exons 6 and 7 both abolished
138 *Pm4b*-based mildew resistance, we conclude from genetic analysis that both alternatively
139 spliced transcripts and their encoded protein isoforms are needed for *Pm4*-mediated
140 resistance.

141 We examined the expression of *Pm4_V1* and *Pm4_V2* on the wild-type *Pm4b* wheat
142 genotype Fed-*Pm4b* after infection with powdery mildew, and the expression of the two
143 transcripts did not significantly differ from each other after mock- and *Bgt96224*-infection.
144 However, the expression of both transcripts was reduced significantly at early infection
145 stages between 12 and 36 hai, suggesting that mildew infection downregulates *Pm4*

146 expression transiently (Fig. 1e). Nearly identical levels of both transcripts suggest that
147 *Pm4b_V1* and *Pm4b_V2* have a similar contribution to resistance.

148 ***Pm4b* confers resistance when stably transformed into a susceptible wheat background**

149 To test if the cloned *Pm4b* candidate gene was sufficient to confer resistance to wheat
150 powdery mildew, we stably co-transformed the *Bgt96224*-susceptible wheat variety Bobwhite
151 S26 with the two full-length cDNAs of *Pm4b_V1* and *Pm4b_V2* (Fig. 2a). All tested
152 transgenic T0 plants contained both the *Pm4b_V1CDS*- and *Pm4b_V2CDS* transgenes
153 indicating complete co-transformation. The T0 plants were self-fertilized, and four events
154 were chosen at random for T1 family infection with *Bgt96224*. The three transgenic events
155 T1Pm4b_V1V2CDS-3, T1Pm4b_V1V2CDS-25 and T1Pm4b_V1V2CDS-52.1 showed a 3:1
156 transgene segregation ratio, suggesting the presence of a single insertion site of
157 *Pm4b_V1V2_CDS*. In contrast, we detected the presence of both transgenes,
158 *Pm4b_V1CDS*- and *Pm4b_V2CDS*, in all T1 plants from family T1Pm4bV1V2CDS-52.2,
159 indicating the presence of the transgene at least at two insertion sites. Importantly, presence
160 of the two transgenes segregated with resistance to *Bgt96224* in T1 families (Fig. 2b). We
161 advanced selected T1 plants to the T2 generation for further analysis. T2 plants expressing
162 *Pm4b_V1* and *Pm4b_V2* also showed resistance to *Bgt* isolates *Bgt96224* and *Bgt94202*,
163 (Fig. 2c and Supplementary Table 3). The analyzed T2 plants showed higher *Pm4*
164 expression levels (*Pm4b_V1* between 1.65- and 44.05-fold; *Pm4b_V2* between 0.67- and
165 62.71-fold) compared to the endogenous *Pm4b* gene in line Fed-*Pm4b*. However, they were
166 all susceptible to the *Pm4a/b*- virulent *BgtJlW2* and *Bgt97251* isolates (Fig. 2c and
167 Supplementary Table 3). These data confirm the race-specific resistance activity provided by
168 the *Pm4* gene, which is unaffected by overexpression in the transgenic lines. Transgenic
169 plants overexpressing both *Pm4b_V1CDS*- and *Pm4b_V2CDS* transgenes did not
170 significantly differ from Bobwhite S26 with respect to measured agronomic traits (Extended
171 Data Fig. 3), which indicates that ectopic defense activation by the *Pm4b_V1CDS*- and
172 *Pm4b_V2CDS* transgenes did not affect plant growth. To further test if both transcript

173 variants are equally needed for *Pm4b*-mediated resistance as indicated by the mutant
174 analyses, we individually transformed Bobwhite S26 with full-length cDNA of *Pm4b_V1* or
175 *Pm4b_V2*. Transgenic events T1Pm4b_V1CDS-9, T1Pm4b_V1CDS-12 and
176 T1Pm4b_V1CDS-19 were fully susceptible to the *Pm4b*-avirulent isolates *Bgt96224* and
177 *Bgt96202* (Extended Data Fig. 4a and Supplementary Table 4). The analyzed T1 plants
178 overexpressing *Pm4b_V1* showed higher *Pm4b_V1* expression levels (between 1.4- and 3.9-
179 fold) compared to the endogenous *Pm4b_V2* transcript in line Fed-*Pm4b*. Similarly, we
180 selected three transgenic events overexpressing *Pm4b_V2*: T2Pm4b_V2CDS-6,
181 T1Pm4b_V2CDS-24 and T1Pm4b_V2CDS-29, all of which were fully susceptible to
182 *Bgt96224* and *Bgt94202*. The analyzed T1 plants overexpressing *Pm4b_V2* transcript
183 showed higher *Pm4b_V2* expression levels (between 1.1- and 20.2-fold) compared to the
184 endogenous *Pm4b_V2* transcript in line Fed-*Pm4b* (Extended Data Fig. 4b and
185 Supplementary Table 4). These data from individual transformation of the two alternative
186 transcripts confirm that both variants must be present to confer resistance, a finding that is in
187 agreement with the mutant analysis.

188 **Silencing of *Pm4b_V1* or *Pm4b_V2* splicing variants compromises powdery mildew** 189 **resistance in Fed-*Pm4b***

190 To further test *Pm4b*-mediated resistance to powdery mildew through VIGS, we designed
191 silencing constructs for either of the two Fed-*Pm4b* splicing variants (Fig. 2d). Both
192 constructs targeting *Pm4b_V1* or *Pm4b_V2* resulted in susceptibility of the *Pm4b*-containing
193 Fed-*Pm4b* wheat genotype, visible as large leaf areas covered by sporulating mildew
194 colonies (Fig. 2d). A comparison of mRNA expression by qRT-PCR in Fed-*Pm4b* leaves
195 infected with BSMV:*Pm4b_V2* with Fed-*Pm4b* plants infected with wild type virus BSMV: γ
196 showed a significant decrease of expression levels of *Pm4b_V2* transcripts. Interestingly, the
197 expression of *Pm4b_V1* decreased also after silencing of *Pm4b_V2*, likely because of the
198 formation of secondary siRNA targeting the mRNA sequence shared by both splicing
199 variants²⁶. However, no decrease of *Pm4b_V1* or *Pmb_V2* expression was observed in

200 BSMV:*Pm4b_V1*-infected Fed-*Pm4b* plants, suggesting that this construct was less efficient
201 in directing silencing²⁷ (Fig. 2e). We conclude that the specific targeting of either *Pm4b_V1*
202 or *Pm4b_V2* expression through VIGS compromised *Pm4b*-mediated resistance.

203 **The *Pm4* gene encodes a putative chimeric kinase-MCTP protein**

204 *Pm4b_V1* and *Pm4b_V2* proteins share the first five exons, predicted to encode a kinase
205 domain with serine/threonine specificity (S_TKc, Fig. 3a,d and Extended Data Fig. 5), but
206 they differ in their C-terminus. *Pm4b_V1* isoform has a single C2C domain, while *Pm4b_V2*
207 contains a C2D domain coupled to a phosphoribosyl transferase C-terminal domain (PRT_C)
208 with two transmembrane domains (Fig. 3a,c). *Pm4b_VF*, a hypothetical protein with a
209 combination of all domains of the two isoforms with protein topology S_TKc-C2C-C2D-
210 PRT_C is similar to proteins containing multiple C2-domain and transmembrane region(s)
211 (MCTPs)^{28,29}. However, the S_TKc domain is absent in MCTPs and *Pm4b_VF* only has the
212 C2C and C2D-PRT_C terminal domains, contrary to the highly conserved domain topology
213 observed in MCTP proteins with three or four C2 domains and a PRT_C domain. Domain
214 *Pm4b_C2D* is more conserved than *Pm4b_C2C* compared to Arabidopsis MCTPs C2
215 domains (Extended Data Fig. 6a,b). The closest Arabidopsis MCTP homologue of *Pm4b_VF*
216 is MCTP6 (Extended Data Fig. 6c) that contributes to flowering time control cooperatively
217 with MCTP1³⁰.

218 The presence of all key conserved residues^{18,31} in *Pm4b-S_TKc* (Extended Data Fig. 5)
219 suggests that it is a functional kinase. Besides, four EMS-derived susceptible mutants
220 (*pm4b_m207*, *pm4b_m293*, *pm4a_m398.1* and *pm4b_m291*) had missense mutations of key
221 conserved residues, implying that *Pm4b-S_TKc* is critical for *Pm4b*-mediated powdery
222 mildew resistance (Extended Data Fig. 5). The closest Arabidopsis homologue to the core
223 kinase domain of *Pm4b* is CRK6 (AT4G23140), a cysteine-rich receptor-like kinase that
224 confers resistance to *Pseudomonas syringae* when overexpressed^{32,33}. Interestingly, the
225 barley orthologue of *CRK6*, *HvCRK1*, is involved in ROS-mediated basal resistance against
226 powdery mildew³⁴. Furthermore, some of the phylogenetically closest kinase-containing

227 resistance proteins to Pm4b (Supplementary Fig. 1) confer resistance to biotrophic
228 pathogens in wheat and barley^{18,20,21,35}.
229 C2 domains are protein signaling motifs with a Ca²⁺-binding region and a polybasic cluster
230 involved in membrane docking^{36,37}. Only Pm4b_C2D might potentially bind Ca²⁺ based on
231 the presence of three conserved aspartate residues and two conserved substitutions
232 (glutamine and asparagine) (Extended Data Fig. 7). The C2C domain might be involved in
233 interaction with phosphoinositides, although it does not contain the characteristic positively
234 charged and aromatic residues in the polybasic cluster but conservative substitutions by
235 amino acids with similar physicochemical properties (Supplementary Fig. 2a). Finally,
236 Pm4b_V2 is predicted to have two transmembrane domains highly conserved with
237 Arabidopsis MCTPs-TM domains (Supplementary Fig. 2b). Notably, Pm4b_V2 has a tandem
238 duplication between the transmembrane domains absent in Arabidopsis MCTPs
239 (Supplementary Fig. 2b).

240 **Allelic variations of the *Pm4* locus**

241 To facilitate the use of *Pm4* in breeding, we designed a diagnostic marker based on *Pm4b*
242 sequences, and verified the presence of the *Pm4* locus and its allelic forms in Fed-*Pm4a*,
243 Fed-*Pm4b* and Tm27d2 (*Pm4d*) after full-length amplification and Sanger sequencing (Fig
244 3b). We tested the *Pm4* haplotype-specific marker in a global wheat collection of 512
245 accessions, among which the *Pm4a* allele was absent, whereas *Pm4b* and *Pm4d* were
246 detected in 19 and 9 genotypes, respectively. Besides, three new *Pm4* alleles, tentatively
247 denoted as *Pm4f*, *Pm4g* and *Pm4h*, were discovered (Fig. 3b). Heterogenic genetic
248 backgrounds with presence of other resistance genes possibly mask the effect of these *Pm4*
249 alleles. Nevertheless, we observed that *Pm4b*- and *Pm4d*-containing lines are resistant to
250 *Bgt94202*, *Bgt96224*, *Bgt97223* and *Bgt97266* but susceptible to *BgtJIW2*, the same
251 resistance pattern observed in the Fed-*Pm4a* and Fed-*Pm4b* NILs. These phenotyping data
252 suggest the functionality of *Pm4b* and *Pm4d*. However, *Pm4f* and *Pm4g*-containing lines
253 were mostly susceptible to the tested *Bgt* isolates, implying that those are susceptible alleles

254 of *Pm4*. Finally, the *Pm4h* allele had a very similar resistance spectrum compared to *Pm4b*-
255 and *Pm4d*-containing genotypes and seems to be active (Supplementary Table 5). *Pm4*
256 alleles contain single SNPs and/or combinations of shared SNPs affecting mainly the kinase
257 domain (Fig. 3b). Intriguingly, most of the SNP lead to amino acid changes in the S_TKc and
258 transmembrane domains (Fig. 3b,e,f).

259 **Pm4b_V1 and Pm4b_V2 form an ER-associated complex**

260 We examined the subcellular localization of eGFP- and TagRFP-tagged Pm4 individual
261 isoforms co-expressed with characterized markers³⁸⁻⁴⁰. eGFP-Pm4b_V2 colocalized with the
262 mCherry-tagged endoplasmic reticulum (ER) marker (Pearson correlation coefficient $0.768 \pm$
263 0.02 , $n = 12$) (Fig. 4b and Supplementary Fig. 3). Notably, MCTPs proteins also contain
264 C2C/C2D and PRT-C domains and localize to the ER as well²⁹. This ER-localization has
265 been proposed to be mediated by the presence of transmembrane domains embedded in the
266 PRT_C domain²⁹, which both Pm4V2 and MCTPs share. In contrast, Pm4b_V1 lacks the
267 PRT_C domain and colocalized with the mCherry-tagged cytosol marker (Pearson
268 correlation coefficient 0.765 ± 0.023 , $n = 12$) (Fig. 4a and Supplementary Fig. 3). These
269 results are in line with localization experiments done with truncated MCTPs proteins, where it
270 was demonstrated that the PRT_C domain is essential for the association with the ER
271 network²⁹. Co-infiltration experiments of eGFP- and TagRFP-Pm4b_V1 and Pm4b_V2
272 revealed a colocalization pattern in the ER (Pearson correlation coefficient 0.765 ± 0.028 , n
273 $= 12$ and 0.782 ± 0.030 , $n = 10$) (Fig. 4c and Supplementary Fig. 3). This suggests that
274 Pm4b_V2 recruits Pm4b_V1 from the cytosol to the ER, possibly by forming an ER-
275 associated complex.

276 To test for potential Pm4b_V1 and Pm4b_V2 homo and heteromeric protein interactions we
277 first performed co-immunoprecipitation assays. HA-Pm4b_V2 co-immunoprecipitated with
278 the Flag-Pm4b_V2 protein and Pm4b_V1-HA was pulled-down with the Pm4b_V1-Flag
279 tagged protein, suggesting the existence of a multimeric complex. Importantly, the Pm4b_V1
280 and Pm4b_V2 proteins associated with each other in a specific manner, as HA-Pm4b_V2

281 and Pm4b_V1-Flag were co-immunoprecipitated (Fig. 4d and Extended Data Fig. 8). These
282 data indicate that Pm4b_V2 and Pm4b_V1 form part of the same complex *in vivo*. To further
283 test if the two isoforms interact with themselves and each other, we performed luciferase
284 complementation imaging (FLuCI) assays⁴¹. We found significantly higher luciferase signals
285 in the Pm4b_V1/Pm4b_V1 and Pm4b_V2/Pm4b_V2 samples compared to the negative
286 controls (Fig. 4e,f). Compared with controls lacking either partner, samples including both
287 Pm4_V1 and Pm4_V2 displayed a significant increase in luciferase signal (Fig. 4g).
288 Interestingly, only N-terminally-tagged N-LUC or C-LUC Pm4b_V2 showed significantly
289 higher luciferase signals, suggesting that domain topology of the C-terminal part of the
290 Pm4b_V2 protein play a critical role in the heteromerisation with Pm4b_V1. To further test
291 whether the two Pm4b variants preferentially establish homo or heteromeric protein
292 interactions, we co-expressed in equal amount the fluorescence tagged Pm4b_V2 protein
293 variant together with Pm4b_V1 / Pm4b_V1 showing high luciferase signal. Similarly,
294 Pm4b_V1 was co-expressed with Pm4b_V2 / Pm4b_V2. In both cases there was a strong
295 reduction of the luciferase signal. This indicates that Pm4b_V1 and Pm4b_V2 protein
296 variants preferentially establish heteromeric rather than homomeric interactions (Extended
297 Data Fig. 9).

298

299 **Evolutionary origin of the *Triticeae*-specific *Pm4*-like gene family**

300

301 We found 18 *Pm4* homologues encoding intact full-length Pm4_V1- and Pm4_V2-like
302 proteins exclusively in various *Triticeae* species (Supplementary Table 6). *Pm4* homologues
303 are present on homeologous group 2 chromosomes of wheat relatives' rye and barley as
304 well as on A, B and D genomes of diploid, tetraploid and hexaploid wheats (Supplementary
305 Fig. 4a,b and Supplementary Table 6). *Pm4* homologues underwent complex evolutionary
306 changes as their clustering did not correspond to 1A, 1B and 1D homologues
307 (Supplementary Fig. 4a,b). Besides, *Pm4* is absent in the wheat reference genome
308 sequence of cv. Chinese Spring (CS)¹, which also lacks a susceptible *Pm4* allele or a

309 homologue, given the low similarity (< 70%) of the CS homologue to *Pm4*. Finally, among
310 the accessions sequenced in the 10+ Wheat Genomes Project genomes
311 (<http://www.10wheatgenomes.com>, <https://wheat.ipk-gatersleben.de/>), cv. SYMattis
312 contained the *Pm4d* allele at the distal region of 2AL chromosome arm (Supplementary Fig.
313 5).

314 *Pm4b* apparently evolved in multiple steps, involving a fusion of gene fragments,
315 duplications and subsequent losses and gains of specific sequences. The gene encoding the
316 closest homolog of the C2 domain of *Pm4b* in Chinese Spring is TraesCS2A01G557900,
317 which is located approximately at position 761 Mb on chromosome 2A, near the position
318 where *Pm4b* maps in SYMattis, and encodes a canonical MCTP protein. The identification of
319 a *Pm4b* homolog in barley indicates that the fusion event occurred already in the *Triticeae*
320 ancestor.

321 We propose that a 3' segment of the ancestor of TraesCS2A01G557900 was duplicated and
322 fused to a gene fragment encoding a kinase domain. Such partial gene duplications to
323 nearby loci can be the result of double-strand break repair⁴². This led to an intermediate form
324 (*Pm4int*) that encodes a kinase in its 5' kinase and three C2 domains in its 3' (Figure 5a).
325 Interestingly, we found this intermediate form on chromosome 2 in both reference genomes
326 for barley⁴³ (cv. Morex) and wheat¹ (cv. Chinese Spring). Our data indicate that *Pm4int*
327 already encodes two different transcripts analogous to those of *Pm4b*. This is in contrast to
328 the donor C2 TraesCS2A01G557900 which is a single long exon. *Pm4int* was then
329 duplicated, giving rise to the *Pm4b* ancestor gene. This gene subsequently lost a segment of
330 exon 6 encoding the first C2 domain and instead acquired a sequence that is unique to
331 *Pm4b* (Figure 5a,b). Interestingly, all three genes (the donor of the C2 domains, *Pm4int* and
332 *Pm4b*) are still all present in a ~1.2 Mb region on barley chromosome 2.

333 Phylogenetic analysis of the C2 domains shows that *Pm4b* and *Pm4int* evolved from the
334 ancestor of TraesCS2A01G557900 (and its barley homolog *HORVU2Hr1G126730*, Fig. 5c).
335 The emergence of *Pm4b* from *Pm4int* apparently occurred soon after, and the phylogenetic

336 tree suggests that there may have been some subsequent gene conversion(s) as the *Pm4b*
337 and *Hv2HG0181350* do not cluster together (Fig. 5c). Molecular dating using fourfold
338 degenerate sites suggest that *Pm4int* and *Pm4b* emerged about 20 million years ago.
339 Consequently, sequence conservation between *Pm4int* and *Pm4b* is limited to CDS while
340 introns are strongly reshuffled (Fig. 5b). Furthermore, branch lengths in the phylogenetic tree
341 indicate that *Pm4b* and *Pm4int* evolved more rapidly than the donor of the C2 domain (Fig.
342 5c).

343

344 Discussion

345

346 We cloned through MutChromSeq²⁴ the wheat powdery mildew resistance gene *Pm4b*,
347 whose functional identity was confirmed by mutagenesis, VIGS and transgenic
348 complementation. While *Pm4b* is relatively widespread in the hexaploid wheat gene pool, the
349 reference genome of wheat genotype Chinese Spring shows a haplotype with complete
350 absence of a *Pm4* allele or homolog.

351 *Pm4* is a valuable gene for use in disease resistance breeding as *Pm4* alleles convey
352 resistance to *Bgt* isolates in economically relevant wheat-growing areas, such as China and
353 USA. The *Pm4* haplotype diagnostic marker developed here will facilitate gene deployment
354 in breeding programs aiming at achieving its long-term effectiveness, for instance, by
355 targeted stacking of *Pm4* alleles matching the corresponding virulence profile of *Bgt*
356 isolates⁴⁴.

357 *Pm4b* race-specific action was conserved in transgenic lines, confirming that overexpressing
358 both *Pm4b_V1* and *Pm4b_V2* did not result in unspecific auto-activity. The molecular basis
359 of race-specificity is well understood in direct or indirect recognition in NLR-based
360 resistance^{14,45}. However, given the novel domain architecture of *Pm4*, the information on
361 NLR-based specificity cannot be easily applied. However, natural diversity of the alleles at
362 the *Pm4* locus reveals some molecular determinants contributing to race-specificity.

363 Possibly, the two amino acid polymorphisms within the activation loop of the S_TKc domain
364 are key determinants of specificity.

365 Microscopic observations revealed that *Pm4*-mediated resistance is phenotypically similar to
366 the canonical NLR-based resistance and is associated with epidermal cell death, although at
367 significantly lower levels. HR can be activated via different cellular pathways⁴⁶, and
368 identification of *Pm4* interacting partners and downstream signaling components will support
369 the characterization of *Pm4*-mediated resistance at the mechanistic level. *Pm4* resistance is
370 based to a large extent on pre-penetration resistance suggesting a rapid and efficient host
371 response upon recognition of the mildew pathogen.

372 *Pm4* undergoes constitutive alternative splicing (AS) generating *Pm4_V1* and *Pm4_V2*
373 splicing variants. While several *NLR* genes were found to undergo AS under pathogen attack
374 via intron retention or in untranslated regions^{47,48}, in *Pm4* we found splicing of mutually
375 exclusive exons. Canonical *NLR* genes undergoing AS usually generate truncated proteins
376 without a clear biological function. In many of those cases it has been shown that alternative
377 variants are not required for resistance, as in the case of the flax *L6*⁴⁹, tomato *BS4*⁵⁰, rice
378 *RGA5*⁵¹ or the wheat resistance genes *WKS1*⁵² and *Lr10*⁵³. On the other hand, resistance
379 provided by the tobacco *N5*⁵⁴, the Arabidopsis *RPS4*⁵⁵ and the *Medicago truncatula* *RCT1*⁵⁶
380 resistance genes depends on AS. In these cases, full immunity only occurs when both
381 regular and alternative transcripts are present, which are subjected to a dynamic abundance
382 ratio under pathogen attack (the case of the *N5*⁵⁴ or *RPS4*⁵⁵ genes). In contrast, *Pm4b_V1*
383 and *Pm4b_V2* show identical expression levels, suggesting an equal contribution to
384 resistance. Importantly, based on the mutant analysis, both transcripts and their encoded
385 protein isoforms are needed for resistance. Indeed, the mutations in either *Pm4b_V1* or
386 *Pm4b_V2* led to full susceptibility whereas in the case of *N5*⁵⁴, *RPS4*⁵⁵ or *RCT1*⁵⁶ genes, the
387 absence of alternative splicing variants did not result in susceptibility but in incomplete
388 resistance, or the overexpression of one transcript variant led to full resistance, like the
389 *RCT1* case⁵⁶.

390 Pm4 encodes a putative kinase-MCTP protein likely resulting from a gene fusion event
391 between a serine/threonine kinase and the C-terminal part of a member of the MCTPs
392 family. *Pm4* homologs are found in different *Triticeae* species but are absent in other grasses
393 within the subfamily *Pooideae* such as rice and *Brachypodium*, suggesting a gene fusion
394 event in the ancestor of the *Triticeae*. Homology-based comparison of the Pm4 core kinase
395 domain with kinase-containing proteins known to be involved in plant immunity points to the
396 functionality of the Pm4 kinase domain. The Pm4 kinase belongs to the RCLK family, many
397 of whose members have been described to be involved in disease resistance⁵⁷.

398 RCLK family members such PBS1 and PBS1-like (PBL) proteins transduce immune signals
399 from the plasma membrane^{58,59} and are also targets of bacterial effectors⁵⁹⁻⁶¹. Similarly, the
400 kinase domain of Pm4 could be targeted by the specific AvrPm4 effector, inducing a defense
401 reaction. Alternatively, the MCTP domain might be the specific sensor detecting effector
402 manipulation at the ER. In this model, Pm4b_V2 would be the sensor and Pm4b_V1 would
403 be a helper protein, similar to NLR-based interactions with sensor and helper proteins⁶².
404 Finally, at this stage we cannot exclude the involvement of an NLR, similar to the Prf/Pto
405 system in tomato and the above-mentioned PBS1 guarded by the NLR RPS5^{61,63,64}. This
406 NLR might be genetically redundant and functionally non-polymorphic in wheat as it was
407 neither identified by genetic mapping nor by mutagenesis.

408 The Arabidopsis protein MCTP1/FTIP interacts via C2 domains with FT, a 175-amino acid
409 length protein part of the mobile flower-promoting signal that promotes the transition from
410 vegetative growth to flowering⁶⁵. It is known that after a fusion event, the resulting gene may
411 acquire a new function through neofunctionalization⁶⁶. It is thus tempting to propose that one
412 of the C2 domains present in Pm4 binds the powdery mildew effector to further trigger
413 disease resistance. Indeed, there are experimental data that might support this hypothesis.
414 For instance, the pepper (*Capsicum*) C2 domain-containing protein SRC2-1 interacts with
415 the *Phytophthora capsici* INF1 elicitor (*PcINF-1*) leading to PcINF-1-induced immunity⁶⁷.
416 Based on the available information along with the work reported here, we present a working

417 model of how Pm4 operates. In this model, Pm4_V1 and Pm4_V2 are in a resting state in the
418 absence of the pathogen forming an ER-associated heterocomplex. After infection by the
419 powdery mildew pathogen (Fig. 6a), there is a rapid, race-specific induction of pre-haustorial
420 resistance in presence of the *Pm4b* gene. We propose that low levels of the yet unknown
421 AvrPm4 effector released at the early stage of haustorium formation (12-24 hai) results in
422 *Pm4b*-mediated, papillae-based pre-haustorial resistance (Fig 6a). At the haustorial stage
423 (48 hours), there is a massive release of the AvrPm4 effector inducing a stronger Pm4-
424 mediated defense reaction resulting in HR. In both the early and weak, as well as the later
425 and strong reaction we assume a direct interaction of Pm4 and AvrPm4. However, the
426 signaling output would be different due to different amounts of AvrPm4 which might bind to
427 one of the C2 or S_TKc domains of either Pm4 variant, resulting in conformational changes
428 of the heteromeric complex, leading to activation of the kinase and disease resistance (Fig.
429 6b). The identification of corresponding effector(s) recognized by Pm4 will be another key
430 element to understand the biological and molecular function of the S_TKc_MCTP based
431 mechanism conferring race-specific resistance to wheat pathogens.

432 ER localization of Pm4b is likely due to the presence of the C-terminal part of a MCTP
433 protein. Extensive work done on Arabidopsis has shown that MCTPs are inserted into the ER
434 via their transmembrane region (TMR)²⁹ as we assume for Pm4b_V2 as well. Likewise, the
435 cytosolic localization of Pm4_V1 (lacking TMR) is in line with the localization observed in
436 MCTPs devoid of TMR²⁹. Finally, we have shown that Pm4b_V1 and Pm4_V2 interact with
437 themselves and each other. We hypothesize that C2 domains play an important role in these
438 interactions. Work done in Arabidopsis has shown that C2 domains are responsible for
439 MCTP physical interaction with other proteins, such as MCTP15/QKY with the receptor-like
440 kinase STRUBBELIG⁶⁹ and binding to lipids and membrane contact sites²⁹.

441 The cloning of the *Pm4* gene broadens our understanding of both immune receptor
442 architecture and the mechanisms of race-specific activation of the plant immune system.
443 Pyramiding resistance genes that operate by different mechanisms possibly increases the

444 durability of resistance gene combinations⁷⁰. The chimeric nature of Pm4 with a MCTP
445 domain reveals a potentially novel biochemical context of resistance activation and expands
446 the toolkit available to breeders for the design of resistance breeding strategies.

447

448 **Online methods**

449 **Wheat germplasm, wheat powdery mildew and infection experiments**

450 The susceptible wheat cultivar Federation (GRIN accession number Cltr47341; with
451 pedigree Purplestraw 14A/Yandilla), its near-isogenic lines (NILs),
452 Khapli/8*Chancellor//8*Federation (derived from Federation BC₈ to Khapli/8*Chancellor) and
453 Federation/W804 (derived from Federation BC₇ to W804) were used in the present study to
454 molecularly identify *Pm4a* and *Pm4b*. Khapli/8*Chancellor//8*Federation, here denoted as
455 Fed-*Pm4a*, harbors the *Pm4a* allele, whose original donor line is Khapli, a tetraploid *Triticum*
456 *turgidum* wheat emmer from which the *Pm4a* gene was transferred to the hexaploid wheat
457 cultivar Chancellor²³. Federation/W804, denoted here as Fed-*Pm4b*, harbors the *Pm4b* allele
458 introgressed from the original donor line W804, to where the *Pm4b* allele was transferred
459 from a tetraploid *T. carthlicum* genotype²². Finally, the wheat genotype Tm27d2, a *Triticum*
460 *monococcum*-derived resistant hexaploid line reported to have the *Pm4d* allele⁷¹ was used to
461 study allelic diversity of the *Pm4* gene. Federation*4/Ulka (derived from Ulka BC₃ to
462 Federation), here denoted as Fed-*Pm2*, carries the *Pm2* resistance gene and was used to
463 compare the resistance reaction at the microscopic level with Fed-*Pm4a* and Fed-*Pm4b*.
464 Finally, a global wheat collection of 512 genotypes, the Whealbi collection, representing a
465 wide spectrum of wheat genetic diversity⁷² was used to study the presence of the *Pm4* locus.
466 Detailed passport information is available at
467 [https://urgi.versailles.inra.fr/download/iwgsc/IWGSC_RefSeq_Annotations/v1.0/iwgsc_refseq](https://urgi.versailles.inra.fr/download/iwgsc/IWGSC_RefSeq_Annotations/v1.0/iwgsc_refseq_v1.0_Whealbi_GWAS.zip)
468 [v1.0_Whealbi_GWAS.zip](https://urgi.versailles.inra.fr/download/iwgsc/IWGSC_RefSeq_Annotations/v1.0/iwgsc_refseq_v1.0_Whealbi_GWAS.zip)

469 *Blumeria graminis* f. sp. *graminis* (*Bgt*) isolates *Bgt96224*, *Bgt94202*, *BgtJIW2* and *Bgt97251*
470 were used for infection tests aimed at the molecular identification and further
471 characterization of the *Pm4* gene because of their avirulence/virulence pattern on *Pm4a* and
472 *Pm4b*. *Bgt96224* and *Bgt94202* are avirulent (no visible symptoms observed) on the *Pm4a/b*
473 lines while *BgtJIW2* and *Bgt97251* are both virulent (leaves fully covered by mycelia). To
474 investigate and compare resistance spectra of *Pm4a* and *Pm4b* against a broad variety of

475 globally collected wheat powdery mildew isolates, infection tests were performed on Fed-
476 *Pm4a* NIL and *Pm4b* NIL Fed-*Pm4b* with 108 genetically diverse contemporary *Bgt*
477 isolates^{73,74,75} (Supplementary Table 1).

478 Plants were grown and challenged with appropriated *Bgt* isolates depending on the
479 experiment as previously described²⁴. Disease levels were assessed 7-9 d after inoculation
480 as one of five classes of host reactions: R = resistance (0-10% of leaf area covered), IR (10-
481 25% of leaf area covered), I (25-50% of leaf area covered), IS (50-75 % of leaf area covered)
482 and S (>75% of leaf area covered).

483 **Microscopic analysis of powdery mildew infection**

484 Infected leaf segments were collected two and six days post infection (dpi) and stained for
485 reactive oxygen species using the 3,3'-diaminobenzidine (DAB)-method⁷⁶. Leaf segments
486 were then fixed⁷⁷ and aerial fungal structures were stained for 45 s using 0.25% Coomassie
487 Brilliant Blue (0.15% in EtOH absolute) followed by three washing steps with H₂O.

488 Microscopic observations were based on five biological replicates, for each of which 100 A-
489 and B-type epidermal cells⁷⁸ with only one attempted penetration were used for the
490 evaluation. Using a conventional bright-field microscope (Leica DM LS phase), powdery
491 mildew-wheat interactions were scored based on three categories: (i) early arrest of conidial
492 growth in the absence of hypersensitive cell-death (HR) at the pre-penetration stage without
493 haustorium formation, (ii) epidermal cells penetrated with a visible haustorium and clear
494 signs of HR (iii) established colonies, with haustorium and production of secondary hyphae
495 but not signs of HR.

496 **Generation and screening of EMS-induced *Pm4a* and *Pm4b* mutants**

497 Mutants were generated treating Fed-*Pm4a* and Fed-*Pm4b* seeds as previously described²⁴.
498 An infection test with the *Pm4a/b*-avirulent isolate *Bgt96224* was done to select potential
499 *pm4a,b* EMS-induced mutants. From a screen of approximately 6,000 M₂ seedlings, we
500 isolated eighteen and twenty-eight putative *pm4a* and *pm4b* mutants, respectively. Progeny

501 test to confirm susceptibility to *Bgt96224* and genotyping with the previously reported *Pm4a*
502 co-segregating marker STS-BCD1231⁷⁹ discarded some of mutants as either they turned out
503 to be resistant or they did not amplify for the STS-BCD1231 marker, a sign that a big
504 chromosomal fragment could have been lost after the EMS treatment. At the end, a total of
505 14 and 18 *pm4a* and *pm4b* mutants, respectively, whose susceptibility to the *Pm4a/b*-
506 avirulent *Bgt96224* isolate was confirmed in the M₃ generation based on ten different M₃
507 plants from each M₂ family.

508 **Primer design and in-house sequencing**

509 All primers used on this study were designed using the Primer blast tool
510 (<https://www.ncbi.nlm.nih.gov/tools/primer-blast/>) and can be found in Supplementary Table
511 7. In-house Sanger sequencing to check integrity of sequences and constructs was
512 performed on an ABI 3730 (Thermo Fischer Scientific, Waltham, Massachusetts, USA).

513 ***Pm4* allele mining**

514 The Whealbi collection was screened for the presence of the *Pm4* locus using the *Pm4*
515 haplotype-specific marker JS717xJS718. Given the difficulty of amplifying the full-length
516 genomic fragment of *Pm4* due to the presence of a 4.5 kb intron between exons 5 and 6 that
517 greatly reduced PCR efficiency, we decided to amplify the gene in two parts. The first part
518 corresponds to the genomic region spanning exons 1 to 5 and the second part to exons 6 to
519 7. To amplify exons 1 to 5, a long range PCR was performed using the primers
520 JS256xJS257 followed by a nested PCR with JS251xJS257. PCR amplification was done
521 using KAPA Hifi HotStart Polymerase (KK2502, Kapa Biosystems) following manufacturer's
522 recommendations and with an annealing temperature of 60°C and extension time of 2:00
523 min. The PCR products were sequenced with the internal primers GH382, GH384, GH385
524 and JS255. For the amplification of the second part of the gene, a long range PCR using the
525 primers JS278xJS261 followed by a nested PCR with JS278xGH407 was done similarly to
526 the PCR dedicated to amplify the first part of the gene but with an annealing temperature of

527 63°C and an extension time of 3:00. The PCR products were sequenced with the internal
528 primers JS280, JS292, GH387, GH397 and GH402.

529 **Assessment of alternative splicing of *Pm4b* mRNA**

530 A first *in silico* annotation of the *Pm4* gene was done based on transcript information from
531 the *Ae. tauschii* gene AET2Gv21296200, given the lack of RNA-seq data from a *Pm4b*-
532 containing genotype and the absence of the gene in the Chinese Spring bread wheat
533 reference genome. We elucidated the genomic structure and splicing pattern of the *Pm4b*
534 gene following a two-steps approach.

535 First, we perform a rapid amplification of cDNA ends (RACE) to determine the transcriptional
536 start (5' RACE) and end (3' RACE) of the *Pm4b* gene. 3'- and 5'-UTR sequences of *Pm4b*
537 were identified by using the SMARTer™ RACE cDNA Amplification Kit (634923; Clontech)
538 according to the protocol using 40 ng of magnetic bead purified and eluted wheat mRNA as
539 described for RT-qPCR. For reverse transcription of cDNA, the 3' SMART CDS Primer II A
540 was replaced by primer GH438 in the 5' RT reaction. Subsequently the same reaction
541 containing the tailed first strand cDNA could be used for both, 3' and 5' race PCR. 5' RACE
542 PCR reaction was made with 2 µl of 1:5 diluted cDNA in a 20µl reaction with KAPA2G
543 Robust PCR Kit (KK5501, Sigma-Aldrich, St. Louis, Missouri, USA) and buffer B, gene
544 specific reverse primer GH432 and the provided UPM primer in the Kit. 30 cycles were run
545 according to the touchdown PCR program 1 described in the SMARTer™ RACE Kit manual.
546 On the other hand, 3' race PCR reaction was made with 4 µl of 1:5 diluted cDNA in a 20µl
547 reaction with KAPA2G Robust PCR Kit and buffer B, gene specific forward primer GH377
548 and a universal reverse primer GH439. After initial denaturation at 95°C for 3 min, a
549 touchdown PCR protocol with 10 cycles of 95°C for 15 secs, 68°C (-0.8°C/cycle) for 30 secs,
550 72°C for 30 secs, then 25 cycles at 95°C for 15 secs, 61°C for 15 secs, 72° for 30 secs was
551 performed with a final extension at 72° C for 5 min. The obtained 3' and 5' race PCR
552 fragments were gel excised, cloned and the sequenced by Sanger sequencing to detect the
553 UTR's. Based on 5'RACE reactions, we could confirm the presence of at least 182-bp 5'UTR

554 consisting split in two exons. The first one starts spans positions 1'028 to 862 bp before start
555 codon. The second one is a small 16-bp string before start codon. Within this 5' UTR, no
556 alternative start codons were found. The 3'UTR of *Pm4b_V1* is at least 270 bp in length
557 while the one of *Pm4b_V2* is 154 bp in length.

558 Second, guided by the 5' and 3' UTRs, we designed primers sitting on both UTRs to study
559 gene structure and splicing. We only found *Pm4b_V1* and *Pm4b_V2* transcripts variants. The
560 amplification of *Pm4b_V1* was achieved using the primers GH398 x GH399 followed by a
561 nested PCR with GH400 x GH401. PCR products were sequenced using primers GH382,
562 GH385, GH387, GH397, JS233 and JS293. For the case of *Pm4b_V2*, transcript
563 accumulation was confirmed by PCR amplification using the primers GH398 x GH407
564 followed by a nested reaction with primers GH400 x GH407. PCR product was sequenced
565 with the internal primers GH382, GH385, GH387, JS233, JS280, JS292, JS298 and JS540.
566 PCR amplifications were done using KAPA Hifi HotStart Polymerase (KK2502, Kapa
567 Biosystems) with an annealing temperature of 60°C and extension time of 2:30 min and 3:00
568 min for amplification of *Pm4b_V1* and *Pm4b_V2*, respectively.

569 **Quantitative Real-Time PCR analysis for detection of *Pm4* expression**

570 Expression of *Pm4a/b_V1* and *Pm4a/b_V2* was quantified in a reverse transcription,
571 quantitative real-time PCR (RT-qPCR) assay, using a CFX96 Real-Time System C1000TM
572 Thermal cycler (Bio-Rad, Hercules, California, USA) and according to MIQE guidelines⁸⁰.
573 The reference genes ADP and ZFL were selected based on a geNorm study made on eight
574 genes as previously described⁸¹. Specificities of amplicons, RT-minus control check, melt
575 curve assessment and efficiency calculation were performed as previously described⁸².
576 Target-specific amplification efficiencies are given in Supplementary Table 8.
577 30 mg leaf material was harvested at the specified time points, shock frozen in liquid nitrogen
578 and stored at -80°. RNA extraction was made with the Dynabeads™ mRNA DIRECT™

579 Purification Kit (61012, Invitrogen) according to the manufacturer's protocol, with 25 μ L of
580 Oligo (dT) 25 per extraction.

581 First-strand cDNA was synthesized from 40 ng mRNA, using 1/2 reaction of the iScript
582 Advanced cDNA Kit (172-5038, Bio-Rad, Hercules, California, USA). RT-qPCR primers used
583 for the targets *Pm4a/b_V1* and *Pm4a/b_V2* and the reference genes *ZFL* and *ADP* are
584 shown in Supplementary Table 8. RT-qPCR was performed with 4 μ L of 20-fold-diluted
585 cDNA in a total reaction volume of 10 μ L in technical duplicates using KAPA SYBR® FAST
586 qPCR Master Mix (KK4601, Sigma-Aldrich, St. Louis, Missouri, USA) and 250 μ M of each
587 primer. Thermocycling conditions were 95 °C for 20 s, followed by 40 cycles of 95 °C for 3 s,
588 then 63 °C for 20 s for targets *Pm4a/b_V1* and *ZFL* or 60 °C for 20 s for targets *Pm4a/b_V2*
589 and *ADP*. Subsequently a melt curve assessment was performed to exclude detection of
590 potential primer dimers. Relative quantities were calculated and normalized to the reference
591 genes *ZFL* and *ADP* revealing the calibrated normalized relative quantities (CNRQ) values,
592 using the program CFX Maestro (Bio-Rad, Hercules, California, USA). To allow comparison
593 of the expression levels between the two splice variants *Pm4a/b_V1* and *Pm4a/b_V2*, the
594 RT-qPCR data were calibrated on the basis of plasmid DNA containing the *Pm4_V1* and
595 *Pm4_V2* construct, respectively. qPCR on equal plasmid concentration showed equal Cq
596 values for both targets in the range observed usually for technical replicates (< 0.5 Cq).

597 **Wheat transformation**

598 The full-length CDS of both splice variants (*Pm4b_V1*CDS: 1.6kb and *Pm4b_V2*CDS: 2.2 kb)
599 were amplified from cDNA with Kapa polymerase (Kapa Biosystems Taq DNA Polymerase
600 (Sigma-Aldrich, St. Louis, Missouri, USA) using the JS274, JS276 (*Pm4b_V1*CDS) and
601 JS274, JS275 (*Pm4b_V2*CDS) primers and introducing *Asc*I and *Pac*I restriction sites, to be
602 cloned into the pGY1 vector. *Pm4b_V1*CDS and *Pm4b_V2*CDS were released from the
603 vector pGY1-*Pm4b_V1/V2* by enzymatic digestion using *Asc*I and *Pac*I (New England
604 Biolabs, Ipswich, MA), to be subsequently cloned into the *Asc*I and *Pac*I sites of the
605 pAHC17 vector under the control of the maize ubiquitin promoter (*ubi*) with the nopaline

606 synthase terminator (nos)⁸³. Furthermore, *Not*I restriction sites were introduced into pAHC17
607 5' in front of the ubi Promoter and after the nos terminator. The gene cassette ubi:PMI was
608 enzymatically released from the pAHC17 vector backbone using *Hind* III and *Not*I, while the
609 gene cassettes ubi:Pm4b_V1CDS and ubi:Pm4b_V2CDS only with *Not*I. Equimolar
610 amounts of each gene cassette was mixed prior to coating with gold particles. As a
611 selectable marker, the phosphomannose isomerase gene was used⁸⁴.

612 The hexaploid spring wheat cultivar Bobwhite S26 was transformed through particle
613 bombardment as previously described⁸¹. Briefly, 1617 immature embryos were isolated from
614 freshly harvested wheat seeds (around 0.5mm, and milkish color), and were co-transformed
615 with ubi:Pm4b_V1CDS, ubi:Pm4b_V2CDS and ubi:Pmi gene cassettes by particle
616 bombardment⁸⁵. Primary T0 transformants were regenerated in tissue culture and selected
617 on mannose-containing media⁸⁶. We obtained 95 putative transgenic plants, among which,
618 Pm4b_V1CDS and Pm4bV2_CDS were detected in 20 T0 plants using specific primers for
619 the two cDNAs forward primers located in the sixth (JS295) and the seventh exon (JS297),
620 respectively. For both cases, primer HZ010 located in the nos terminator was used as
621 reverse primer. Both PCRs were performed with the following parameters: 30 cycles of 30s
622 at 35°C 95°C, 15s at 61°C, and 40s at 72°C. Transgenic plants with both the Pm4b_V1CDS
623 and Pm4b_V2CDS transgenes were self-fertilized, and four events were chosen at random
624 for T1 family characterization.

625 **Virus Induced Gene Silencing (VIGS)**

626 To specifically silence each splicing variant individually, we focused on exons 6 and 7 of
627 *Pm4b* to define the VIGS targets. To minimize the possibility of off-target silencing, we
628 blasted the coding sequences of exons six and seven against our own sequencing data
629 obtained from flow-sorted chromosome 2A of Fed-*Pm4b* as well as against the reference
630 genome assembly of wheat (Chinese Spring¹) choosing fragments of 150-250 bp with no
631 homology to other genes. For amplifying Pm4b_V1_target_1 and Pm4b_V2_target_2,
632 primers JS189xJS190 and JS498x499 were used, respectively. Note that primers were

633 designed with *NotI* and *PacI* restriction sites in antisense direction to lead to an antisense
634 insertion in the pBS-BSMV- γ vector. Equimolar amount of pBS-BSMV- α , pBS-BSMV- β and
635 pBS-BSMV- γ transcripts carrying Pm4b_V1_target_1 or Pm4b_V2_target_2 were used to
636 inoculate full-expanded first leaves of Fed-*Pm4b* seedlings, using the wild type (γ) viral
637 genome as control as previously described⁸⁷⁻⁸⁹. For in vitro synthesis of viral RNA, the
638 Invitrogen™ mMMESSAGE mMACHINE™ T7 Transcription Kit (Thermo Fischer Scientific,
639 Waltham, Massachusetts, USA) was used according to the manufacturer's
640 recommendations. Seeds from Fed-*Pm4b* cultivar were stratified at 4°C during five days.
641 Seedlings were then placed in a growth chamber (Conviron, Winnipeg, Canada) cycled at
642 23°C/16°C, 16/8h photoperiod with 60% humidity and a light intensity regime of 350
643 $\mu\text{mol}/(\text{s}\cdot\text{m}^2)$. Fed-*Pm4b* plants were inoculated when the first leaf was fully developed as
644 previously described^{90,91}. 14 days after virus infection the 3rd and 4th leaves were detached
645 and infected with the Pm4a/b avirulent isolate *Bgt96224*, adding 10g/L Benzylaminopurine
646 (BAP)⁹² to 0.5% agar plates. 7 days later, powdery mildew phenotypes were documented
647 and around 1 cm² highly mildew infected leaf pieces were sampled for further gene silencing
648 expression analyses as explained before in the section Quantitative Real-Time PCR analysis
649 for detection of Pm4 expression.

650 **Plasmids constructs for protein interaction and localization studies**

651 To generate constructs for the Split-Luciferase complementation assay, cDNA from Fed-
652 *Pm4b* was used to amplify the full-length Pm4b_V1 CDS with primers JS483 (common
653 forward) and JS486 (stop codon) or JS487 (without stop codon). Likewise, the full-length
654 Pm4b_V2 CDS was amplified using primers JS483 and JS484 (stop codon) or JS485
655 (without stop codon). All the fragments were cloned into pENTR/D-TOPO vector (Invitrogen)
656 following manufacturer's recommendations. For the expression clones, the pENTR
657 subclones were recombined into the destination vectors 35S: gwnLUC, 35S: nLUCgw, 35S:
658 gwcLUC, 35S: cLUCgw⁴¹, using LR Clonase II (ThermoFisher Scientific) following the
659 manufacturer's recommendations.

660 To generate constructs for the co-immunoprecipitation assay, similarly to before, entry
661 clones were generated for full-length Pm4b_V1 CDS using JS483 and JS486 (stop codon) or
662 JS487 (without stop codon) primers. For full-length amplification of Pm4b_V2 CDS primers
663 JS483 and JS484 (stop codon) or JS485 (without stop codon) were used. The subclones
664 were then cloned into expression vector pIPKb004⁹³, using LR Clonase II (ThermoFisher
665 Scientific) and following manufacturer's recommendations. Introduction of genes encoding
666 fusion proteins into the destination vectors was made by site-directed mutagenesis,
667 amplifying the CDS in the expression clones adding HA/Flag tags by PCR with the Primers,
668 JS589&JS590 (N-terminal Flag), JS593&594 (C-terminal Flag), JS601&JS602 (N-terminal
669 HA), JS488&JS489 (C-terminal HA).

670 To generate the constructs for fluorescence localization, the pENTR subclones generated for
671 the Split-luciferase complementation assay were recombined into the expression vectors
672 35S:pGWB505³⁸ and 35S: pMpGWB228⁹⁴, by LR Clonase II (ThermoFisher Scientific)
673 according to manufacturer's recommendations. Likewise, the mRFP-fused cytosolic
674 localization sequence (pGWB455³⁸), ER-marker (ER-ck, CD3-959³⁹) and plasma membrane-
675 marker (35S:REM 1.2 m_RFP⁴⁰) were cloned into *A. tumefaciens* GV3101.

676 **Agroinfiltrations**

677 Binary plasmids were transformed via freeze-thaw approach⁹⁵ into *Agrobacterium*
678 *tumefaciens* GV3101, which were grown overnight with vigorous shaking (200 rpm) at 28°C
679 in Luria-Bertani (LB) medium supplemented with appropriate selective medium depending on
680 constructs carried. 200µl of this culture was used to inoculate 15 ml LB medium and grown
681 overnight under the same conditions. Bacteria were harvested by centrifugation at 2'500 x g
682 for 15min and then resuspended and diluted in infiltration medium (10 mM MgCl₂, 0.1M
683 acetosyringone) to an optimal density at 600 nm = 0.8-1.0. After 2 to 4h of incubation at room
684 temperature, one or more cultures were mixed in a 1:1 ratio with an equally treated
685 *Agrobacterium* p19-silencing-suppressor strain⁹⁶ and were infiltrated with a needleless

686 syringe into the abaxial side of leaves from 2- to 4-week-old *Nicotiana benthamiana*
687 plantlets.

688 **Split - luciferase complementation assay**

689 For the *in vivo* split-luciferase assay in *N. benthamiana*, the CDS of *Pm4b_V1* and *Pm4b_V2*
690 were fused in frame with nLUCgw/gwnLUC and cLUCgw/gwcLUC. As negative controls N-
691 and C-terminal fusions of the Pm17 resistance protein⁹⁷ to nLUC or cLUC were used. As
692 positive controls, we used the AvrPm3b C-terminally fused to nLUC and cLUC. All the fusion
693 constructs were transformed into *A. tumefaciens* GV3101 strain. Equal amounts of bacteria
694 producing the nLUC or cLUC, N- or C-terminally-fused proteins were infiltrated in 2-4 weeks
695 old *N. benthamiana* leaves. The luciferase luminescence signals were imaged 4 days after
696 infiltration using an *in vivo* plant imaging system (Spark, multimode microplate reader,
697 TECAN, Switzerland).

698 **Plant protein extraction and co-immunoprecipitation**

699 Tissue for co-immunoprecipitation was harvested three days post infiltration and immediately
700 flash frozen in liquid nitrogen. Leaf material (50 mg) was ground to a fine powder and
701 proteins were extracted with Triton-X100 (100mM Tris-HCL pH7.4, 50mM NaCl, 5mM NaF,
702 5mM NaVo4, 0.5% Triton X-100, PMSF) or Brij-58 (100mM Tris-HCL pH7.4, 50mM NaCl,
703 5mM NaF, 5mM NaVo4, 0.5% Brij-58, PMSF) lysis buffers (1 mL), and subsequently
704 precipitated by anti HA magnetic beads (10 µl) (mouse, monoclonal, 88837, Thermo
705 Scientific). Precipitates were washed five times with Triton X-100 or Brij-58. Proteins from
706 crude extracts (input) and precipitated proteins were detected by immunoblotting with
707 protein-specific antibodies. The elution, IP, washing and detection were performed at 4°C.
708 Proteins were separated by SDS-PAGE and transferred to a nitrocellulose membrane (GE
709 Healthcare, Chicago, Illinois, USA). The membrane was then blocked in TBST buffer
710 containing 5% non-fat dry milk under gentle shaking. The blocked membrane was incubated
711 with specific antibodies dissolved in TBST 5% non-fat dry milk powder at a ratio of 1:10'000

712 (Anti-Flag) or 1:3'000 (Anti-HA-HRP) and incubated at 25°C by shaking at 100rpm for 2
713 hours, followed by three washes (10 min each) with TBST. The detection of the antibodies
714 was performed with WesternBright ECL HRP substrate (Advansta, San Jose, California,
715 USA), before photographing using the Fusion FX system (Vilber Lourmat, Eberhardzell,
716 Germany). Blotted proteins were stained with Ponceau S. The primary antibodies used in
717 this study were anti-Flag (mouse monoclonal, clone M2, F3165, Sigma-Aldrich, St. Louis,
718 Missouri, USA), anti-HA-HRP (rat monoclonal, clone 3F10, 12013819001, Roche, Basel,
719 Switzerland), and Anti-GFP (mouse monoclonal, clone B34, 902601, BioLegend, San Diego,
720 USA). Anti-mouse immunoglobulin G(IgG) (LabForce, sc2357) was used as a secondary
721 antibody for Flag-tag and GFP detection at a working dilutions of 1:10'000 and 1:5'000,
722 respectively.

723 **Confocal Laser Scanning Microscopy**

724 Confocal images of infiltrated *N. benthamiana* leaves were taken as previously described⁹⁸.
725 Briefly, a Leica SP5 confocal laser scanning microscopy system (Leica, Wetzlar, Germany)
726 equipped with Argon and DPSS lasers and hybrid detectors was used. eGFP fluorescence
727 was observed using excitation wavelengths of 488nm and its fluorescence emission was
728 collected at 495 to 550 nm. Tag- and m-RFP fluorescence was observed using excitation
729 wavelengths of 561nm and its fluorescence emission was collected at 575 to 650nm. Leaf
730 samples of 5x5 mm were transferred between a glass slide and a cover slip in a drop of
731 water. Experiments were performed using identical confocal acquisition parameters (e.g.
732 laser power, gain, zoom factor, resolution, and emission wavelengths reception), with
733 detector settings optimized for low background and no pixel saturation.

734 Pseudo-colored images were obtained using “Green” and “Magenta” look-up-table (LUT) of
735 Fiji software⁹⁹ (<http://rsb.info.nih.gov/ij/>). To calculate the most quantitative estimate of co-
736 localization, known as the Pearson correlation coefficient that depends on the amount of
737 colocalized signals in both channels (magenta and green) in a nonlinear manner, we
738 performed the analysis as previously described¹⁰⁰ in Image J (<http://rsb.info.nih.gov/ij/>). In

739 brief, it was made sure that the images acquired have low noise levels and no bleed through,
740 and that the optical setup used for each color lead to the same point of spread function
741 (PSF). In addition, after splitting the images and removing the blue channel, the background
742 was subtracted and then the Coloc 2 Image J plug in was run.

743 **Chromosome flow sorting, sequencing and MutChromSeq-based identification of a *Pm4b*** 744 **candidate gene**

745 Chromosome flow sorting and sequencing was performed in WT and eight mutants
746 (Supplementary Table 2). Briefly, cycling cells in root tips of young seedlings were
747 accumulated at mitotic metaphase and chromosomes were isolated by mechanical
748 homogenization of formaldehyde-fixed meristem tips as previously described¹⁰¹.
749 Chromosomes in suspension were fluorescently labelled using (GAA)₇-FITC as previously
750 described¹⁰², chromosomal DNA was stained by DAPI (2 µg/ml) and the suspension was
751 analyzed by FACSaria SORP II flow sorter (BD Biosciences, San Jose, USA). 30,000 copies
752 of chromosome 2A corresponding to 50 ng of DNA were flow-sorted from each line into PCR
753 tube containing 40 µl deionized water using the sort window shown in Extended Data Fig. 10.
754 To estimate the extent of contamination by other chromosomes, 2,000 chromosomes 2A
755 were flow-sorted onto a microscopic slide, labelled by FISH with GAA microsatellite and Afa-
756 family probes (inset of Extended Data Fig. 10) and evaluated microscopically¹⁰³. The purities
757 in the sorted fractions ranged from 90 to 99% Chromosomal DNA was purified and amplified
758 by Illustra GenomiPhi V2 DNA amplification Kit (GE Healthcare, Piscataway, USA) as
759 previously described¹⁰⁴.

760 **MutChromSeq-based identification of a *Pm4b* candidate gene**

761 Illumina raw reads of flow-sorted chromosomes of EMS-derived mutants were analyzed for
762 their quality using FastQC (<http://www.bioinformatics.bbsrc.ac.uk/projects/fastqc>). For
763 sequencing adapter removal and quality trimming, cutadapt¹⁰⁵ and sickle
764 (<https://github.com/najoshi/sickle>), with the sickle parameter -q = 25 and -l = 20, were used.

765 MutChromSeq was performed as described previously
766 (<https://github.com/steuernb/MutChromSeq>)²⁴ with minimum adjustments in the Pileup2XML
767 command (-a 0.1 -c 8) and MutChromSeq command (-a 0 -c 8 -n 3 -z 1). It is important to
768 note, that manual inspection of the MutChromSeq pipeline is advisable. For example,
769 mutations of *pm4b_m207* and *pm4b_m256* contig_18057 were not identified as such
770 because neither of the two did meet the stringency criteria of the pipeline. *pm4b_m207* had
771 a G->A SNP at contig_18057 position 3723, but was only covered by 4 reads. The
772 *pm4b_m256* showed a G->A SNP at contig_18057 position 11,157 but was only
773 supported by eight out of nine reads, and therefore, not meeting the allele frequency
774 demands of the pipeline.

775 **Protein sequence and domain analysis**

776 Prediction of core domain kinase of Pm4b and resistance proteins displayed in Extended
777 Data Fig. 5 and Supplementary Fig. 1 was done based on Conserved Domain Database
778 (CDD) from NCBI¹⁰⁶ (<https://www.ncbi.nlm.nih.gov/Structure/cdd/wrpsb.cgi>). Prediction and
779 delimitation of Pm4b C2 domains was done as previously described²⁹. Prediction of
780 transmembrane helices was performed with TMHMM server v.2.0¹⁰⁷
781 (<http://www.cbs.dtu.dk/services/TMHMM/>) and Phobius¹⁰⁸ (<http://www.phobius.sbc.su.se>).
782 Only transmembrane domains predicted for both applications were considered. 3D structure
783 modelling was done using Phyre2 using intensive modelling mode. Crystal structures served
784 as best templates, % of confidentiality and p-values for each 3D structure modelling are
785 indicated in the legends of the corresponding figures. The structural graphics were
786 generated using PyMOL (The PyMOL Molecular Graphics System, Version 2.0 Schrödinger,
787 LLC).

788 **Phylogenetic analysis of *Pm4* homologues**

789 To reduce complexity and shorten computation time in the search of *Pm4* homologues, we
790 created *in silico* a hypothetical protein called Pm4_VF, without alternative splicing and with

791 exons 6 and 7 both included in the coding gene (STKc-C2C-C2D-PRT_C). The Pm4b_VF
792 amino acid sequence was used as a query to identify *Pm4* homologues via BlastP on
793 genome assemblies of barley *H. vulgare*¹⁰⁹ (Genome assembly: Barley Pseudomolecules
794 Morex v2.0 2019, https://webblast.ipk-gatersleben.de/barley_ibsc/), goatgrass *Ae. tauschii*
795 ¹¹⁰ (Genome assembly, Aet_v4.0 https://plants.ensembl.org/Aegilops_tauschii/Info/Index),
796 rye *S. cereale* (<https://webblast.ipk-gatersleben.de/ryeselect/>), *T. urartu*¹¹¹ (accession
797 G1812) wild emmer wheat *T. turgidum dicoccoides*¹¹² (Genome assembly, Zavitan
798 pseudomolecules), durum wheat *T. turgidum durum*¹¹³ (Genome assembly, Svevo
799 pseudomolecules) and common wheat¹ (Genome assembly, Chinese Spring
800 pseudomolecules, IWGSC RefSeq v1.0). We retrieve a total of 18 *Pm4* homologues
801 encoding intact full-length Pm4_V1- and Pm4_V2-like proteins, whose predicted sequences
802 were aligned with Clustalw at default parameters. Phylogenetic trees for *Pm4_V1* and
803 *Pm4b_V2* homologs were done with MrBayes¹¹⁴, summarized using a burn-in of 25% and
804 visualized with FigTree (<http://tree.bio.ed.ac.uk/software/figtree/>). All software was obtained
805 from ubuntu repositories (ubuntu.com)

806 **Phylogenetic analysis of kinase domain-containing proteins.**

807 A BlastP search of the NCBI non-redundant protein database was used to find proteins
808 described in disease resistance with a kinase domain similar to one present in Pm4b.
809 Considering the increasing evidence of a blurred PTI-ETI dichotomy¹¹⁵, we did not
810 differentiate between PTI- or ETI-related resistance proteins but instead focus on homology.
811 Alignment and phylogenetic tree was conducted in the same way as for the *Pm4*
812 homologues described above.

813 **Divergence estimates**

814 Predicted protein sequences were aligned with the program Water. From this alignment, a
815 codon-by-codon DNA alignment was deduced. All protein alignments were inspected by eye
816 and poor alignments were removed. For divergence time estimates, only fourfold degenerate

817 sites were used (i.e. third codon bases for Ala, Gly, Leu, Pro, Arg, Ser, Thr and Val. For Leu,
818 Arg and Ser (which have six possible codons), we used only those codons starting with CT,
819 TC and CG, respectively (where the third base can be exchanged without amino acid
820 change). Divergence time estimates for gene pairs were calculated as previously
821 described¹¹⁶ using a substitution rate of 1.3E-9 substitutions per site per year¹¹⁷.

822 **Statistical analysis**

823 Detailed statistical description is provided in the figure legends, including the type of
824 statistical tests used and the sample size. All analyses were performed using R Statistical
825 Software (R version 3.6.2)¹¹⁸.

826

827 **Acknowledgements**

828 This project was financially supported by the University of Zurich, Swiss National Science
829 Foundation grant 310030B_182833 to B.K., the European Research Council under the Grant
830 Agreement 773153 (grant IMMUNO-PEPTALK) to C.Z., and the European Molecular Biology
831 Organization (EMBO Long-Term Fellowships 438-2018) to J.G. M.C.K has received funding
832 from the European Union's Horizon 2020 research and innovation program under the Marie
833 Skłodowska-Curie grant agreement No 674964. B.K. and J.S.M sincerely thank Dr. Volker
834 Mohler from the Bavarian State Research Center for Agriculture (LfL) for providing seeds
835 from the hexaploid line Tm27d2. J.S.M. sincerely thanks Dr. Nina Chumak from the
836 Department of Plant and Microbial Biology (UZH) for providing the ER-marker (ER-ck, CD3-
837 959).

838

839 **Author Contributions**

840 J.S.M. and B.K. conceived the project. M.K. and J.D. performed chromosome flow sorting
841 and preparation of chromosomal DNA. T.W., J.S.M., M.H., C.R.P., B.S., and M.C.K.
842 performed bioinformatics analysis. H.Z. performed VIGS. G.H. carried out gene expression
843 studies. J.G. and V.W. performed confocal microscopy. V.W. did validation by transgenic
844 complementation. V.W., J.S.M., L.S., and J.I. performed biochemistry experiments. J.S.M.
845 and L.S. carried out allele mining. C.Z. provided theoretical contributions to the project.
846 J.S.M. and B.K. analyzed the data. J.S.M. and B.K. wrote the manuscript, and all authors
847 revised the manuscript.

848 **Competing Interests statement**

849 The authors declare no competing interests.

850

851 **Data availability statement**

852 All data is available in the main text or the supplementary materials. Sequence data were deposited at
853 the NCBI GenBank under the accession numbers MT783929 (Pm4b_V1 CDS) and MT783930
854 (Pm4b_V2 CDS), and at the NCBI short read archive (SRA) database under the accession number

855 PRJNA646941 (flow-sorted chromosome 2A of eight Fed-*Pm4b* mutants and the wild-type Fed-
856 *Pm4b*). All *Blumeria graminis* f. sp. *tritici* (*Bgt*) isolates listed in Supplementary Table 1 are kept alive
857 in the Department of Plant and Microbial Biology of the University of Zurich and are available upon
858 request. Any additional data that support the findings of this study are available from the
859 corresponding author upon reasonable request. The databases that we used are all publicly available,
860 please see Methods and the [Nature Research Reporting Summary](#) linked to this article.

861

862 **References**

- 863 1. Appels, R. *et al.* Shifting the limits in wheat research and breeding using a fully annotated
864 reference genome. *Science* (80-.). (2018) doi:10.1126/science.aar7191.
- 865 2. Savary, S. *et al.* The global burden of pathogens and pests on major food crops. *Nat. Ecol.*
866 *Evol.* **3**, 430-439 (2019).
- 867 3. Singh, R. P. & Rajaram, S. Breeding for disease resistance in wheat. in *Bread wheat:*
868 *improvement and production.* (Food and Agriculture Organization of the United Nations, 2002).
- 869 4. Pink, D. A. C. Strategies using genes for non-durable disease resistance. in *Euphytica* vol. 124
870 227-236 (2002).
- 871 5. Koller, T., Brunner, S., Herren, G., Hurni, S. & Keller, B. Pyramiding of transgenic Pm3 alleles
872 in wheat results in improved powdery mildew resistance in the field. *Theor. Appl. Genet.* **131**,
873 861-871 (2018).
- 874 6. Mundt, C. C. Use of multiline cultivars and cultivar mixtures for disease management. *Annu.*
875 *Rev. Phytopathol* **40**, 381-410 (2002).
- 876 7. Jones, J. D. G. & Dangl, J. L. The plant immune system. *Nature* **444**, 323-329 (2006).
- 877 8. Dodds, P. N. & Rathjen, J. P. Plant immunity: towards an integrated view of plant-pathogen
878 interactions. *Nat. Rev. Genet.* **11**, 539-548 (2010).
- 879 9. Marchal, C. *et al.* BED-domain-containing immune receptors confer diverse resistance spectra
880 to yellow rust. *Nat. Plants* **4**, 662-668 (2018).
- 881 10. Wang, H., Zou, S., Li, Y., Lin, F. & Tang, D. An ankyrin-repeat and WRKY-domain-containing
882 immune receptor confers stripe rust resistance in wheat. *Nat. Commun.* (2020)
883 doi:10.1038/s41467-020-15139-6.
- 884 11. Sarris, P. F., Cevik, V., Dagdas, G., Jones, J. D. G. & Krasileva, K. V. Comparative analysis of
885 plant immune receptor architectures uncovers host proteins likely targeted by pathogens. *BMC*
886 *Biol.* (2016) doi:10.1186/s12915-016-0228-7.
- 887 12. Le Roux, C. *et al.* A receptor pair with an integrated decoy converts pathogen disabling of
888 transcription factors to immunity. *Cell* (2015) doi:10.1016/j.cell.2015.04.025.
- 889 13. Sarris, P. F. *et al.* A plant immune receptor detects pathogen effectors that target WRKY
890 transcription factors. *Cell* (2015) doi:10.1016/j.cell.2015.04.024.
- 891 14. Kourelis, J. & Van Der Hoorn, R. A. L. Defended to the nines: 25 years of resistance gene
892 cloning identifies nine mechanisms for R protein function. *Plant Cell* (2018)
893 doi:10.1105/tpc.17.00579.
- 894 15. Saintenac, C. *et al.* Wheat receptor-kinase-like protein Stb6 controls gene-for-gene resistance
895 to fungal pathogen *Zymoseptoria tritici*. *Nat. Genet.* (2018) doi:10.1038/s41588-018-0051-x.
- 896 16. Kema, G. H. J. *et al.* Stress and sexual reproduction affect the dynamics of the wheat
897 pathogen effector AvrStb6 and strobilurin resistance. *Nat. Genet.* **50**, 375-380 (2018).
- 898 17. Zhong, Z. *et al.* A small secreted protein in *Zymoseptoria tritici* is responsible for avirulence on
899 wheat cultivars carrying the *Stb6* resistance gene. *New Phytol.* **214**, 619-631 (2017).
- 900 18. Klymiuk, V. *et al.* Cloning of the wheat Yr15 resistance gene sheds light on the plant tandem
901 kinase-pseudokinase family. *Nat. Commun.* (2018) doi:10.1038/s41467-018-06138-9.
- 902 19. Brueggeman, R. *et al.* The barley stem rust-resistance gene Rpg1 is a novel disease-
903 resistance gene with homology to receptor kinases. *Proc. Natl. Acad. Sci. U. S. A.* **99**, 9328-
904 9333 (2002).
- 905 20. Chen, S. *et al.* Wheat gene Sr60 encodes a protein with two putative kinase domains that
906 confers resistance to stem rust. *New Phytol.* (2020) doi:10.1111/nph.16169.

- 907 21. Lu, P. *et al.* A rare gain of function mutation in a wheat tandem kinase confers resistance to
908 powdery mildew. *Nat. Commun.* (2020) doi:10.1038/s41467-020-14294-0.
- 909 22. The, T. T., McIntosh, R. A. & Bennett, F. G. A. Cytogenetical Studies in Wheat . IX . *
910 Monosomic Analyses , Telocentric Mapping and Linkage Relationships of Genes Sr21, Pm4
911 and Mle. *Aus* **32**, 115-126 (1979).
- 912 23. Briggie, L. W. Transfer of Resistance to Erysiphe graminis f. sp. tritici from Khapli Emmer and
913 Yuma Durum to Hexaploid Wheat 1 . *Crop Sci.* (1966)
914 doi:10.2135/cropsci1966.0011183x000600050020x.
- 915 24. Sánchez-Martín, J. *et al.* Rapid gene isolation in barley and wheat by mutant chromosome
916 sequencing. *Genome Biol.* **17**, (2016).
- 917 25. Stam, M., Mol, J. N. M. & Kooter, J. M. The silence of genes in transgenic plants. *Annals of*
918 *Botany* (1997) doi:10.1006/anbo.1996.0295.
- 919 26. Carbonell, A. Secondary small interfering RNA-based silencing tools in plants: An update.
920 *Frontiers in Plant Science* (2019) doi:10.3389/fpls.2019.00687.
- 921 27. Wang, P. H. *et al.* RNase I f-treated quantitative PCR for dsRNA quantitation of RNAi trait in
922 genetically modified crops. *BMC Biotechnol.* (2018) doi:10.1186/s12896-018-0413-6.
- 923 28. Liu, L., Li, C., Liang, Z. & Yu, H. Characterization of multiple C2 domain and transmembrane
924 region proteins in arabidopsis. *Plant Physiol.* (2018) doi:10.1104/pp.17.01144.
- 925 29. Brault, M. L. *et al.* Multiple C2 domains and transmembrane region proteins (MCTP s) tether
926 membranes at plasmodesmata . *EMBO Rep.* (2019) doi:10.15252/embr.201847182.
- 927 30. Liu, L. *et al.* FTIP1 is an essential regulator required for florigen transport. *PLoS Biol.* (2012)
928 doi:10.1371/journal.pbio.1001313.
- 929 31. Hanks, S. K., Quinn, A. M. & Hunter, T. The protein kinase family: Conserved features and
930 deduced phylogeny of the catalytic domains. *Science (80-).* (1988)
931 doi:10.1126/science.3291115.
- 932 32. Yeh, Y. H., Chang, Y. H., Huang, P. Y., Huang, J. B. & Zimmerli, L. Enhanced Arabidopsis
933 pattern-triggered immunity by overexpression of cysteine-rich receptor-like kinases. *Front.*
934 *Plant Sci.* (2015) doi:10.3389/fpls.2015.00322.
- 935 33. Chen, K., Du, L. & Chen, Z. Sensitization of defense responses and activation of programmed
936 cell death by a pathogen-induced receptor-like protein kinase in Arabidopsis. *Plant Mol. Biol.*
937 (2003) doi:10.1023/B:PLAN.0000009265.72567.58.
- 938 34. Rayapuram, C. *et al.* Regulation of basal resistance by a powdery mildew-induced cysteine-
939 rich receptor-like protein kinase in barley. *Mol. Plant Pathol.* (2012) doi:10.1111/j.1364-
940 3703.2011.00736.x.
- 941 35. Brueggeman, R. *et al.* The barley stem rust-resistance gene Rpg1 is a novel disease-
942 resistance gene with homology to receptor kinases. *Proc. Natl. Acad. Sci. U. S. A.* (2002)
943 doi:10.1073/pnas.142284999.
- 944 36. Corbalan-Garcia, S. & Gómez-Fernández, J. C. Signaling through C2 domains: More than one
945 lipid target. *Biochimica et Biophysica Acta - Biomembranes* (2014)
946 doi:10.1016/j.bbamem.2014.01.008.
- 947 37. Shin, O. H., Hau, W., Wang, Y. & Südhof, T. C. Evolutionarily conserved multiple C2 domain
948 proteins with two transmembrane regions (MCTPs) and unusual Ca²⁺ binding properties. *J.*
949 *Biol. Chem.* (2005) doi:10.1074/jbc.M407305200.
- 950 38. Nakagawa, T. *et al.* Improved gateway binary vectors: High-performance vectors for creation of
951 fusion constructs in transgenic analysis of plants. *Biosci. Biotechnol. Biochem.* (2007)
952 doi:10.1271/bbb.70216.
- 953 39. Nelson, B. K., Cai, X. & Nebenführ, A. A multicolored set of in vivo organelle markers for co-
954 localization studies in Arabidopsis and other plants. *Plant J.* (2007) doi:10.1111/j.1365-

- 955 313X.2007.03212.x.
- 956 40. Bücherl, C. A. *et al.* Plant immune and growth receptors share common signalling components
957 but localise to distinct plasma membrane nanodomains. *Elife* (2017) doi:10.7554/eLife.25114.
- 958 41. Gehl, C. *et al.* Quantitative analysis of dynamic protein-protein interactions in planta by a
959 floated-leaf luciferase complementation imaging (FLuCI) assay using binary Gateway vectors.
960 *Plant J.* (2011) doi:10.1111/j.1365-313X.2011.04607.x.
- 961 42. Wicker, T., Buchmann, J. P. & Keller, B. Patching gaps in plant genomes results in gene
962 movement and erosion of colinearity. *Genome Res.* (2010) doi:10.1101/gr.107284.110.
- 963 43. Mascher, M. *et al.* A chromosome conformation capture ordered sequence of the barley
964 genome. *Nature* **544**, 427-433 (2017).
- 965 44. Sánchez, J. & Beat, M. Contribution of recent technological advances to future resistance
966 breeding. *Theor. Appl. Genet.* (2019) doi:10.1007/s00122-019-03297-1.
- 967 45. Barsoum, M., Sabelleck, B., D. Spanu, P. & Panstruga, R. Rumble in the Effector Jungle:
968 Candidate Effector Proteins in Interactions of Plants with Powdery Mildew and Rust Fungi.
969 *CRC. Crit. Rev. Plant Sci.* (2019) doi:10.1080/07352689.2019.1653514.
- 970 46. Greenberg, J. T. & Yao, N. The role of regulation of programmed cell death in plant-pathogen
971 interactions. *Cellular Microbiology* (2004) doi:10.1111/j.1462-5822.2004.00361.x.
- 972 47. Yang, S., Tang, F. & Zhu, H. Alternative splicing in plant immunity. *International Journal of*
973 *Molecular Sciences* (2014) doi:10.3390/ijms150610424.
- 974 48. Lai, Y. & Eulgem, T. Transcript-level expression control of plant NLR genes. *Molecular Plant*
975 *Pathology* (2018) doi:10.1111/mpp.12607.
- 976 49. Ayliffe, M. A. *et al.* Analysis of alternative transcripts of the flax L6 rust resistance gene. *Plant*
977 *J.* (1999) doi:10.1046/j.1365-313X.1999.00377.x.
- 978 50. Schornack, S. *et al.* The tomato resistance protein Bs4 is a predicted non-nuclear TIR-NB-LRR
979 protein that mediates defense responses to severely truncated derivatives of AvrBs4 and
980 overexpressed AvrBs3. *Plant J.* (2004) doi:10.1046/j.1365-313X.2003.01937.x.
- 981 51. Cesari, S. *et al.* The Rice Resistance Protein Pair RGA4/RGA5 Recognizes the Magnaporthe
982 oryzae Effectors AVR-Pia and AVR1-CO39 by Direct Binding. *Plant Cell* **25**, 1463-1481 (2013).
- 983 52. Gou, J. Y. *et al.* Wheat stripe rust resistance protein WKS1 reduces the ability of the thylakoid-
984 associated ascorbate peroxidase to detoxify reactive oxygen species. *Plant Cell* (2015)
985 doi:10.1105/tpc.114.134296.
- 986 53. Sela, H. *et al.* Ancient diversity of splicing motifs and protein surfaces in the wild emmer wheat
987 (*Triticum dicoccoides*) LR10 coiled coil (CC) and leucine-rich repeat (LRR) domains. *Mol. Plant*
988 *Pathol.* (2012) doi:10.1111/j.1364-3703.2011.00744.x.
- 989 54. Dinesh-Kumar, S. P. & Baker, B. J. Alternatively spliced N resistance gene transcripts: Their
990 possible role in tobacco mosaic virus resistance. *Proc. Natl. Acad. Sci. U. S. A.* (2000)
991 doi:10.1073/pnas.020367497.
- 992 55. Zhang, X. C. & Gassmann, W. RPS4-Mediated Disease Resistance Requires the Combined
993 Presence of RPS4 Transcripts with Full-Length and Truncated Open Reading Frames. *Plant*
994 *Cell* (2003) doi:10.1105/tpc.013474.
- 995 56. Tang, F., Yang, S., Gao, M. & Zhu, H. Alternative splicing is required for RCT1-mediated
996 disease resistance in *Medicago truncatula*. *Plant Mol. Biol.* (2013) doi:10.1007/s11103-013-
997 0068-6.
- 998 57. Liang, X. & Zhou, J.-M. Receptor-Like Cytoplasmic Kinases: Central Players in Plant Receptor
999 Kinase-Mediated Signaling. *Annu. Rev. Plant Biol.* (2018) doi:10.1146/annurev-arplant-
1000 042817-040540.
- 1001 58. Lu, D. *et al.* A receptor-like cytoplasmic kinase, BIK1, associates with a flagellin receptor

- 1002 complex to initiate plant innate immunity. *Proc. Natl. Acad. Sci. U. S. A.* (2010)
1003 doi:10.1073/pnas.0909705107.
- 1004 59. Zhang, J. *et al.* Receptor-like cytoplasmic kinases integrate signaling from multiple plant
1005 immune receptors and are targeted by a *Pseudomonas syringae* effector. *Cell Host Microbe*
1006 (2010) doi:10.1016/j.chom.2010.03.007.
- 1007 60. Feng, F. *et al.* A *Xanthomonas* uridine 5'-monophosphate transferase inhibits plant immune
1008 kinases. *Nature* (2012) doi:10.1038/nature10962.
- 1009 61. Shao, F. *et al.* Cleavage of Arabidopsis PBS1 by a bacterial type III effector. *Science* (80-.).
1010 (2003) doi:10.1126/science.1085671.
- 1011 62. Adachi, H., Derevnina, L. & Kamoun, S. NLR singletons, pairs, and networks: evolution,
1012 assembly, and regulation of the intracellular immunoreceptor circuitry of plants. *Current*
1013 *Opinion in Plant Biology* (2019) doi:10.1016/j.pbi.2019.04.007.
- 1014 63. Ade, J., DeYoung, B. J., Golstein, C. & Innes, R. W. Indirect activation of a plant nucleotide
1015 binding site-leucine-rich repeat protein by a bacterial protease. *Proc. Natl. Acad. Sci. U. S. A.*
1016 (2007) doi:10.1073/pnas.0608779104.
- 1017 64. Qi, D. *et al.* Recognition of the protein kinase AVRPPHB SUSCEPTIBLE1 by the disease
1018 resistance protein RESISTANCE TO PSEUDOMONAS SYRINGAE5 Is dependent on S-
1019 acylation and an exposed loop in AVRPPHB SUSCEPTIBLE. *Plant Physiol.* (2014)
1020 doi:10.1104/pp.113.227686.
- 1021 65. Corbesier, L. *et al.* FT protein movement contributes to long-distance signaling in floral
1022 induction of Arabidopsis. *Science* (80-.). (2007) doi:10.1126/science.1141752.
- 1023 66. Freeling, M. Bias in Plant Gene Content Following Different Sorts of Duplication: Tandem,
1024 Whole-Genome, Segmental, or by Transposition. *Annu. Rev. Plant Biol.* (2009)
1025 doi:10.1146/annurev.arplant.043008.092122.
- 1026 67. Liu, Z. Q. *et al.* SRC2-1 is required in PclNF1-induced pepper immunity by acting as an
1027 interacting partner of PclNF1. *J. Exp. Bot.* (2015) doi:10.1093/jxb/erv161.
- 1028 68. Bushnell, W. R. Aggregation of Host Cytoplasm and the Formation of Papillae and Haustoria in
1029 Powdery Mildew of Barley. *Phytopathology* (1975) doi:10.1094/phyto-65-310.
- 1030 69. Vaddepalli, P. *et al.* The C2-domain protein QUIRKY and the receptor-like kinase
1031 STRUBBELIG localize to plasmodesmata and mediate tissue morphogenesis in Arabidopsis
1032 thaliana. *Dev.* (2014) doi:10.1242/dev.113878.
- 1033 70. Lowe, I., Cantu, D. & Dubcovsky, J. Durable resistance to the wheat rusts: Integrating systems
1034 biology and traditional phenotype-based research methods to guide the deployment of
1035 resistance genes. *Euphytica* (2011) doi:10.1007/s10681-010-0311-z.
- 1036 71. Schmolke, M., Mohler, V., Hartl, L., Zeller, F. J. & Hsam, S. L. K. A new powdery mildew
1037 resistance allele at the Pm4 wheat locus transferred from einkorn (*Triticum monococcum*). *Mol.*
1038 *Breed.* (2012) doi:10.1007/s11032-011-9561-2.
- 1039 72. Pont, C. *et al.* Tracing the ancestry of modern bread wheats. *Nat. Genet.* (2019)
1040 doi:10.1038/s41588-019-0393-z.
- 1041 73. McNally, K. E. *et al.* Distinct domains of the AVRPM3A2/F2 avirulence protein from wheat
1042 powdery mildew are involved in immune receptor recognition and putative effector function.
1043 *New Phytol.* (2018) doi:10.1111/nph.15026.
- 1044 74. Menardo, F. *et al.* Hybridization of powdery mildew strains gives rise to pathogens on novel
1045 agricultural crop species. *Nat. Genet.* **48**, 201-205 (2016).
- 1046 75. Zeng, F. S. *et al.* Virulence and diversity of *Blumeria graminis* f. sp. *tritici* populations in China.
1047 *J. Integr. Agric.* **13**, 2424-2437 (2014).
- 1048 76. Thordal-Christensen, H., Zhang, Z., Wei, Y. & Collinge, D. B. Subcellular localization of H₂O₂
1049 in plants. H₂O₂ accumulation in papillae and hypersensitive response during the barley-

- 1050 powdery mildew interaction. *Plant J.* (1997) doi:10.1046/j.1365-313X.1997.11061187.x.
- 1051 77. Sánchez-Martín, J., Rubiales, D. & Prats, E. Resistance to powdery mildew (*Blumeria graminis*
1052 f.sp. *avenae*) in oat seedlings and adult plants. *Plant Pathol.* **60**, 846-856 (2011).
- 1053 78. Rubiales, D. & Carver, T. L. W. Defence reactions of *Hordeum chilense* accessions to three
1054 formae speciales of cereal powdery mildew fungi. *Can. J. Bot.* (2000) doi:10.1139/cjb-78-12-
1055 1561.
- 1056 79. Ma, Z. Q., Wei, J. B. & Cheng, S. H. PCR-based markers for the powdery mildew resistance
1057 gene Pm4a in wheat. *Theor. Appl. Genet.* (2004) doi:10.1007/s00122-004-1605-0.
- 1058 80. Bustin, S. A. *et al.* The MIQE guidelines: Minimum information for publication of quantitative
1059 real-time PCR experiments. *Clin. Chem.* (2009) doi:10.1373/clinchem.2008.112797.
- 1060 81. Brunner, S. *et al.* Transgenic Pm3 multilines of wheat show increased powdery mildew
1061 resistance in the field. *Plant Biotechnol. J.* **10**, 398-409 (2012).
- 1062 82. Hurni, S. *et al.* The maize disease resistance gene Htn1 against northern corn leaf blight
1063 encodes a wall-associated receptor-like kinase. *Proc. Natl. Acad. Sci. U. S. A.* **112**, 8780-5
1064 (2015).
- 1065 83. Christensen, A. H. & Quail, P. H. Ubiquitin promoter-based vectors for high-level expression of
1066 selectable and/or screenable marker genes in monocotyledonous plants. *Transgenic Res.*
1067 (1996) doi:10.1007/BF01969712.
- 1068 84. Reed, J. *et al.* Phosphomannose isomerase: An efficient selectable marker for plant
1069 transformation. *Vitr. Cell. Dev. Biol. - Plant* (2001) doi:10.1007/s11627-001-0024-z.
- 1070 85. Brunner, S. *et al.* Transgenic Pm3b wheat lines show resistance to powdery mildew in the field.
1071 *Plant Biotechnol. J.* **9**, 897-910 (2011).
- 1072 86. Wright, M. *et al.* Efficient biolistic transformation of maize (*Zea mays* L.) and wheat (*Triticum*
1073 *aestivum* L.) using the phosphomannose isomerase gene, *pmi*, as the selectable marker. *Plant*
1074 *Cell Rep.* (2001) doi:10.1007/s002990100318.
- 1075 87. Bhullar, N. K., Street, K., Mackay, M., Yahiaoui, N. & Keller, B. Unlocking wheat genetic
1076 resources for the molecular identification of previously undescribed functional alleles at the
1077 Pm3 resistance locus. *Proc. Natl. Acad. Sci. U. S. A.* **106**, 9519-9524 (2009).
- 1078 88. Holzberg, S., Brosio, P., Gross, C. & Pogue, G. P. Barley stripe mosaic virus-induced gene
1079 silencing in a monocot plant. *Plant J.* (2002) doi:10.1046/j.1365-313X.2002.01291.x.
- 1080 89. Loutre, C. *et al.* Two different CC-NBS-LRR genes are required for Lr10-mediated leaf rust
1081 resistance in tetraploid and hexaploid wheat. *Plant J.* **60**, 1043-1054 (2009).
- 1082 90. Scofield, S. R., Huang, L., Brandt, A. S. & Gill, B. S. Development of a virus-induced gene-
1083 silencing system for hexaploid wheat and its use in functional analysis of the Lr21-mediated
1084 leaf rust resistance pathway. *Plant Physiol.* (2005) doi:10.1104/pp.105.061861.
- 1085 91. Bhullar, N. K., Street, K., Mackay, M., Yahiaoui, N. & Keller, B. Unlocking wheat genetic
1086 resources for the molecular identification of previously undescribed functional alleles at the
1087 Pm3 resistance locus. *Proc. Natl. Acad. Sci. U. S. A.* (2009) doi:10.1073/pnas.0904152106.
- 1088 92. Xing, L. *et al.* Pm21 from *Haynaldia villosa* Encodes a CC-NBS-LRR Protein Conferring
1089 Powdery Mildew Resistance in Wheat. *Molecular Plant* (2018) doi:10.1016/j.molp.2018.02.013.
- 1090 93. Himmelbach, A. *et al.* A set of modular binary vectors for transformation of cereals. *Plant*
1091 *Physiol.* **145**, 1192-200 (2007).
- 1092 94. Ishizaki, K. *et al.* Development of gateway binary vector series with four different selection
1093 markers for the liverwort *Marchantia polymorpha*. *PLoS One* (2015)
1094 doi:10.1371/journal.pone.0138876.
- 1095 95. Hofgen, R. & Willmitzer, L. Storage of competent cells for *Agrobacterium* transformation.
1096 *Nucleic Acids Res.* **16**, 9877 (1988).

- 1097 96. Voinnet, O., Rivas, S., Mestre, P. & Baulcombe, D. An enhanced transient expression system
1098 in plants based on suppression of gene silencing by the p19 protein of tomato bushy stunt
1099 virus. *Plant J.* (2003) doi:10.1046/j.1365-313X.2003.01676.x.
- 1100 97. Singh, S. P. *et al.* Evolutionary divergence of the rye Pm17 and Pm8 resistance genes reveals
1101 ancient diversity. *Plant Mol. Biol.* **98**, 249-260 (2018).
- 1102 98. Gronnier, J. *et al.* Structural basis for plant plasma membrane protein dynamics and
1103 organization into functional nanodomains. *Elife* (2017) doi:10.7554/eLife.26404.
- 1104 99. Hu, J. *et al.* Abràmoff, M. D., Magalhães, P. J., & Ram, S. J. (2004). Image processing with
1105 ImageJ. *Biophotonics international*, 11(7), 36-42. *Opt. Express* (2011)
1106 doi:10.1201/9781420005615.ax4.
- 1107 100. French, A. P., Mills, S., Swarup, R., Bennett, M. J. & Pridmore, T. P. Colocalization of
1108 fluorescent markers in confocal microscope images of plant cells. *Nat. Protoc.* (2008)
1109 doi:10.1038/nprot.2008.31.
- 1110 101. Vrana, J. *et al.* Flow sorting of mitotic chromosomes in common wheat (*Triticum aestivum* L.).
1111 *Genetics* **156**, 2033-2041 (2000).
- 1112 102. Giorgi, D. *et al.* FISHIS: Fluorescence In Situ Hybridization in Suspension and Chromosome
1113 Flow Sorting Made Easy. *PLoS One* **8**, (2013).
- 1114 103. Kubaláková, M. *et al.* Analysis and sorting of rye (*Secale cereale* L.) chromosomes using flow
1115 cytometry. *Genome* **46**, 893-905 (2003).
- 1116 104. Šimková, H., Čihalíková, J., Vrána, J., Lysák, M. A. & Doležel, J. Preparation of HMW DNA
1117 from plant nuclei and chromosomes isolated from root tips. *Biol. Plant.* (2003)
1118 doi:10.1023/A:1024322001786.
- 1119 105. Martin, M. Cutadapt removes adapter sequences from high-throughput sequencing reads.
1120 *EMBnet.journal* (2011) doi:10.14806/ej.17.1.200.
- 1121 106. Marchler-Bauer, A. *et al.* CDD: A Conserved Domain Database for the functional annotation of
1122 proteins. *Nucleic Acids Res.* (2011) doi:10.1093/nar/gkq1189.
- 1123 107. Krogh, A., Larsson, B., Von Heijne, G. & Sonnhammer, E. L. L. Predicting transmembrane
1124 protein topology with a hidden Markov model: Application to complete genomes. *J. Mol. Biol.*
1125 (2001) doi:10.1006/jmbi.2000.4315.
- 1126 108. Käll, L., Krogh, A. & Sonnhammer, E. L. L. Advantages of combined transmembrane topology
1127 and signal peptide prediction-the Phobius web server. *Nucleic Acids Res.* (2007)
1128 doi:10.1093/nar/gkm256.
- 1129 109. Mascher, M. *et al.* A chromosome conformation capture ordered sequence of the barley
1130 genome. *Nature* (2017) doi:10.1038/nature22043.
- 1131 110. Luo, M. C. *et al.* Genome sequence of the progenitor of the wheat D genome *Aegilops tauschii*.
1132 *Nature* (2017) doi:10.1038/nature24486.
- 1133 111. Ling, H. Q. *et al.* Genome sequence of the progenitor of wheat A subgenome *Triticum urartu*.
1134 *Nature* (2018) doi:10.1038/s41586-018-0108-0.
- 1135 112. Avni, R. *et al.* Wild emmer genome architecture and diversity elucidate wheat evolution and
1136 domestication. *Science (80-.)*. (2017) doi:10.1126/science.aan0032.
- 1137 113. Maccaferri, M. *et al.* Durum wheat genome highlights past domestication signatures and future
1138 improvement targets. *Nat. Genet.* (2019) doi:10.1038/s41588-019-0381-3.
- 1139 114. Ronquist, F. *et al.* Mrbayes 3.2: Efficient bayesian phylogenetic inference and model choice
1140 across a large model space. *Syst. Biol.* (2012) doi:10.1093/sysbio/sys029.
- 1141 115. Cook, D. E., Mesarich, C. H. & Thomma, B. P. H. J. Understanding Plant Immunity as a
1142 Surveillance System to Detect Invasion. *Annu. Rev. Phytopathol.* (2015) doi:10.1146/annurev-
1143 phyto-080614-120114.

- 1144 116. Buchmann, J. P., Matsumoto, T., Stein, N., Keller, B. & Wicker, T. Inter-species sequence
1145 comparison of Brachypodium reveals how transposon activity corrodes genome colinearity.
1146 *Plant J.* (2012) doi:10.1111/j.1365-313X.2012.05007.x.
- 1147 117. Ma, J. & Bennetzen, J. L. Rapid recent growth and divergence of rice nuclear genomes. *Proc.*
1148 *Natl. Acad. Sci. U. S. A.* (2004) doi:10.1073/pnas.0403715101.
- 1149 118. R Development Core Team. *R Development Core Team, R: a language and environment for*
1150 *statistical computing. R: A Language and Environmental for Estatistical Computing* (2020).
- 1151 119. Omasits, U., Ahrens, C. H., Müller, S. & Wollscheid, B. Protter: Interactive protein feature
1152 visualization and integration with experimental proteomic data. *Bioinformatics* (2014)
1153 doi:10.1093/bioinformatics/btt607.
- 1154 120. Kelley, L. A., Mezulis, S., Yates, C. M., Wass, M. N. & Sternberg, M. J. E. The Phyre2 web
1155 portal for protein modeling, prediction and analysis. *Nat. Protoc.* (2015)
1156 doi:10.1038/nprot.2015.053.
- 1157 121. Zeng, F. S. *et al.* Virulence and diversity of *Blumeria graminis* f. sp. *tritici* populations in China.
1158 *J. Integr. Agric.* (2014) doi:10.1016/S2095-3119(13)60669-3.
- 1159 122. Pont, C. *et al.* Tracing the ancestry of modern bread wheats. *Nat. Genet.* **51**, 905-911 (2019).
1160
1161

1162 Figure Legends

1163 **Fig. 1 | Molecular identification and characterization of a *Pm4b* candidate gene.** **a**, host
1164 reactions of Fed-*Pm4a*, Fed-*Pm4b*, Fed-*Pm2* and Fed challenged with *Bgt96224* isolate at 2
1165 and 6 dpi. Left, percentage of pre-penetration resistance arresting conidia growth without
1166 hypersensitive cell-death (HR). Middle, percentage of epidermal cells with haustorium
1167 associated with HR. Right, percentage of established colonies. Different letters indicate
1168 significant differences using ANOVA followed by Tukey honest significant difference (HSD)
1169 test ($P < 0.05$). Scale bar, 50 μ m. **b**, Powdery mildew infection of seedlings from resistant
1170 *Pm4b* wheat cv. Fed-Pm4b, eight EMS-derived susceptible mutants and the susceptible
1171 control Federation. Scale bar, 1 cm **c**, Gene structure and alternative splicing of the *Pm4b*
1172 gene. Exons are indicated as blue boxes. Mutations identified by MutChromSeq are shown
1173 in red. In purple, mutants affected on exons six and seven subjected to expression analysis.
1174 Please note that m256 was subjected to flow-sorting and gene expression analysis. **d**,
1175 Pm4b_V1 and Pm4b_V2 protein isoforms with domains indicated by colours: yellow, serine-
1176 threonine kinase; light-blue, C2; gray, phosphoribosyltransferase C-terminal. Black and
1177 orange vertical lines indicate *pm4a* and *pm4b* EMS-derived mutants, respectively. Each
1178 mutation, letter after amino acid and its position in the wild-type, is only indicated in one of
1179 the two Pm4 isoforms. Asterisks denote early stop codons. Complete information can be
1180 found in Supplementary Table 2. Scale bars: 100 aa. **e**, Transcripts levels of the *Pm4_V1*
1181 and *Pm4_V2* splice variants in mock-inoculated or *Bgt*-inoculated Fed-*Pm4b* plants. Error
1182 bars denoting s.e.m. are based on four biological replicates. Statistical analysis was done
1183 using a two-tailed *t*-test at $p < .05$ (mock vs infected) based on $n = 4$ biological replicates.
1184 Exact *p* values are shown above bars.

1185 **Fig. 2 | Confirmation of the functional identity of the *Pm4b* gene by transgenic**
1186 **complementation and VIGS.** **a**, Schematic diagram of the two constructs with the coding
1187 sequences (CDS) Pm4b_V1CDS and Pm4b_V2CDS, used for transformation of susceptible
1188 Bobwhite S26 (BW). Blue and green bars above the schematic diagrams of constructs

1189 indicate regions targeted for construct-specific PCR amplification using transgene specific
1190 primers displayed in Supplementary Table 7 **b**, Screening of T1 progeny from T1 family
1191 Pm4bV1V2CDS-25. The presence (+) or absence (-) of the *Pm4bV1_CDS* (top row) and
1192 *Pm4bV2_CDS* (lower row) transgenes corresponded to the resistance/susceptibility
1193 phenotype for the individual tested T₁ plants. **c**, Expression levels of *Pm4bV1_CDS* (blue)
1194 and *Pm4bV2_CDS* (turquoise) transgenes in selected T2 progenies compared to the
1195 endogenous *Pm4b_V1* and *Pm4b_V2* transcripts in the wild-type Fed-Pm4b (second bar).
1196 The data points are technical replicates (double quantifications) on single T2 progenies. On
1197 top of each bar, number corresponds to the x-fold expression compared to *Pm4b_V1* or
1198 *Pm4b_V2* in the wild-type Fed-*Pm4b* genotype. Below each T2 progeny, representative
1199 images of disease reactions after infection with the *Pm4alb*-avirulent *Bgt96224* isolate and
1200 with the *Pm4alb*-virulent *BgtJ1W2* isolate are shown. **d**, Schematic diagram of *Pm4b_V1* and
1201 *Pm4b_V2* splicing variants, where blue and green bars indicate regions selected as VIGS
1202 targets. Black bars below the diagrams indicate regions targeted for qRT-PCR amplification
1203 using transcript-specific primers displayed in Supplementary Table 7. Symptoms of the third
1204 and fourth leaves of representative plants subjected to VIGS and after infection with the
1205 *Pm4b*-avirulent *Bgt96224* isolate. **e**. Expression levels of the *Pm4bV1* (light green bars) and
1206 *Pm4bV2* splicing variants (turquoise bars) of BSMV:γ-, BSMV:*Pm4b_V1*- and
1207 BSMV:*Pm4b_V2*-infected Fed-*Pm4b* plants assessed by quantitative reverse-transcription
1208 PCR (qRT-PCR). Statistical analysis was done using a two-tailed *t*-test at *p* < .05 (BSMVγ vs
1209 BSMV:Pm4V1 or BSMV:Pm4V2) based on *n* = 4-8 biological replicates, where black and
1210 grey dots represent the 3rd and 4th leaves, respectively. Error bars, mean ± s.e.m. Exact *P*
1211 values are shown above bars.

1212 **Fig. 3 | The Pm4 protein variants differ in the S_TKc and transmembrane domains** **a**, Pm4
1213 protein isoforms, Pm4_V1 (left) and Pm4_V2 (right), differ in few amino acid changes (red
1214 bars) among the six *Pm4* alleles described. Protein domains are indicated by colours
1215 corresponding to the ones displayed in Fig. 1d. Scale bar, 100 amino acids. **b**, Protein

1216 sequence comparison of the Pm4 variants, where dots represent identical amino acids to
1217 Pm4a. **c**, Topological model of Pm4b_V2 modified from Protter¹¹⁹ displaying the two
1218 transmembrane domains. Below, sequence alignment of the second transmembrane domain
1219 of the Pm4a, b and g protein variants, indicating their start and the endpoints at protein level.
1220 Dots represent identical amino acids compared to Pm4a. **d**, Cartoon model of the core
1221 domain of the Pm4b S_TKc done using the Phyre2¹²⁰ server based on the crystal structure of
1222 human IKK1 (PDB: 5EBZ, Fold library id: c5ebzF) with 25% of identity and 100.0 % of
1223 confidence. In purple, the activation loop, in blue, the catalytic loop and in pink, the DFG
1224 motif. **e**, WebLogo graphical representation of sequence alignment for positions 126, 205
1225 and 208 in Pm4 protein variants compared the kinase-containing resistance proteins
1226 described in Extended Data Fig. 5. Note that x-axis numbers correspond to numbers in the
1227 alignment of Extended Data Fig. 5. In position 121 (126 in Pm4), kinase-containing
1228 resistance proteins mostly have negatively charged amino acids while Pm4g has a Lysine,
1229 positively charged. In position 195 (205 in Pm4), Pm4a is the only one, together with BSK1,
1230 having a positively charged amino acid. Finally, in position 198 (208 in Pm4) mostly occupied
1231 by aliphatic amino acids, Pm4a shows a Tryptophan, which is unique among all the kinases.
1232 These amino acid changes might play a fundamental role in differentiating race-specificity
1233 among Pm4 protein variants. **d**, close-up of the catalytic and activation loops of Pm4b (top)
1234 and Pm4a (bottom) highlighting the occurring amino acid changes.

1235 **Fig. 4 | Pm4_V1 and Pm4_V2 form an ER-associated complex.** **a**, Confocal micrographs
1236 depicting surface views of *N. benthamiana* epidermal cells co-expressing Pm4b_V1-eGFP
1237 with a marker of the cytosol, **b**, Pm4b_V2-eGFP with the marker of the endoplasmic
1238 reticulum and **c**, Pm4b_V2-eGFP with Pm4b_V1-TagRFP. Scale bar of 10 μ m applies to all
1239 images. Localization experiments were repeated five times independently with similar
1240 results. **d**, Identification of potential Pm4b_V1 and Pm4b_V2 homo- and heterodimeric
1241 protein interactions via Co-IP. Pm4b_V2 was tagged N-terminally HA- and Flag-tagged.
1242 Pm4b_V1 was C-terminally with HA- and Flag-tagged. Representative results of HA

1243 pulldown experiments, top panel, where + sign states the presence of the protein. Proteins
1244 were detected using anti-HA and anti-Flag antibodies following SDS-PAGE and membrane
1245 transfer (bottom panel). First and second columns show homomer formations of Pm4b_V2
1246 and Pm4b_V1, respectively and the third column heteromer formation between Pm4b_V2
1247 and Pm4b_V1. Ponceau staining of the Western blot membrane is depicted at the bottom.
1248 Co-immunoprecipitation experiments were repeated three times with similar results. **e**, Split-
1249 luciferase complementation assays showing dimerization of Pm4b_V1 isoform, **f**, Pm4b_V2
1250 isoform and **g**, interaction between Pm4b_V1 and Pm4b_V2 isoforms. At the top of each
1251 panel the tested combination is displayed, specifying if the N- or C-terminal part of LUC was
1252 cloned at the beginning or the end of the protein. For simplicity, V1 and V2 refer to Pm4b_V1
1253 and Pm4b_V2, respectively. The first boxplot corresponds to the positive control, AvrPm3b-
1254 AvrPm3b. Second boxplot corresponds to the combination tested, specified at the top in
1255 each panel, and the last two to the negative controls used: each component of the test
1256 combination with the complementary N-LUC or C-LUC Pm17 tagged. In the boxplots, center
1257 lines show the medians; box limits indicate the 25th and 75th percentiles as determined by
1258 the `geom_boxplot` function of the `ggplot2` R package; whiskers extend 1.5 times the
1259 interquartile range from the 25th and 75th percentiles, individual data points are represented
1260 by dots. Significant differences were determined by Krustal-Wallis test followed by Dunn's
1261 multiple comparisons test with two-sided 95.0% confidence interval with Bonferroni
1262 correction based on $n = 24$ (8 technical and 3 biological replicates). Exact P values are
1263 shown above bars.

1264 **Fig. 5 | Evolutionary origin of Pm4b.** **a**, Model for the evolution of Pm4b. A Kinase domain
1265 (blue) was fused to a fragment of a gene encoding a protein with four C2 domains (yellow).
1266 The product (*Pm4int*) encodes two alternative transcripts and comprises 7 exons.
1267 Subsequent duplication of *Pm4int* led to the rise of *Pm4b* which undergoes re-shuffling of
1268 intron 5, leading to loss of the CDS of one C2 domain and to the introduction of a unique
1269 sequence in exon 6 (red). **b**, Comparison of genomic regions of *Pm4int* (top) and *Pm4b*

1270 (bottom). The two alternative transcripts are depicted on different levels. Sequences that can
1271 be aligned at the DNA level are indicated with shaded areas, with sequence identify shown in
1272 different shades of grey. **c**, Phylogenetic tree of the CDS for the C2 domains. Distant
1273 homologs 7Ag403500 and 6Ag246700 were used to root the tree. Pm4int and Pm4b from
1274 wheat and barley cluster with the descendants of the proposed donor of the C2 domains.

1275 **Fig. 6 | A possible working model of Pm4-mediated resistance. a**, A schematically drawn
1276 wheat epidermal cell attacked by a mature powdery mildew germling. An early release of
1277 small amounts of effectors at around 12 hours translates ① into induction of Pm4b-
1278 dependent pre-haustorial resistance ②. Later, when large amounts of effectors are present
1279 ③, the recognition of AvrPm4 (light blue) by Pm4b protein complex will lead to Pm4b-
1280 mediated hypersensitive response (HR) ④. ER, endoplasmic reticulum. **b**, Schematic model
1281 of a possible activation mechanism of Pm4 upon a hypothetical AvrPm4 recognition. In the
1282 absence of the AvrPm4, Pm4_V1 and Pm4_V2 are in a resting state, forming a
1283 heterocomplex interacting via C2 domains. This heterocomplex is anchored into the
1284 membrane of the ER and it is inactive (yellow star in the S_TKc domains). Upon AvrPm4
1285 recognition by the C2C/D or the kinase domains the heterocomplex undergoes
1286 conformational changes, leading to activation of the kinase activity (red star in the S_TKc
1287 domains) and disease resistance. Numbers indicate the sequence of steps of the proposed
1288 model.

1289

1290 **Extended Data Fig. 1 | *Pm4a* and *Pm4b* convey resistance to a wide range of *Bgt* isolates. a,**
1291 Disease reactions of Fed-*Pm4a* and Fed-*Pm4b* NILs to 108 genetically diverse
1292 contemporary *Bgt* isolates^{73,74,121}. **b,** Selection of *Bgt* isolates for which Fed-*Pm4a* and Fed-
1293 *Pm4b* NILs showed a differential resistance/susceptibility pattern. The outer and inner circle
1294 represent the reaction pattern of Fed-*Pm4a* and Fed-*Pm4b*, respectively. Disease reaction
1295 was evaluated seven days post-inoculation. Five classes of host reactions were
1296 distinguished: R = resistance (0-10% of leaf area covered), IR (10-25% of leaf area covered),
1297 I (25-50% of leaf area covered), IS (50-75 % of leaf area covered) and S (>75% of leaf area
1298 covered). CHN: China, ISR: Israel; CHE; Switzerland; FRA: France; USA: United States;
1299 GRB: Great Britain; JPN; Japan.

1300 **Extended Data Fig. 2 Expression profiling of *Pm4b* mutants following infection with**
1301 ***Bgt96224*.** Transcripts levels of the *Pm4_V1* and *Pm4_V2* splice variants in mock-inoculated
1302 or *Bgt*-inoculated Fed-*Pm4b* plants. Statistical analysis was done using a two-tailed *t*-test at
1303 $p < .05$ (mock vs infected) based on $n = 4$ biological replicates. Error bars, mean \pm s.e.m.
1304 Exact *P* values are shown above bars

1305 **Extended Data Fig. 3 Agronomically-related traits of selected T₂ transgenic families**
1306 **overexpressing *Pm4b_V1CDS* and *Pm4b_V2CDS* transgenes. a,** Plant growth of
1307 representative T₂ transgenics from families T2#52-1.4 and T2#52-3.11 compared to
1308 Bobwhite S26 in the following order: Bobwhite S26, T2#52-1.4_1.10, T2#52-1.4_1.9, T2#52-
1309 3.11_1.2 and T2#52-3.11_1.3 **b,** Plant height of the T₂ families overexpressing
1310 *Pm4b_V1CDS* and *Pm4b_V2CDS* transgenes presented in Fig 3c and Supplementary Table
1311 3. Names are indicated in the x-axis. **c,** Thousand Grain Weight for the same T₂ families.
1312 Selected representative of the same T₂ family are displayed with the same color: T2#3 in
1313 cyan, T2#25 lime green and T2#52 in magenta. In the boxplots, center lines show the
1314 medians; box limits indicate the 25th and 75th percentiles as determined by the
1315 `geom_boxplot` function of the `ggplot2` R package; whiskers extend 1.5 times the interquartile
1316 range from the 25th and 75th percentiles, individual data points are represented by dots. On

1317 top of each boxplot, p values based on two-tailed *t*-test at $p < .05$ (transformants versus
1318 Bobwhite S26). Above p values, n = the number of T2 progeny.

1319 **Extended Data Fig. 4 Gene expression in transgenic wheat plants overexpressing single**
1320 **splice variants of the *Pm4b* gene. a,** Expression levels of *Pm4bV1_CDS* transgenes in
1321 selected T1 progeny for three independent transgenic events (T1#9, T1#12, T1#12)
1322 overexpressing full-length cDNA of *Pm4b_V1* compared to the endogenous *Pm4b_V1*
1323 transcripts in the wild-type Fed-*Pm4b* (second bar). **b,** Expression levels of *Pm4bV2_CDS*
1324 transgenes in selected T1 progeny for three independent transgenic events (T1#6, T1#24,
1325 T1#29) overexpressing full-length cDNA of *Pm4b_V2* compared to the endogenous
1326 *Pm4b_V2* transcripts in the wild-type Fed-*Pm4b* (second bar). For a and b, data points are
1327 technical replicates (triple quantifications) on single T1 progenies. Error bars, mean \pm s.e.m.
1328 of three technical replicates. On top of each bar, the number corresponds to the x-fold
1329 expression compared to *Pm4b_V1* or *Pm4b_V2* in the wild-type Fed-*Pm4* genotype. Below
1330 each T1 progeny, representative images of disease reactions after infection with the
1331 *Pm4alb*-avirulent *Bgt96224* and *Bgt94202* isolates are shown.

1332 **Extended Data Fig. 5 | Predicted Pm4 kinase catalytic domain.** A multiple amino acid
1333 sequence alignment of 38 protein kinase catalytic domains involved in disease resistance
1334 was used to infer the Pm4b kinase domain architecture. In Pm4b (indicated with a red
1335 rectangle) all the 14 key conserved residues of protein kinases are present. In the alignment,
1336 red arrowheads mark invariant residues (G⁵², K⁷², E⁹¹, D¹⁶⁶, N¹⁷¹, D¹⁸⁴, G¹⁸⁶, E²⁰⁸, R²⁸⁰), which
1337 are numbered with upper case numbers corresponding to their position in the α form of the
1338 cAMP-dependent protein kinase catalytic unit (cAPK). Likewise, black arrowheads indicate
1339 the mostly invariant residues (G⁵⁰, V⁵⁷, F¹⁸⁵, D²²⁰, G²²⁵). Based on the presence of a L residue
1340 at position R¹⁶⁵ of cAPK in subdomain VI, Pm4 Kinase was classified as a non-RD kinase.
1341 Moreover, conserved residues in subdomain VI (D¹⁶⁶ -> N¹⁷¹, DLKPAN in Pm4b vs.
1342 DLPKPEN in cAPK) and VIII (GTMGYLAPE in Pm4b vs. GT/SXXY/FXAPE in cAPK) indicate
1343 that the Pm4 kinase domain is a serine/threonine protein kinase.

1344 Labels: red and black arrowheads, key invariant and nearly invariant residues in the protein
1345 kinase catalytic domains, respectively. Light blue diamond points to the RD or non-RD
1346 kinase determination site. Black asterisks, substrate binding site. Green arrowheads, ATP
1347 binding site. Core conserved, diagnostic regions of subdomains I, II, VI, and VIII are
1348 highlighted by grey bars labelled with Roman numerals. On top of the wrapped alignment,
1349 EMS mutagenized line designations affecting the Pm4 kin domain in *Pm4a* or *Pm4b* genes
1350 and corresponding amino acid changes are indicated. Violet squares indicate polymorphic
1351 amino acids within the kinase domain among the Pm4 allelic variants described in this study.
1352 Numbers above violet squares indicate the position on the alignment based on the cAPK
1353 sequence.

1354 **Extended Data Fig. 6 | Sequence alignment of Pm4 C2 domains with homologous C2**
1355 **domains of Arabidopsis MCTPs. a**, sequence alignment of Pm4b-C2C with C2C domains
1356 from Arabidopsis MCTPs. **b**, likewise alignment of C2D domains. C2 domains were delimited
1357 based on Conserved Domain Database (CDD) from NCBI¹⁰⁶. The location of the domain is
1358 indicated by the sequence range numbers. C2 domains in Pm4 (black background) are
1359 indicated with a red rectangle. **c**, Phylogenic tree of C2C and C2D domains of Arabidopsis
1360 MCTPs and Pm4b-C2C/C2D domains. The human DySF dysferlin C2C/D domains was used
1361 as outgroup.

1362 **Extended Data Fig. 7 | Determination of aspartate residues predicted to be involved in Ca²⁺-**
1363 **binding in Pm4b C2 domains. a**, Sequence alignment of Pm4b-C2C and Pm4b-C2D domains
1364 with C2 domains previously described to bind Ca²⁺. UniProt entry names followed by the
1365 specific C2 domain displayed are located on the left. The region of the C2 domain displayed
1366 is indicated by the sequence range numbers. Conserved aspartate residues involved in
1367 Ca²⁺-binding are highlighted in pink. Pm4b_C2C (fourth row from the bottom) does not have
1368 conserved aspartate residues and exhibits diverse amino acid substitutions, including D -> E,
1369 A or I. However, Pm4b_CD2 (third row from the bottom) has three conserved aspartate
1370 residues (positions I, III and IV) and two conservative substitutions, asparagine (position II)

1371 and glutamine (position V), both polar and relatively small amino acids. Interestingly,
1372 Pm4_C2D contains an insertion of eight amino acids (green) just before the predicted Ca^{2+}
1373 binding region 3 that shifts the position of the conserved aspartate residues at position III and
1374 IV (highlighted in red) (see Extended Data Fig. 6). Rectangles denote calcium-binding
1375 regions (CBR) 1 and 3, respectively. **b**, Structured-based alignment of C2D Pm4b_V2
1376 (turquoise) and the C2 domain from PKC α (pink) (Protein kinase C alpha type, PDB: 1DSY).
1377 The predicted structural model of the Pm4bC2 domain was done using the Phyre2 server on
1378 the basis of the crystal structure of rat otoferlin c2a (PDB: 3L9B, Fold library id: c3l9bA) with
1379 14% of identity and 99.9% of confidence. **c**, On top, calcium binding regions (CBR) CBR1
1380 and 3 of PKC α . In the middle, CBR1 and 3 of Pm4b_C2D domain. On the bottom part,
1381 overall alignment of CBRs 1 and 3 of Pm4b_C2D domain (turquoise) and PKC α (dark blue).
1382 **d**, Three-dimensional structure of C2D domain of Pm4b using the Phyre2¹²⁰ server based on
1383 the crystal structure of rat otoferlin c2a (PDB: 3L9B, Fold library id: c3l9bA) with 14% of
1384 identity and 99.9 % of confidence highlighting in blue CBR 1 and 3, with predicted residues
1385 involved in Ca^{2+} -binding labelled. Calcium ions are shown as grey balls.

1386 **Extended Data Fig. 8 | Negative controls for the Pm4b interaction.** **a**, Pm4b_V1 does not
1387 interact with the ER-marker ER_ck_CD3_953³⁹. **b**, Pull-down with anti-HA beads is specific
1388 for the presence of HA-tagged Pm4b variants. Co-immunoprecipitation experiments were
1389 repeated two times with similar results.

1390 **Extended Data Fig. 9 | Binding ability of Pm4b variants for homo- and heteromeric**
1391 **interactions.** **a**, Split-LUC combinations showing luciferase signal for Pm4b_V1 homomeric
1392 interaction in Fig. 4e were co-infiltrated with fluorescence-tagged Pm4b_V2 protein variants.
1393 **b**, Split-LUC combinations showing luciferase signal for Pm4b_V2 homomeric interaction in
1394 Fig. 4f were co-infiltrated with fluorescence-tagged Pm4b_V1 protein variants. The data are
1395 displayed following the same logic as presented in Figure 4: in each of the 18 panels, the
1396 first boxplot corresponds to the positive control, AvrPm3b_N-LUC & AvrPm3b_C_LUC. The
1397 second boxplot (orange color) corresponds to the tested combination, displayed at the top of

1398 each panel. For simplicity, V1 and V2 refer to Pm4b_V1 and Pm4b_V2, respectively. Finally,
1399 the last two boxplots in each panel correspond to the negative controls co-infiltrated.
1400 Significant differences were determined by Krustal-Wallis test followed by Dunn's multiple
1401 comparisons test with two-sided 95.0% confidence interval with Bonferroni correction based
1402 on $n = 24$ (8 technical and 3 biological replicates). Exact P values are shown above bars. In
1403 the boxplots, center lines show the medians; box limits indicate the 25th and 75th percentiles
1404 as determined by the `geom_boxplot` function of the `ggplot2` R package; whiskers extend 1.5
1405 times the interquartile range from the 25th and 75th percentiles, individual data points are
1406 represented by dots.

1407 **Extended Data Fig. 10 | Bivariate flow karyotype GAA-FITC vs. DAPI obtained after the**
1408 **analysis of chromosomes isolated from mutant *pm4b_m256*.** The population representing
1409 chromosome 2A, which was flow-sorted, is highlighted in orange. Inset: Flow-sorted
1410 chromosomes were identified microscopically after FISH with probes for GAA microsatellites
1411 (green) and Afa repeat (red). The fluorescent labeling pattern allowed chromosome
1412 identification and estimation of the contamination of sorted fractions by other chromosomes.
1413 Chromosomes were counterstained by DAPI (blue).

1414 **Supplementary Fig. 71 | Phylogenetic analysis of core kinase domains of described**
1415 **resistance proteins and Pm4b.** The phylogenetic tree is based on the core kinase domains
1416 delimited based on Conserved Domain Database (CDD) from NCBI¹⁰⁶. The location of the
1417 domain is indicated by the sequence range numbers. In red, the core kinase domain of
1418 Pm4b. cAPK-alpha was used as outgroup.

1419 **Supplementary Fig. 92 | Pm4b-C2C/C2D domain analysis for lysine-rich clusters involved in**
1420 **interaction with phosphoinositides. a,** Sequence-based alignment of Pm4b C2C and C2D
1421 domains (first two rows) with C2 domains reported to bind phosphoinositides, for example,
1422 the C2 domain of PKC α (1DSY). Protein identification and PDB codes are located on the left.
1423 Conserved residues that form the lysine-rich cluster (YxKx_{n1}KxKx_{n2}W(Y/L/C)x_{n3}N) are
1424 depicted as white letters on dark blue background. Yellow letters in C2C and C2D domains

1425 correspond to homologues residues compared to the classical lysine-rich cluster. Pm4 C2D
1426 domain exhibits diverse amino acid substitutions, including K -> V or T disrupting the
1427 presence of conserved positive charged and aromatic residues present characteristic of the
1428 lysine-rich cluster. However, in Pm4 C2C domain, although lacking the characteristic
1429 positively charged (K) and aromatic (Y, W) amino acids present in typical lysine-rich clusters,
1430 there are substitutions by amino acids with similar physicochemical properties. In the third
1431 position, instead of a Lysine, there is an Arginine, another positively charged polar amino
1432 acid. In the fifth position, tryptophan is substituted by another nonpolar amino acid, Valine.
1433 Finally, in position sixth, Asparagine is substitute by glutamic acid, another polar and
1434 relatively small amino acid. **b**, Alignment of the terminal part of Arabidopsis MCTPs and
1435 Pm4b_V2, underlined on purple. Transmembrane domains are depicted as red squares. The
1436 characteristic duplication present in Pm4b_V2 is indicated in blue. The protein region
1437 displayed is indicated by the sequence range numbers.

1438 **Supplementary Fig. 103 | Co-localization analysis of Pm4b_V1 and Pm4b_V2 with**
1439 **characterized markers.** Pm4b_V1 and Pm4b_V2 isoforms were co-infiltrated with the plasma
1440 membrane-marker (35S:REM 1.2 m_RFP⁴⁰), the mRFP-fused cytosolic localization
1441 sequence (pGWB455³⁸) and the ER-marker (ER-ck, CD3-959³⁹) to examine their subcellular
1442 localization. Pm4b_V1 mainly co-localizes with the cytosolic marker while Pm4b_V2 with the
1443 ER marker. High Pearson correlation coefficients of Pm4b_V1 and Pm4b_V2 indicate their
1444 co-localization when co-expressed. On top of each boxplot, number of observations and
1445 means. Different letters indicate significant differences using ANOVA followed by Tukey
1446 honest significant difference (HSD) test ($P < 0.05$). At least $n = 10$ single-scanned cell images
1447 per experiment were collected and analyzed using the same conditions of laser intensity,
1448 pinhole size, and gain levels. In the boxplots, center lines show the medians; box limits
1449 indicate the 25th and 75th percentiles as determined by the geom_boxplot function of the
1450 ggplot2 R package; whiskers extend 1.5 times the interquartile range from the 25th and 75th
1451 percentiles, individual data points are represented by dots.

1452 **Supplementary Fig. 4 | Phylogenetic analysis of Pm4 homologues.** The tree on the top
1453 corresponds to full-length predicted proteins based on Pm4b_V1 isoform. Likewise, isoform
1454 Pm4_V2 is displayed in the bottom. In red, Pm4b_V1/V2. For both cases, the kinase domain
1455 of the rice Os04g30030 was used as outgroup.

1456 **Supplementary Fig. 5 | Sequence comparison of the contig_18057 in wheat cultivars Fed-**
1457 ***Pm4b* and SYMattis.** Dotplot alignment of the *Pm4* contig_18057 from Fed-*Pm4b* (horizontal)
1458 and SYMattis (vertical). On top of the dotplot, it is displayed a schematic drawing of the Pm4
1459 CDS. The first blue box corresponds to exons one to five. The second and third blue boxes,
1460 to exons six and seven, respectively. SYMattis contained the *Pm4* contig_18057 sequence
1461 spanning physical positions 788'726'801-788'747'264, at the very distal end of chromosome
1462 arm 2AL. Around 27 bp downstream of the stop codon of *Pm4b_V2* lies a novel TE of the
1463 Mutator superfamily ([https://www.botinst.uzh.ch/en/research/genetics/thomasWicker/trep-](https://www.botinst.uzh.ch/en/research/genetics/thomasWicker/trep-db.html)
1464 [db.html](https://www.botinst.uzh.ch/en/research/genetics/thomasWicker/trep-db.html)). Since this TE lies so close to the gene, it provides downstream regulatory
1465 sequences to *Pm4*. For example, two putative poly-adenylation signals are located inside
1466 this TE.

1467

1468 **Supplementary Fig. 16 | Pm4a and Pm4b coding sequences.** GenBank submission of
1469 genomic DNA, noncontiguous genomic sequences, with internal introns removed for
1470 Pm4b_V1 (NCBI GenBank accession number MT783929) and Pm4b_V2 (NCBI GenBank
1471 accession number MT783930).

1472 **Supplementary Table 1 | List of *Bgt* isolates used to characterize the resistance spectra of**
1473 ***Pm4a* and *Pm4b*.** The first column corresponds to the name of the *Bgt* isolate, followed by
1474 the geographic origin and collection site (if available) and the source. The last two columns
1475 show the disease reactions of Fed-*Pm4a* and Fed-*Pm4b* NILs distinguishing five classes of
1476 host reactions R = resistance (0-10% of leaf area covered), IR (10-25% of leaf area
1477 covered), I (25-50% of leaf area covered), IS (50-75 % of leaf area covered) and S (>75% of

1478 leaf area covered. Infection test is based on four biological replicates. CHN: China, ISR:
1479 Israel; CHE; Switzerland; FRA: France; USA: United States; GRB: Great Britain; JPN; Japan.

1480 **Supplementary Table 2 | List of EMS-induced *Pm4a* and *Pm4b* mutants used in this study.**

1481 The given name of each mutant (first column) is followed by the donor line, Fed-*Pm4a* or
1482 Fed-*Pm4b*, where the EMS treatment was performed. In the column Mutation, the first letter
1483 indicates the amino acid in the wild-type followed by the position and the amino acid change
1484 in the corresponding mutant. Last column denotes the predicted domain based delimited
1485 based on Conserved Domain Database (CDD) from NCBI¹⁰⁶, where S_TKc (cl21453)
1486 corresponds to the serine/threonine kinase domain, C2C and C2D (cl14603) to C2 domain
1487 third and fourth repeat found in Multiple C2 domain and Transmembrane regions Proteins
1488 (MCTP). Finally, PRT_C (pfam08372) denotes the plant phosphoribosyltransferase C-
1489 terminal domain.

1490 **Supplementary Table 3 | Disease reactions of selected T2 families challenged with selected**

1491 ***Bgt* isolates.** The first column displays the name of each progeny. Second and third column
1492 indicates the presence (+) or absence (-) of the transgenes *Pm4b_V1CDS*- and
1493 *Pm4b_V2CDS* (See Methods). The remaining columns show the disease reaction of each T2
1494 line challenged with two *Pm4a/b*-avirulent (*Bgt96224* and *Bgt94202*) and two *Pm4a/b*-
1495 virulent (*BgtJIW2* and *Bgt97251*) isolates. Top four rows show the disease reactions of the
1496 *Pm4a* NIL Fed-*Pm4a* and the *Pm4b* NIL Fed-*Pm4b* genotypes, Bobwhite S26, the
1497 susceptible background where transgenic complementation assays were performed, and
1498 Kanzler, a highly susceptible cultivar to *Bgt*. Five classes of host reactions were considered.
1499 R = resistance (0-10% of leaf area covered), IR (10-25% of leaf area covered), I (25-50% of
1500 leaf area covered), IS (50-75 % of leaf area covered) and S (>75% of leaf area covered).
1501 Evaluation was done 7-9 dpi based on four biological replicates.

1502

1503 **Supplementary Table 4 | Disease reactions of selected T1 transgenic lines overexpressing**

1504 ***Pm4b_V1* or *Pm4b_V2* challenged with selected *Bgt* isolates.** The first column displays the

1505 name of each progeny. Second column displays the Pm4b splicing variant transformed:
1506 either Pm4b_V1CDS or Pm4b_V2CDS. The third column, named detection, indicates the
1507 presence (+) or absence (-) of the corresponding transgenes: *Pm4b_V1CDS* or
1508 *Pm4b_V2CDS*. The remaining columns show the disease reaction of each T1 transgenic line
1509 challenged with two *Pm4a/b*-avirulent (*Bgt96224* and *Bgt94202*) and one *Pm4a/b*-virulent
1510 (*BgtJlW2*). Top four rows show the disease reactions of the Fed-*Pm4a*, Fed-*Pm4b*, Bobwhite
1511 S26, the susceptible background where transgenic complementation assays were
1512 performed, and Kanzler, a highly susceptible cultivar to *Bgt*. Five classes of host reactions
1513 were considered. R = resistance (0-10% of leaf area covered), IR (10-25% of leaf area
1514 covered), I (25-50% of leaf area covered), IS (50-75 % of leaf area covered) and S (>75% of
1515 leaf area covered).

1516 **Supplementary Table 5 | Disease reactions of wheat cultivars carrying the Pm4 locus**
1517 **challenged with selected *Bgt* isolates.** In the first column, WW refers to Whealbi Wheat lines
1518 from Pont et al¹²². Detailed passport information is available at
1519 [https://urgi.versailles.inra.fr/download/iwgsc/IWGSC_RefSeq_Annotations/v1.0/iwgsc_refseq](https://urgi.versailles.inra.fr/download/iwgsc/IWGSC_RefSeq_Annotations/v1.0/iwgsc_refseq_v1.0_Whealbi_GWAS.zip)
1520 [v1.0_Whealbi_GWAS.zip](https://urgi.versailles.inra.fr/download/iwgsc/IWGSC_RefSeq_Annotations/v1.0/iwgsc_refseq_v1.0_Whealbi_GWAS.zip). Second column specifies the Pm4 allele. From third column on,
1521 disease reaction of each wheat line to selected *Bgt* isolates, where letters refer to the five
1522 host reactions: R = resistance (0-10% of leaf area covered), IR (10-25% of leaf area
1523 covered), I (25-50% of leaf area covered), IS (50-75 % of leaf area covered) and S (>75% of
1524 leaf area covered. Infection test is based on four biological replicates. Note that disease
1525 reactions of the *Pm4a* NIL Fed-*Pm4a* and the *Pm4b* NIL Fed-*Pm4b* genotypes are included
1526 in the top to facilitate the comparison of resistance spectra among Pm4 alleles. In general,
1527 *Pm4b*-, *Pm4d*- and *Pm4h*-containing lines exhibit a very similar pattern compared to *Pm4a*
1528 NIL Fed-*Pm4a* and the *Pm4b* NIL Fed-*Pm4b*, for example susceptible to *BgtJlW2* and
1529 *Bgt97251* but resistant to *Bgt96224*, *Bgt94202*, *Bgt97223* and *Bgt97266*.

1530

1531 **Supplementary Table 6 | List of *Pm4* homologues found in different species within the**
1532 **Triticeae tribe.** The first column displays the given name used in Supplementary Fig. 84. If
1533 annotated in the corresponding reference assembly (last column), the real name of each
1534 *Pm4* homologue is given in the second column. Third column specifies the species where is
1535 found the *Pm4* homologue, followed by the chromosome and its length and the hit positions
1536 corresponding to the beginning and end of the gene. chr: chromosome. Note that if a
1537 homologue does not have assigned a chromosome is due to the fact that that homologue
1538 was located in the “*unknown*” (Un) chromosome. If this was the case, the given name
1539 includes “Un”.

1540 **Supplementary Table 7 | Primers used in this study.**

1541 **Supplementary Table 8 | Target-specific amplification efficiencies of the splicing variants**
1542 ***Pm4b_V1* and *Pm4b_V2* and the reference genes used in this study.**

1543

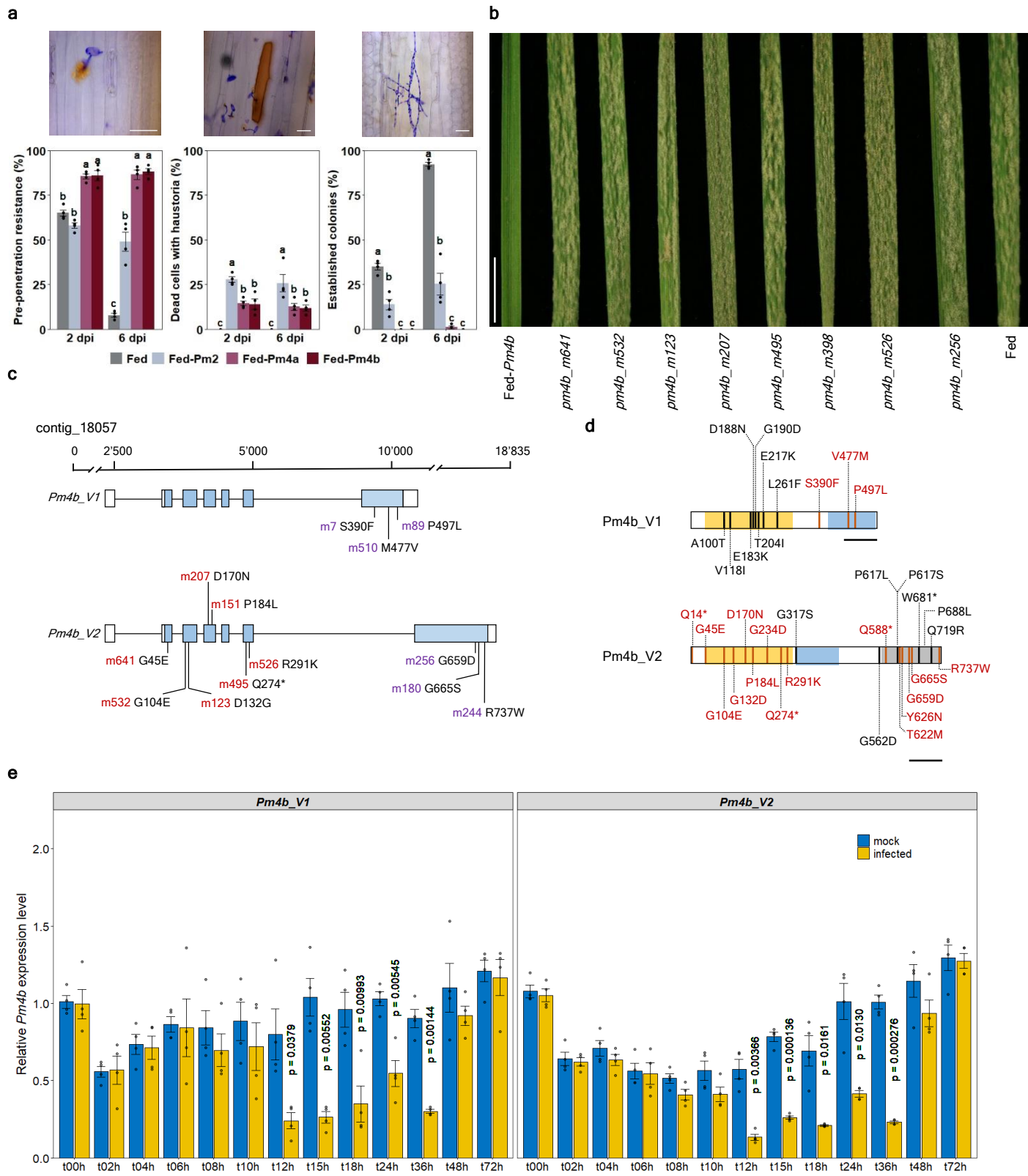


Fig. 1

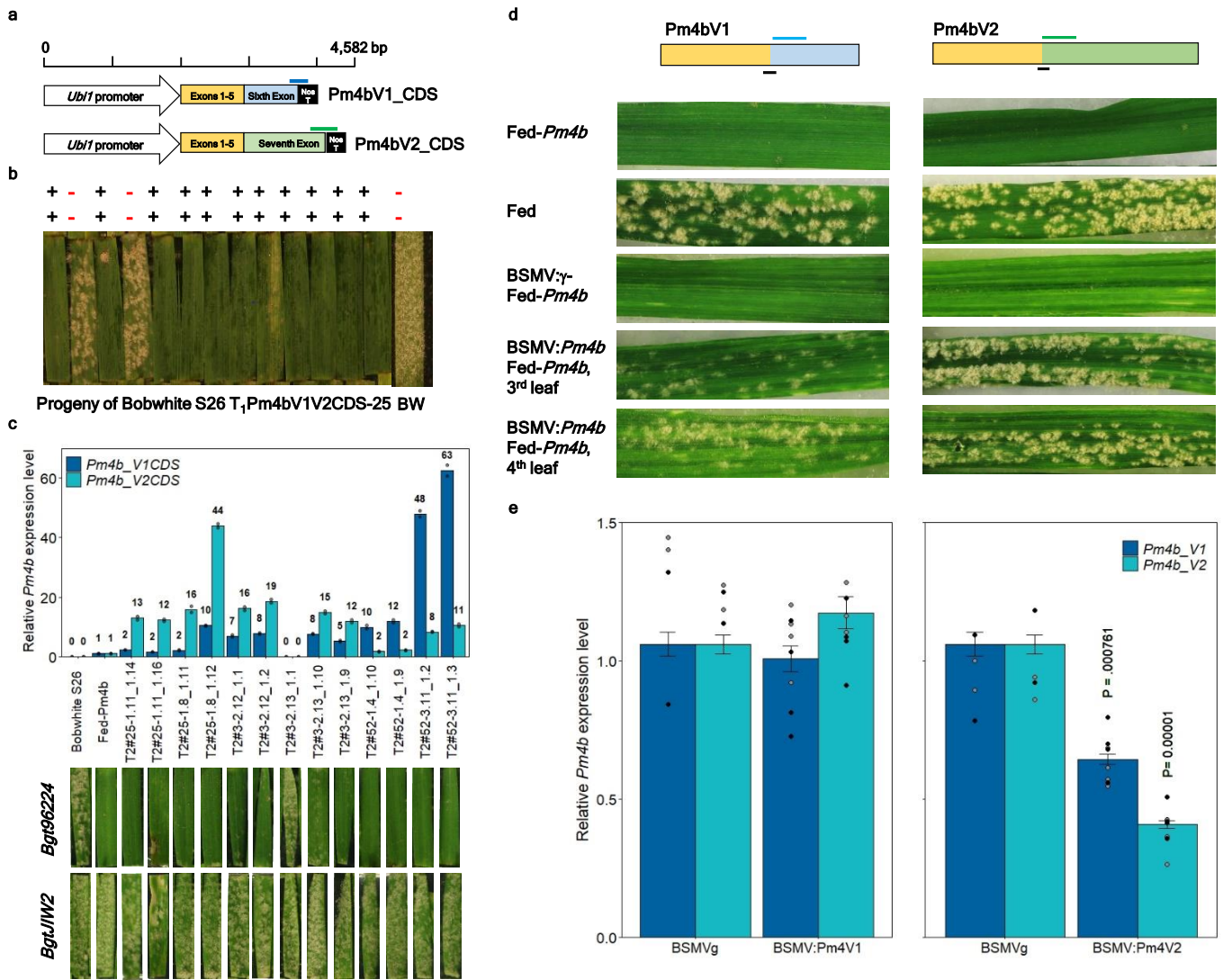


Fig. 2

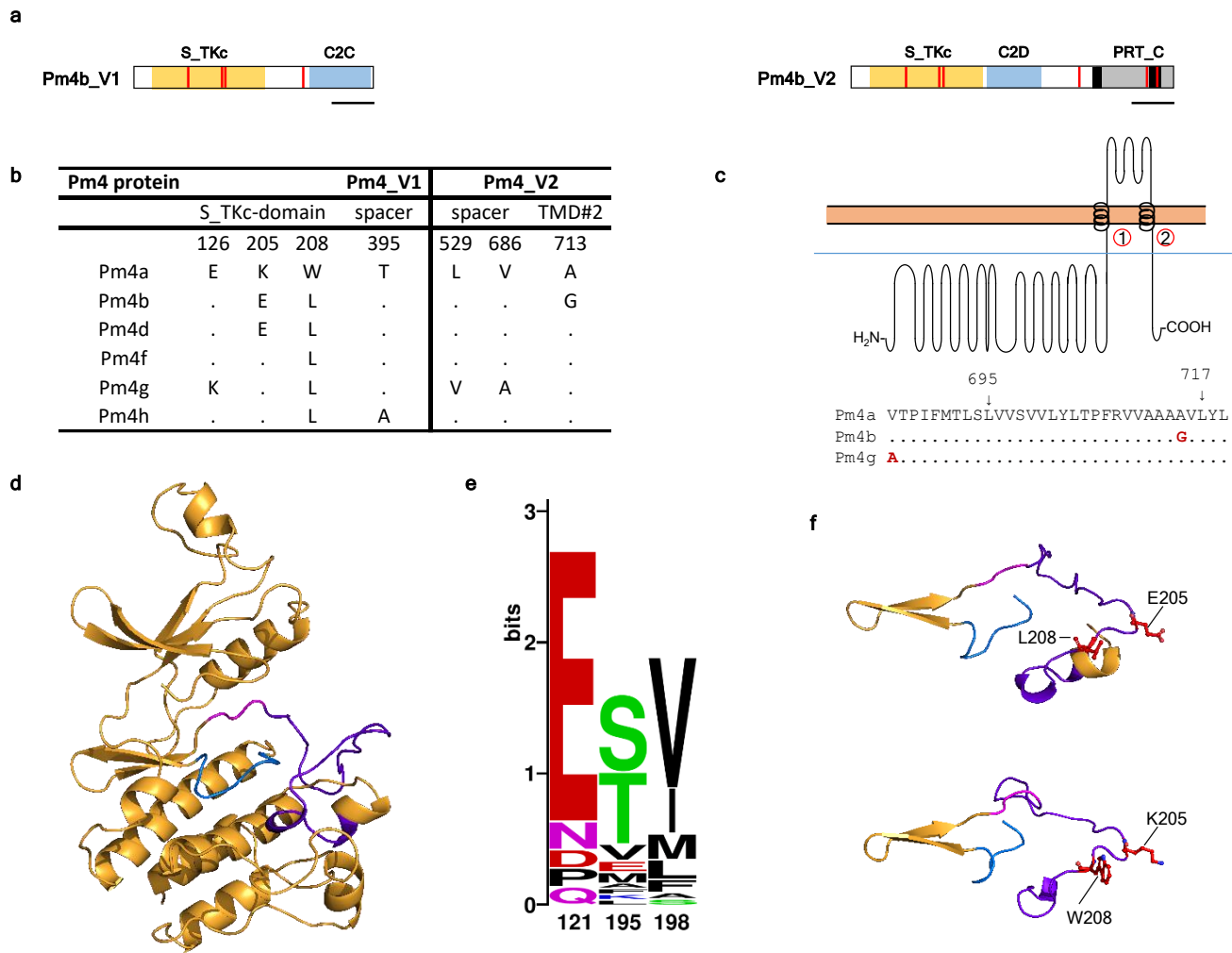


Fig. 3

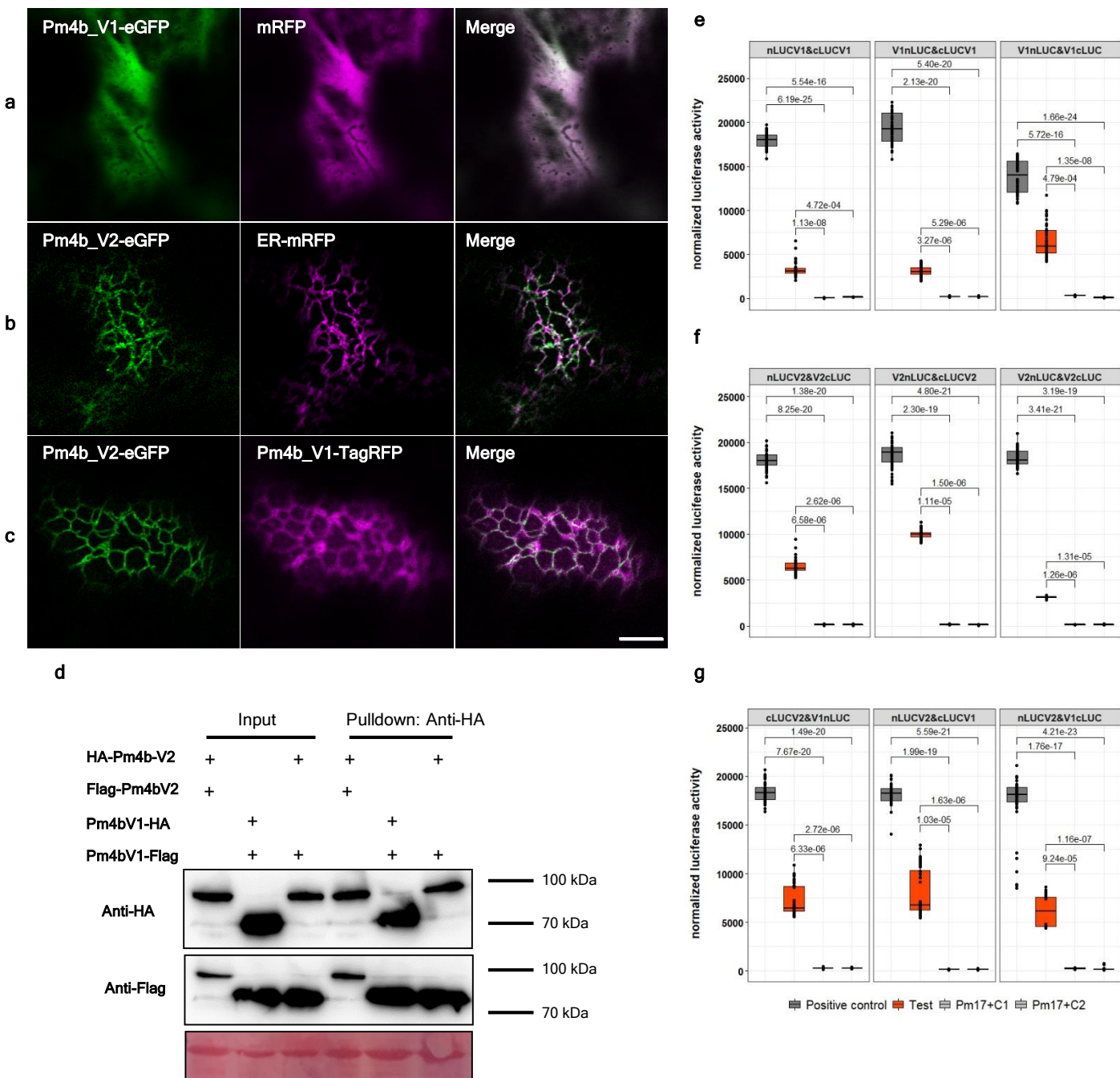


Fig. 4

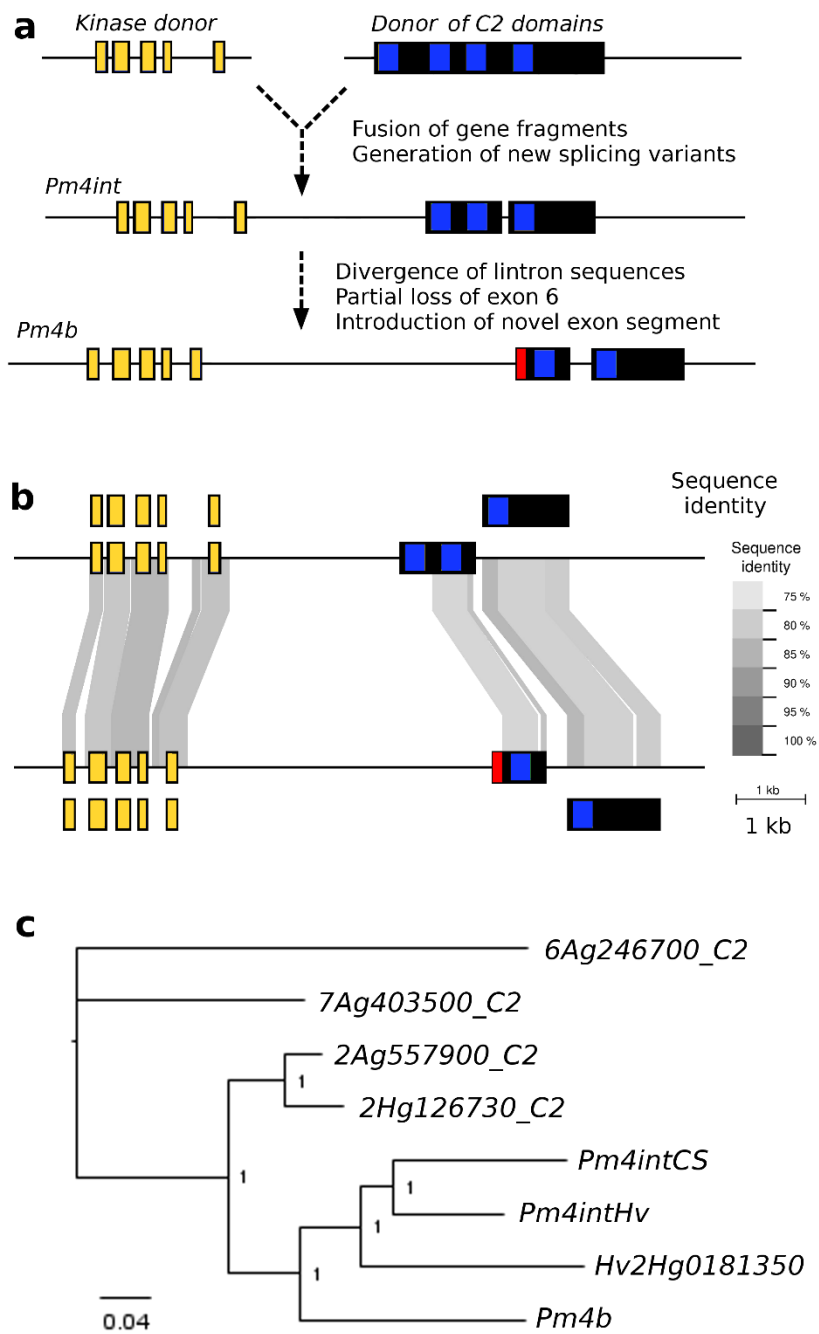
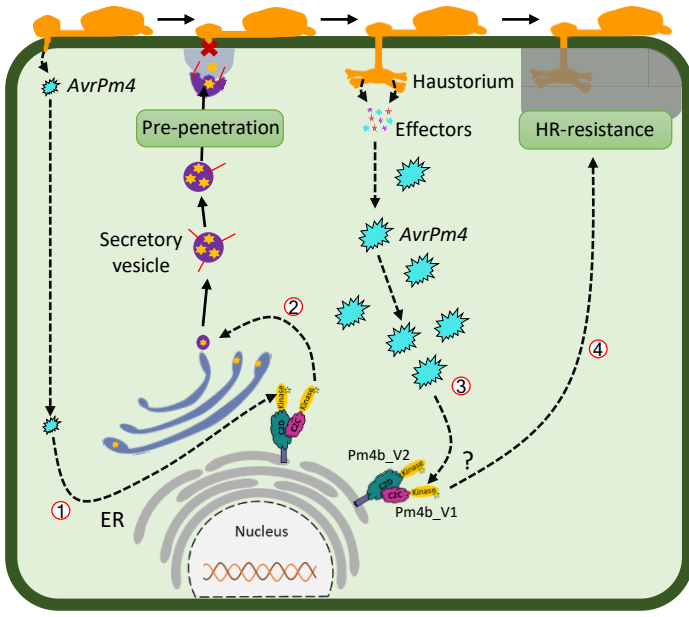


Fig. 5

a



b

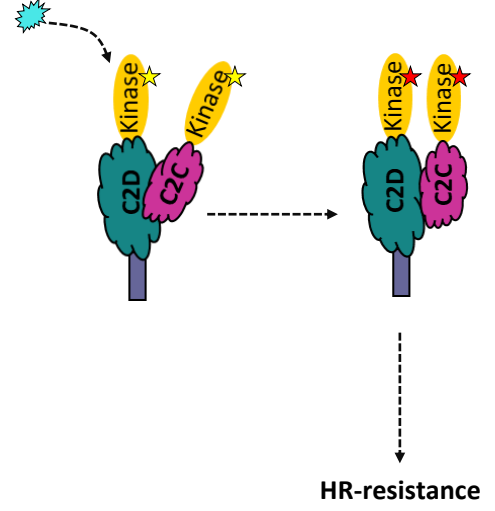
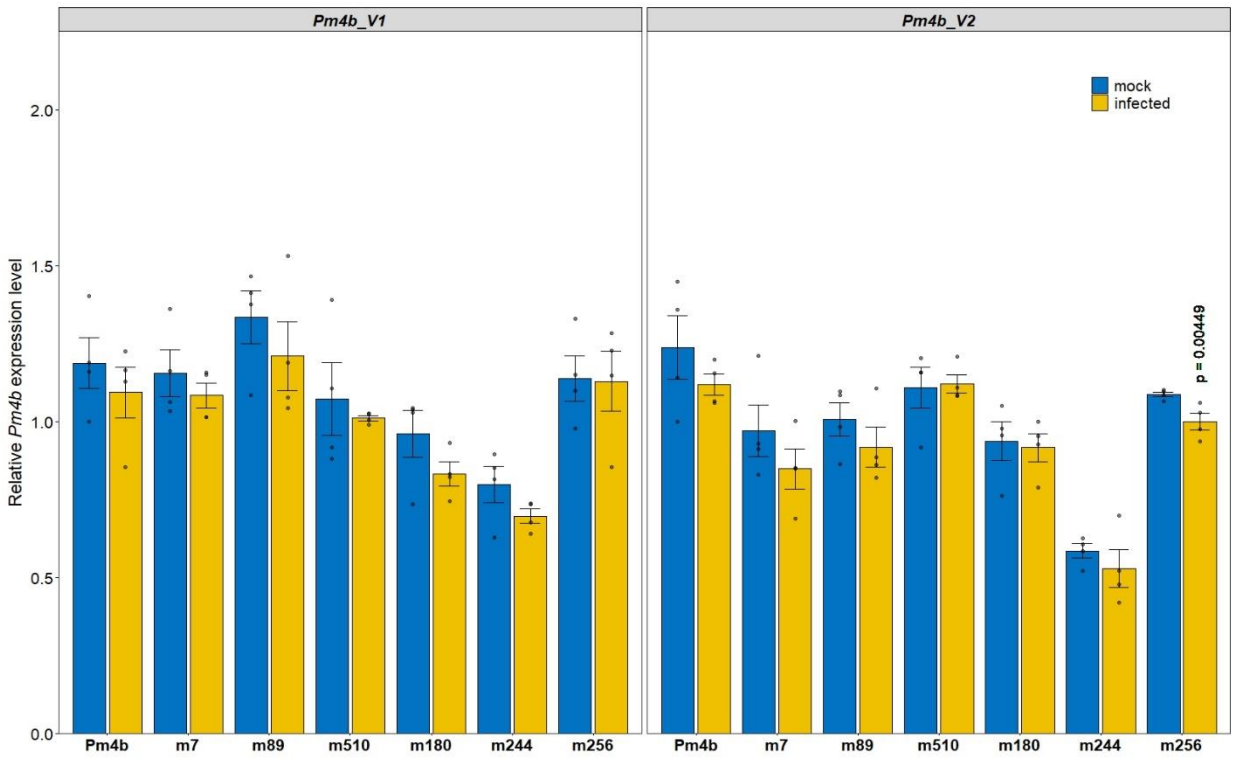
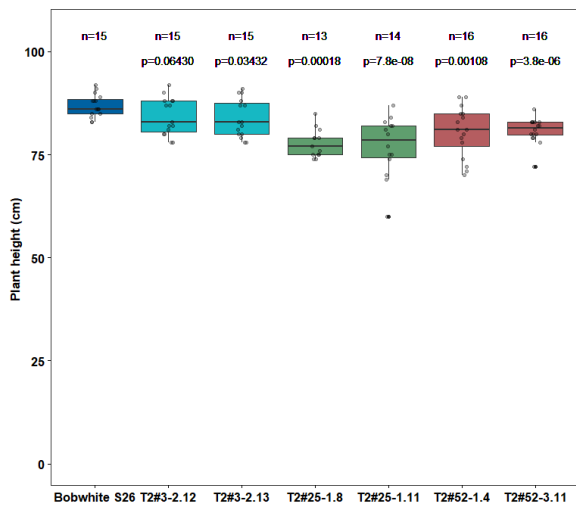
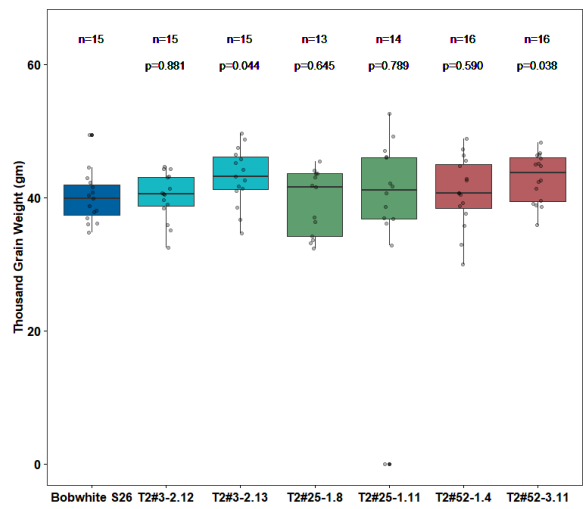


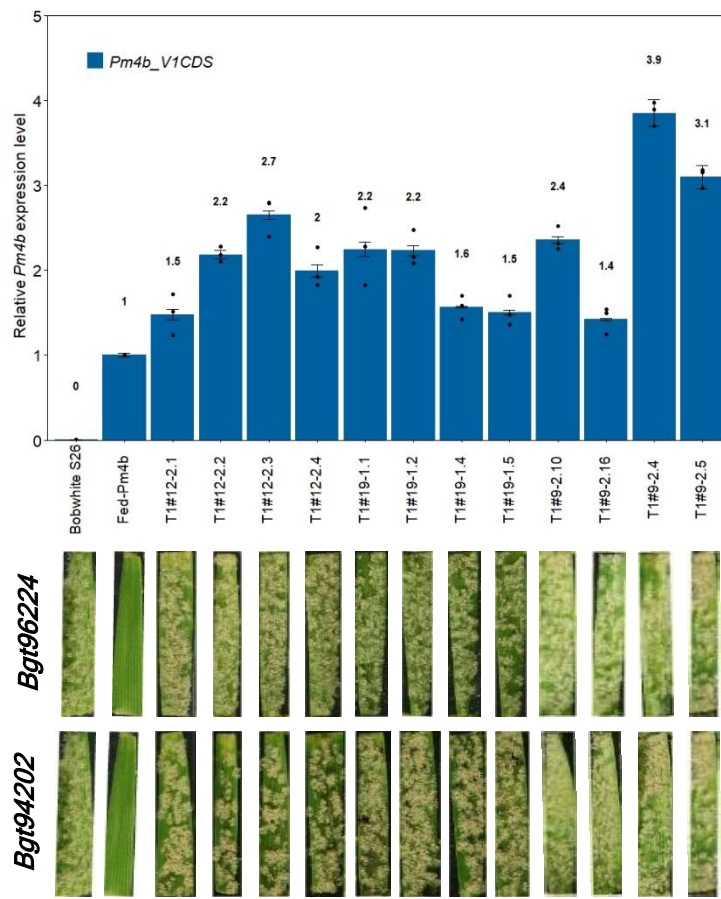
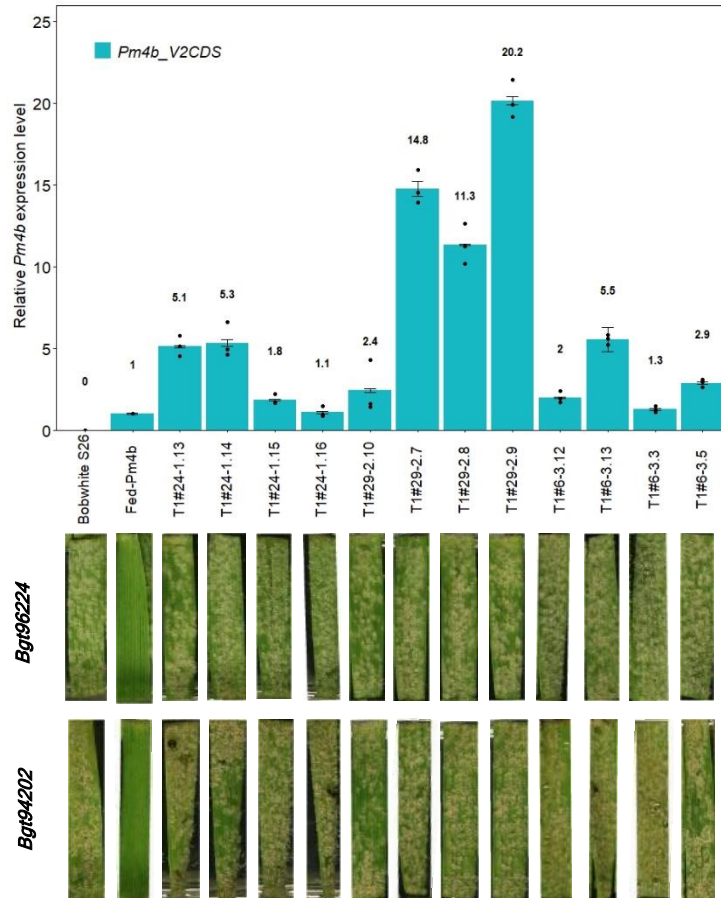
Fig. 6

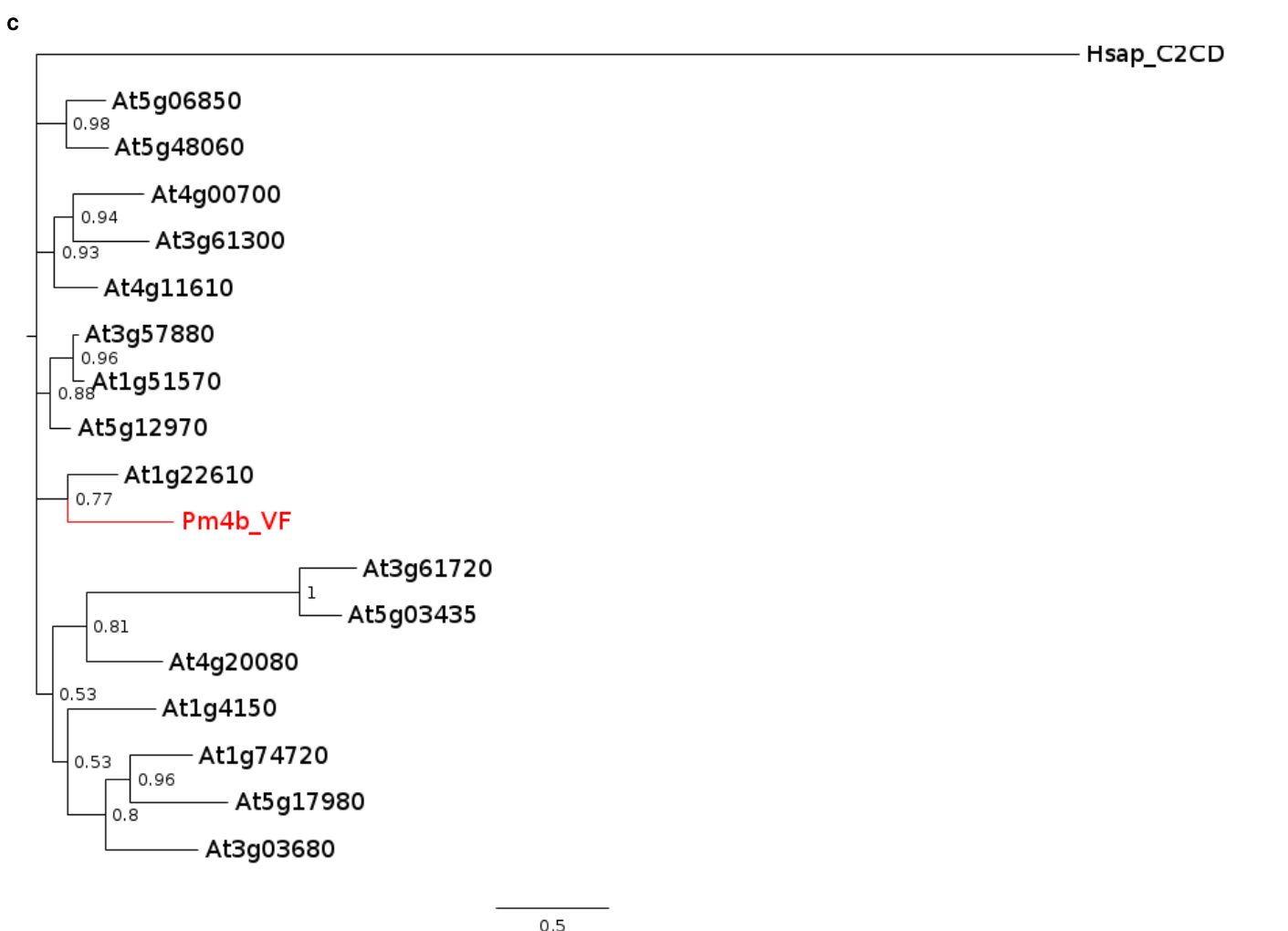
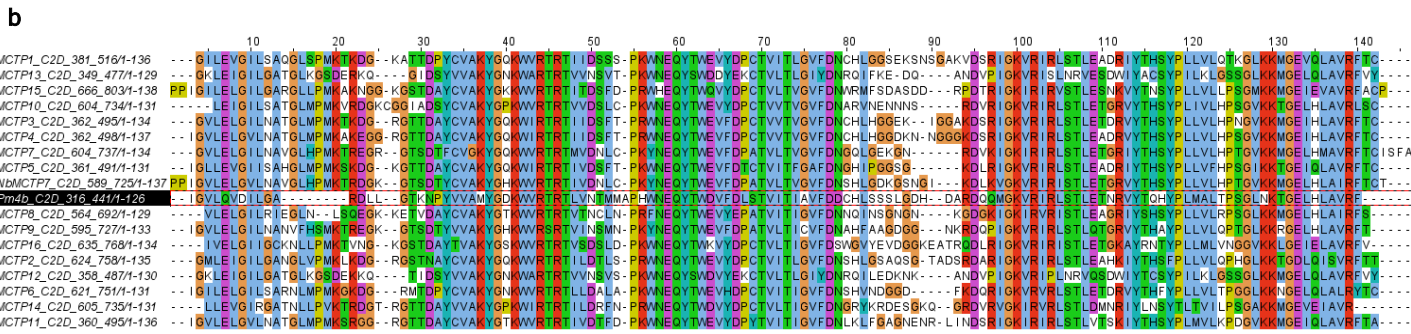
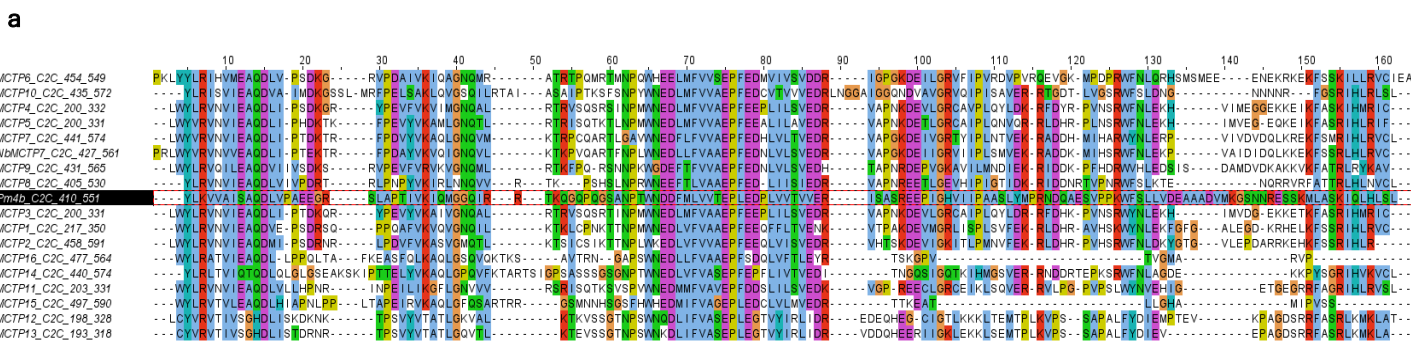


Extended Data Fig. 2

a**b****c**

Extended Data Fig. 3

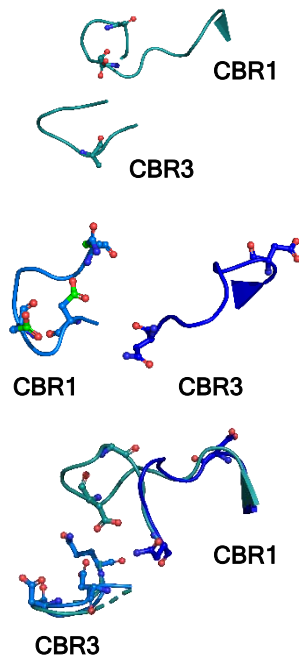
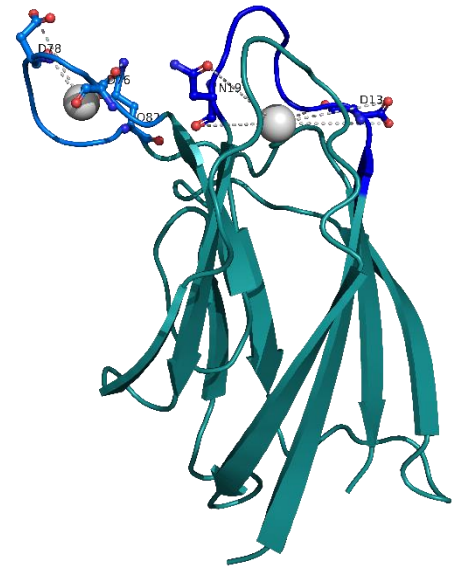
a**b**



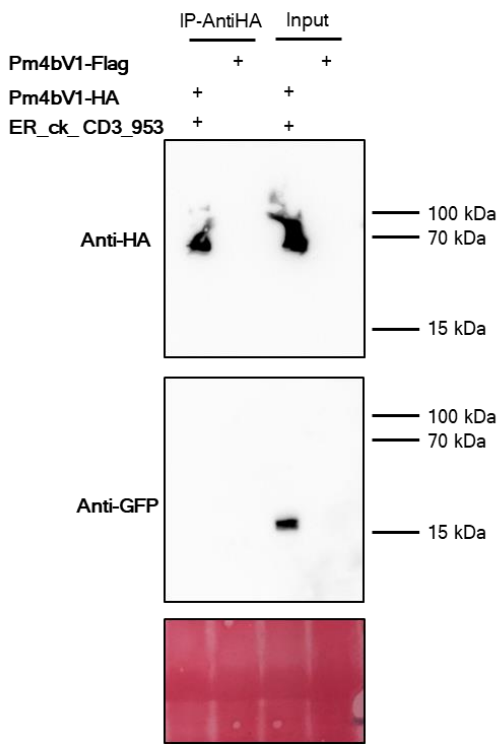
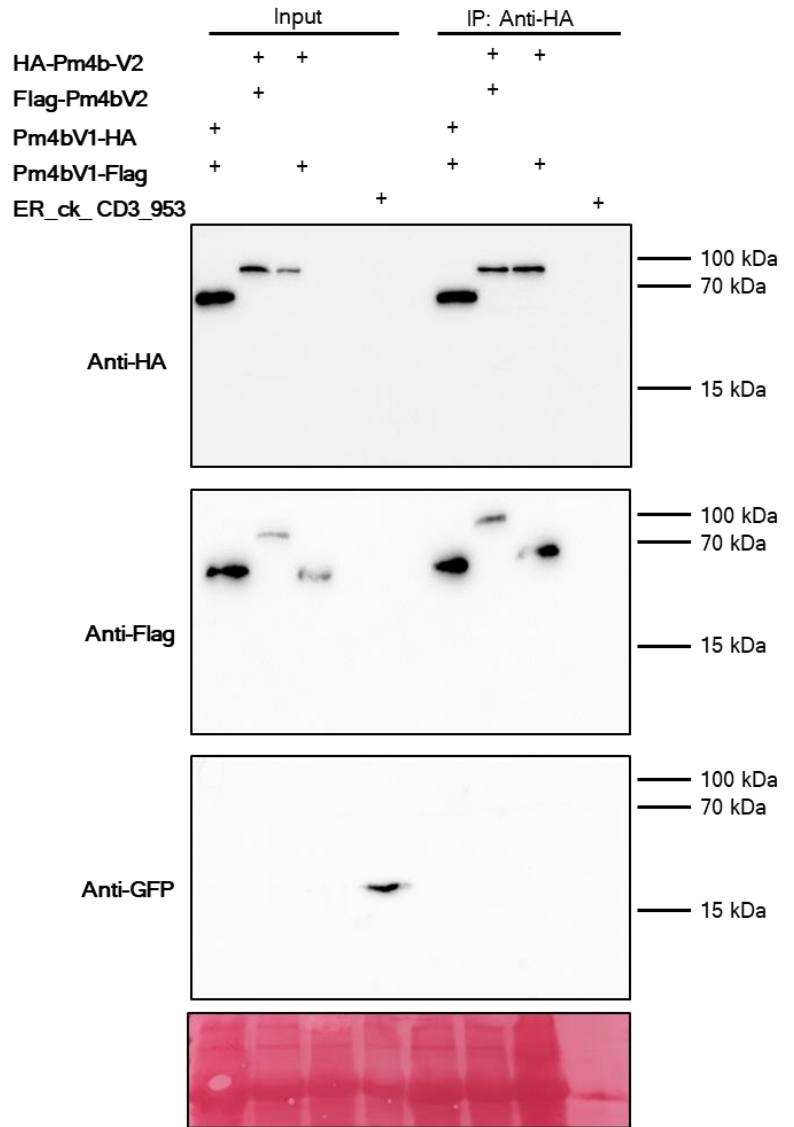
Extended Data Fig. 6

a

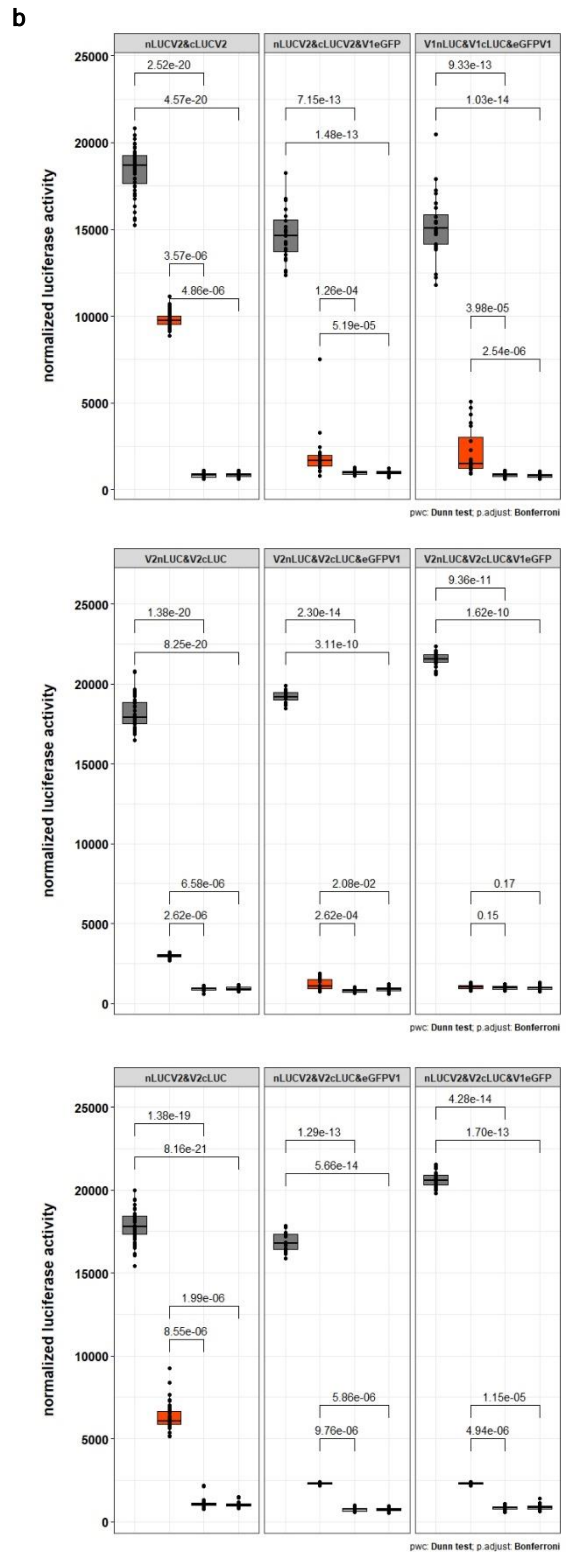
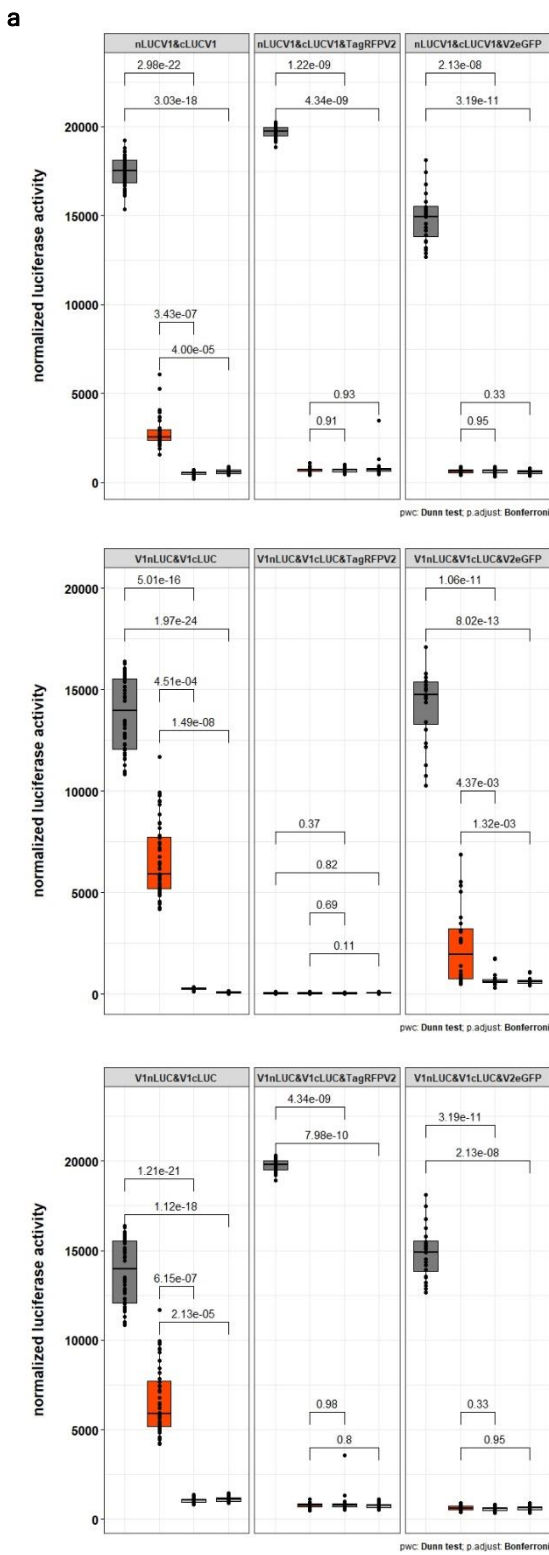
	CBR1							CBR3			
	10	20	30	40	50	60	70	80	90		
P3C2A_MOUSE-C2B_1584-1665	LVTEEDGADP	NP--YVKTYLLPDP	THKTSKRRTK	ISRKTRNPT	FNEMLVVSGYSK	ETLRQRELQLSVLS	S	A	SLREN--F	FLGGITLPL	
RIMS2_RAT-C2_770-854	IPSRFDGRPN	NP--YVKIYFLPDR	SDKNKRRTKT	VKKTLPEKWN	QTFIYSPVHRREF	RERMLEITLWD		Q	RVREEESE	FLGELIEL	
KPCA_RAT-C2_183-263	IPMDPNGLSD	NP--YVKLKLIPDP	KNESKQKTKT	IRSTLNQWNES	FTFK-LKPSDKDRR	-LSVEIWD		W	DRTRRN--	DFMGSLSGV	
KPCB_RAT-C2_183-262	IPMDPNGLSD	NP--YVKLKLIPDP	KSESQKTKT	IKCSLNPEWNET	FRFQ-LKESDKDRR	-LSVEIWD		W	DLTSRN--	DFMGSLSPG	
KPCG_HUMAN-C2_183-263	IPMDPNGLSD	NP--YVKLKLIPDP	RNLTKQKTRT	VKATLNPNVNET	FVFN-LKPGDVERR	-LSVEIWD		W	DRTSRN--	DFMGAMSGV	
SYT1_RAT-C2B_299-380	IKKMDVGLSD	NP--YVKIHLMQN	GKRLKKKTKT	IKKNTLNPNYNE	SFSFE-VPEEQIQKV	QVVVTVD		Y	KLIGN--	DAIGVFVGY	
SYT7_MOUSE-C2_293-374	IKAMDIGGTS	NP--YVKVWLMYK	DRVEKKTVT	KRNLNPIFNES	FAFD-IPTEKLR	ETTTIITVMD		K	DKLSRN--	DVIGKIYLSW	
SYT4_RAT-C2_314-395	IPKSDVSGLS	NP--YVKVNLVHAK	KRISKKTHV	KCTPNAVFNEL	VFD-IPCESLEEI	SVEFLVD		S	ERGSRN--	EVIGRLVGA	
SYT1_RAT-C2A_168-262	IPALDMGGTS	NP--YVKVFLPD	DK--KKFETV	HRKTLNPNVNE	QTFK-VPYSELG	GKTLVMAYD		F	DRFSKH--	DIIGEFKVP	
SYT7_HUMAN-C2B_162-242	IPAKDFSGTS	NP--YVKIYLLP	DK--HKLETV	KVRKLNPNVNE	TFLFEGFPY	EKVVQRILYQVLD		Y	DRFSRN--	DFMGAMSGV	
RP3A_RAT-C2B_567-648	IAAMDANGYSD	NP--FVKLWLKPD	MGKAKKHTQ	IKKTLNPNFNE	EEFYD-IKHSDL	LAKKSLDISVWD		Y	DIGKSN--	DYIGGCQLGI	
RP3A_RAT-C2A_409-491	IKPMDNSGLAD	NP--YVKLHLLP	GASKSNKLR	TTLRNRNPNVNET	LQYHGITEED	MQRKTLRISVCD		E	DKFGHN--	DFIGTRFSL	
MCTP1_HUMAN_C2C_638-699	IMAADVTGKSD	NP--FCV--ELN	NDRLLTHTVY	KNLNPEWNV	FTFN--IKDIHSV	-LEVTVD		E	DRDRSA--	DFLGKVAIPL	
MCTP2_HUMAN_C2C_521-582	ILAADFSGKSD	NP--FCL--ELG	NDRLQTHTVY	KNLNPEWNV	FTFP--IKDIHDV	-LEVTVD		E	DGDKPP--	DFLGKVAIPL	
MCTP1_HUMAN_C2A_273-335	IAARDRGGTS	NP--YVKF--K	IGGEVFRSKI	IHKNLNPNVNE	EKACIL--VDHLREP	-LYIKVD		Y	DGLQD--	DFMGSAFLDL	
MCTP2_HUMAN_C2A_206-267	IVVDRRCGTS	NP--YVKF--K	LNKGTLYKSK	VIVYKLNPNVNE	IVVLP--IQSLDQK	-LRVKVD		R	L-TTS--	DFMGSAFVLL	
MCTP1_HUMAN_C2B_483-544	KAMDSNGLSD	NP--YVKFRLG	---HQYKYSK	IMPKTLNPNVNE	TQWREQDFH--LYEER	GGVIDITAWD		K	DAGKRD--	DFIGRCQVLD	
MCTP2_HUMAN_C2B_363-427	LEKKNVSGGSM	TEM--FVQLKLG	---DQRYKSK	TLCKSANPNQ	WQEQDFH--YFSDRM	GILDIEVWG		K	NKKHE--	ERLGTCKVDI	
Pm4b_C2C_421-496	IVPAEGRSL	NP--IVKIQMG	---GQIRRTK	QGGPQGSAN	PTWDDFMLV--VTEPLE	DLVVTVV		R	SASRE--	PIGHVIT--	
Pm4b_C2D_324-404	IGARLLGTK	NP--YVVAMY	---GDKWVR	TRLVNTMMAPH	WNEQYTWDD--VFDLSTV	-ITIAVFD		D	CHLSSS	CDHARD--	QMGKVRIT--
RIMS1_RAT-C2_1486-1566	LTQKPGSKS	TPAPYVKVYL	LENGACIAK	KKTKIAR	KTLDLPYQ	QSIVFD--ESPQ	GKVLQVIVWG		Y	GRMDHK--	CFMGVAQILL
SYT13_HUMAN-C2_185-262	SNHDGGCD	NP--YVQGSVAN	RTG--SVEAQT	ALKRQLHTT	WEGLVLP-LABEEL	PTATLTTLRT		C	DRFSRH--	SVIGELRLLG	

b**c****d**

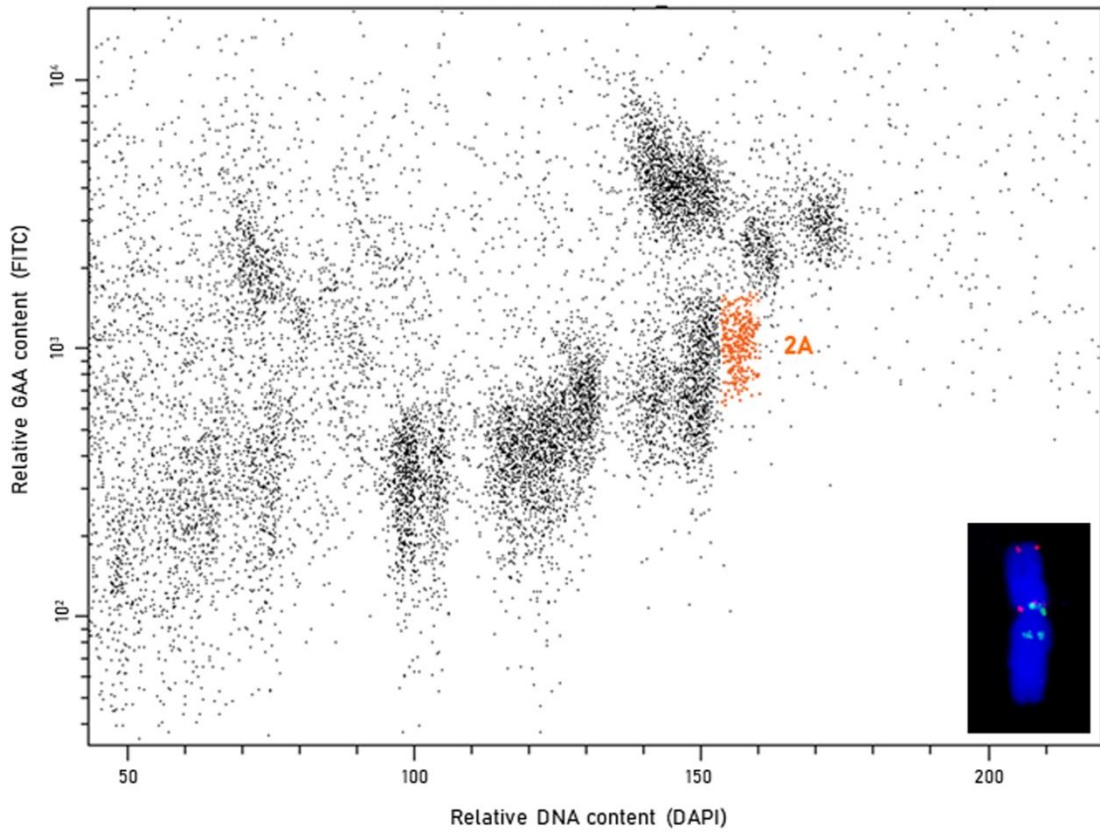
Extended Data Fig. 7

a**b**

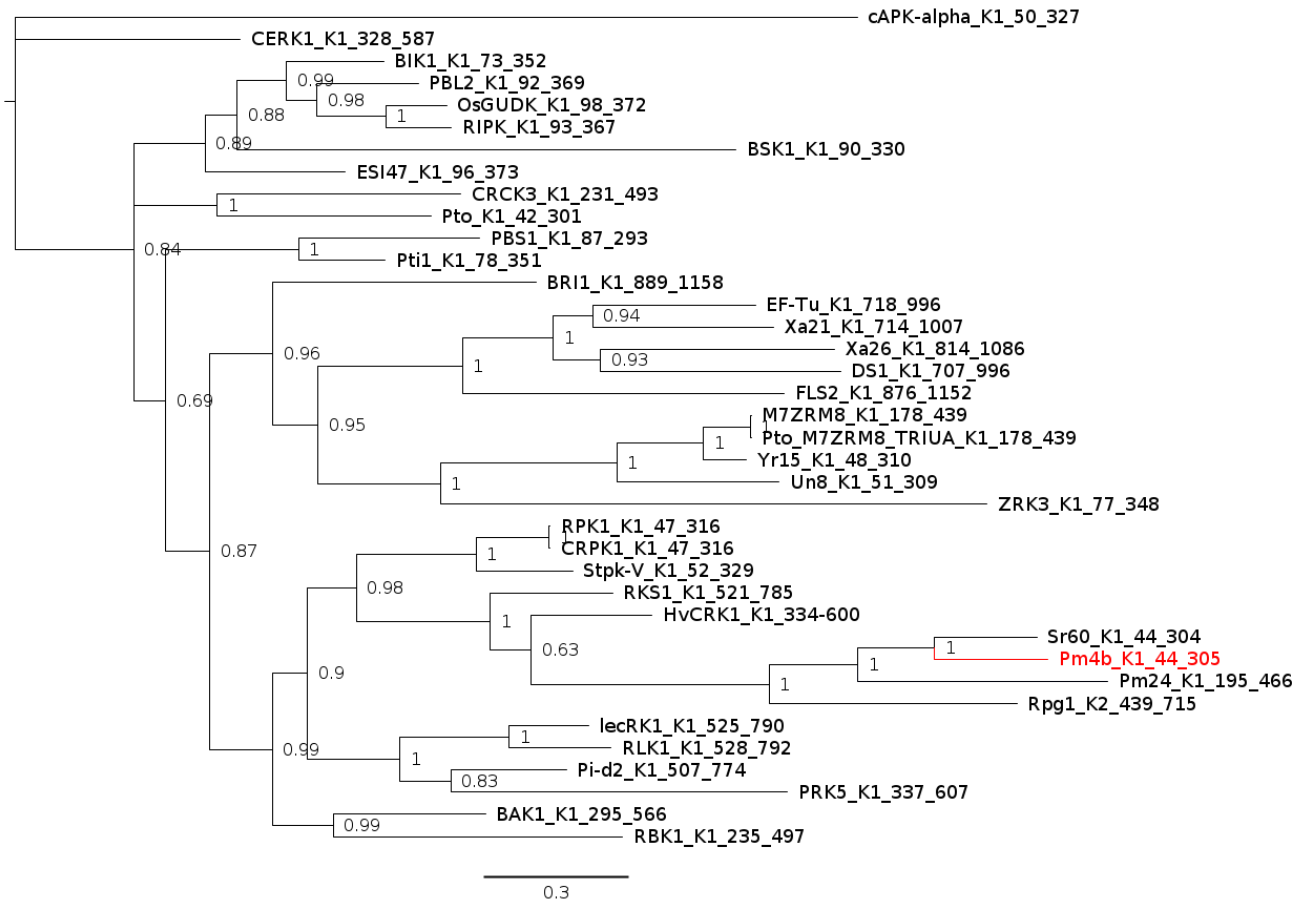
Extended Data Fig. 8



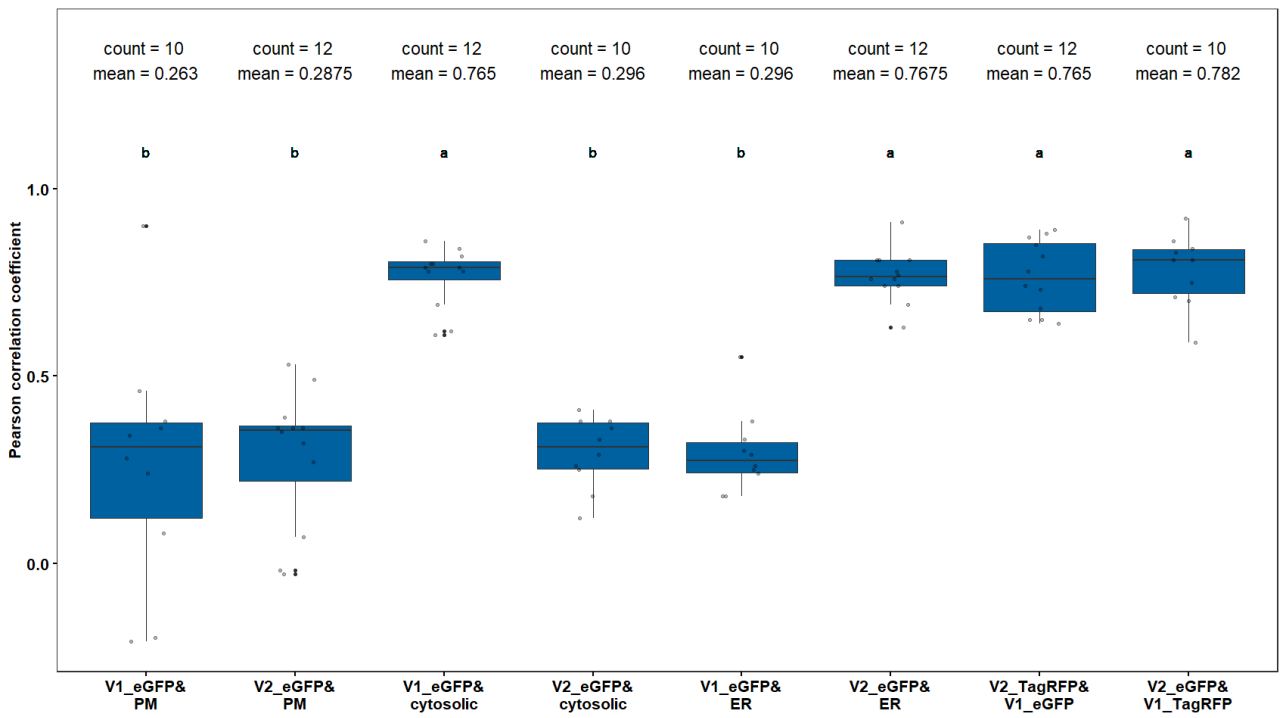
Extended Data Fig. 9

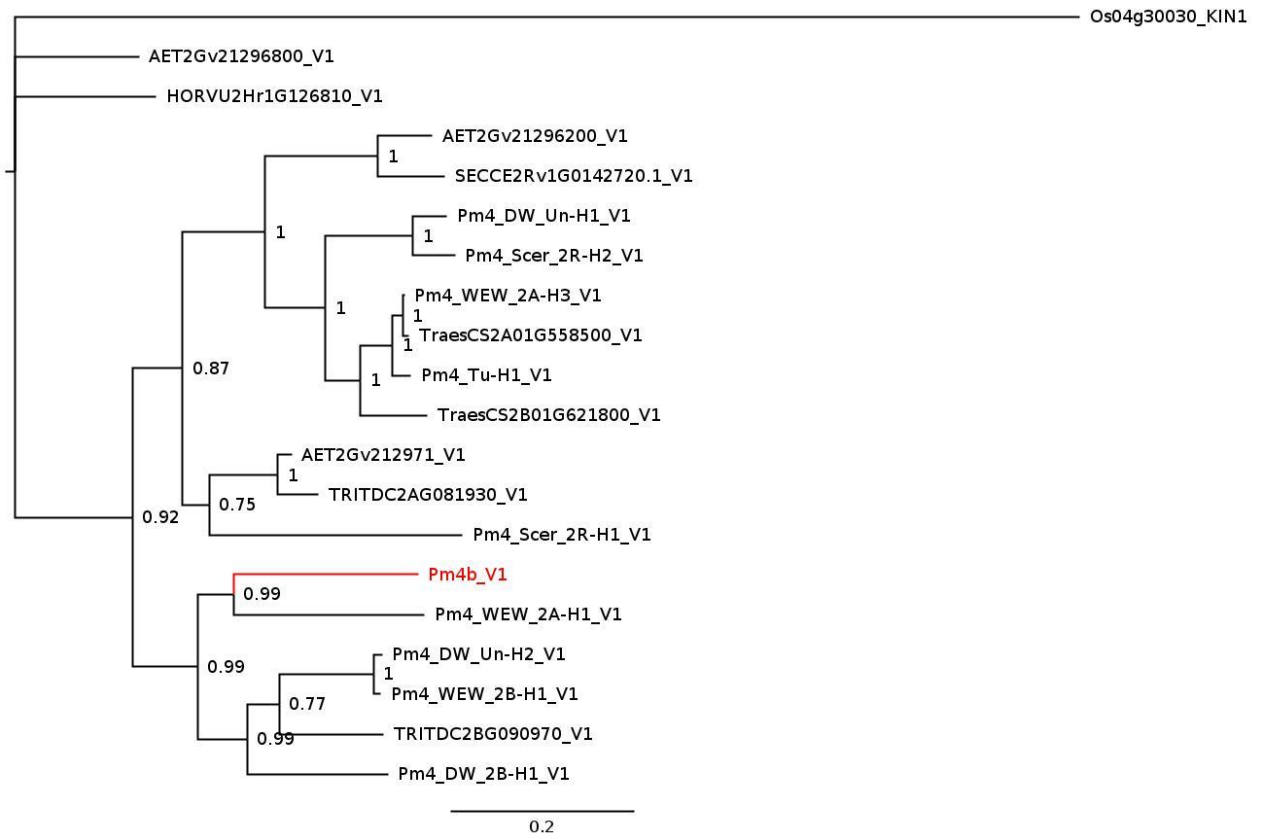
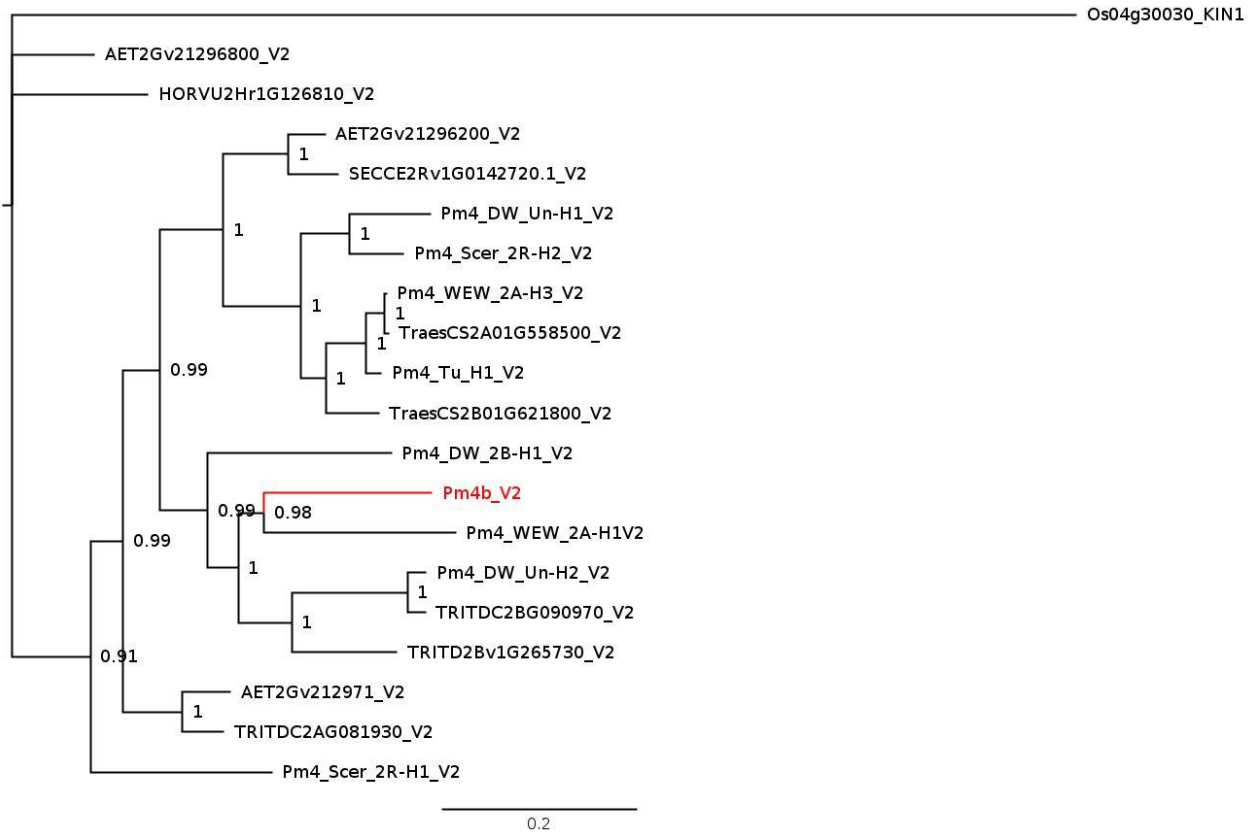


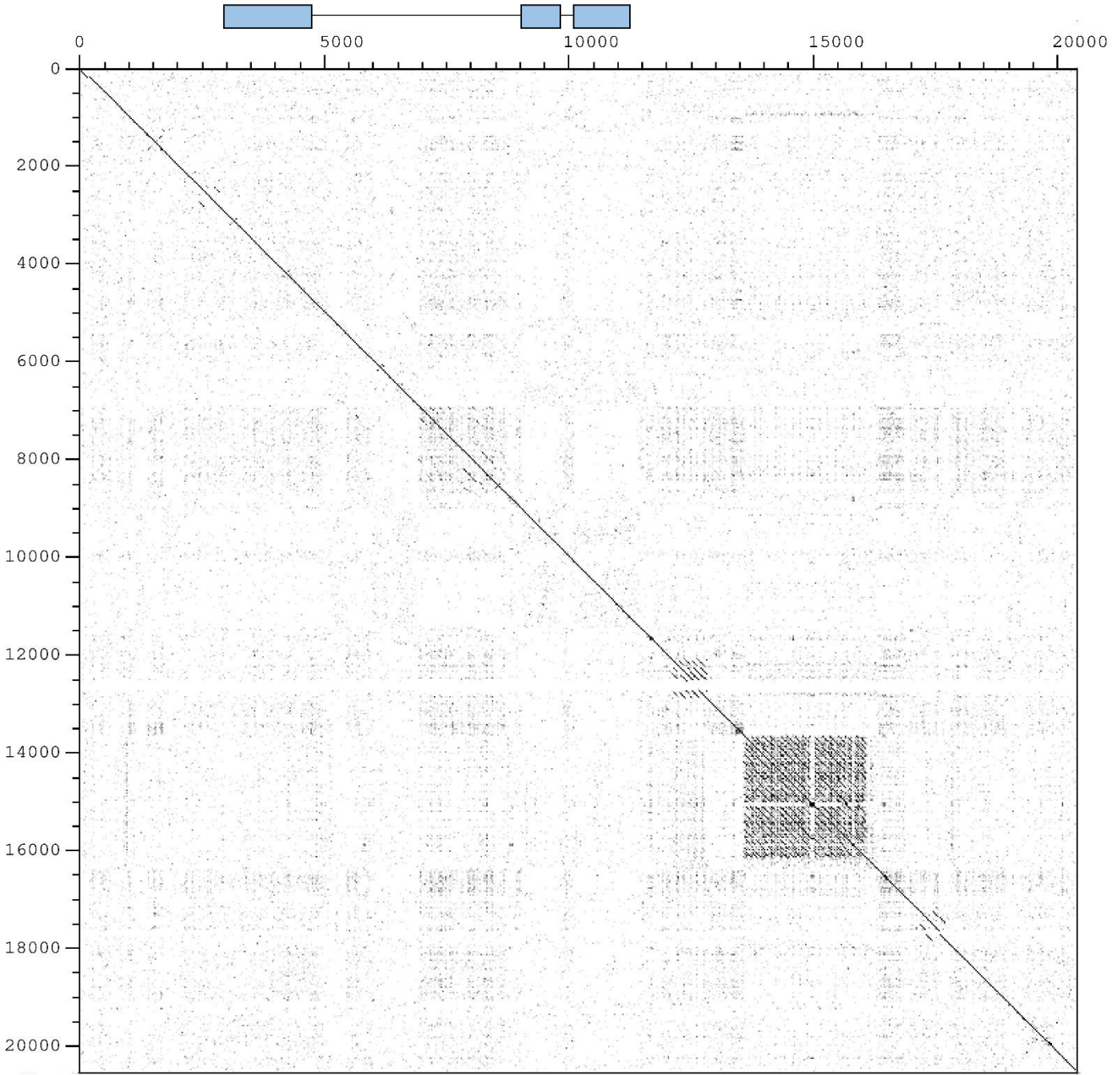
Extended Data Fig. 10



Supplementary Fig. 1

a**Supplementary Fig. 3**

a**b**



Supplementary Fig. 5

Supplementary Table 1 | List of *Bgt* isolates used to characterize the resistance spectra of *Pm4a* and *Pm4b*. The first column corresponds to the name of the *Bgt* isolate, followed by the geographic origin and collection site (if available) and the source. The last two columns show the disease reactions of Fed-*Pm4a* and Fed-*Pm4b* NILs distinguishing five classes of host reactions R = resistance (0-10% of leaf area covered), IR (10-25% of leaf area covered), I (25-50% of leaf area covered), IS (50-75 % of leaf area covered) and S (>75% of leaf area covered). Infection test is based on four biological replicates. CHN: China, ISR: Israel; CHE; Switzerland; FRA: France; USA: United States; GRB: Great Britain; JPN; Japan.

<i>Bgt</i>	Origin	Collection site	Source ¹⁻⁴	Fed- <i>Pm4a</i>	Fed- <i>Pm4b</i>
CHE_94202	CHE		Wicker et al. 2013	R	R
CHE_96224	CHE		Wicker et al. 2013	R	R
CHE_96249	CHE		in-house collection	R	R
CHE_97223	CHE		in-house collection	R	R
CHN_10_8	CHN	Yunnan province	Zeng et al. 2014	R	R
CHN_12_50	CHN	Guizhou province	Zeng et al. 2014	R	R
CHN_19_11	CHN	Jiangsu province	Zeng et al. 2014	R	R
CHN_28_9	CHN		Zeng et al. 2014	R	R
CHN_36_70	CHN	Hebei province	Zeng et al. 2014	R	R
CHN_39_1	CHN		Zeng et al. 2014	R	R
CHN_46_31	CHN	Gansu province	Zeng et al. 2014	R	R
CHN_6_69	CHN	Shannxi province	Zeng et al. 2014	R	R
CHN_7_8	CHN	Shannxi province	Zeng et al. 2014	R	R
FRA_B_Stone_95-45	FRA		McNally et al. 2018	R	R
ISR_1	ISR	Hula	McNally et al. 2018	R	R
ISR_103I	ISR	Amiad	Menardo et al. 2016	R	R
ISR_103K	ISR		Menardo et al. 2016	R	R
ISR_113	ISR	Amiad	McNally et al. 2018	R	R
ISR_13	ISR	Hula	McNally et al. 2018	R	R
ISR_16	ISR	Nahal Oz	McNally et al. 2018	R	R
ISR_20	ISR	Ein Hanaziv	McNally et al. 2018	R	R
ISR_204	ISR		Menardo et al. 2016	R	R
ISR_217	ISR		Menardo et al. 2016	R	R
ISR_218	ISR	Tel Far	McNally et al. 2018	R	R
ISR_219	ISR	Bizaron	McNally et al. 2018	R	R
ISR_30P	ISR	Talmei Yafe	McNally et al. 2018	R	R
ISR_30w	ISR	Talmei Yafe	McNally et al. 2018	R	R
ISR_37	ISR	Nahal Oz	McNally et al. 2018	R	R
ISR_43	ISR	Yesodot	McNally et al. 2018	R	R
ISR_44	ISR	Negev	McNally et al. 2018	R	R
ISR_50	ISR	Nahal Oz	McNally et al. 2018	R	R
ISR_52	ISR	DirEIBalakh	McNally et al. 2018	R	R
ISR_6	ISR	Hula	McNally et al. 2018	R	R
ISR_67	ISR	Lahav	McNally et al. 2018	R	R
ISR_70	ISR		Menardo et al. 2016	R	R
ISR_94	ISR	Ein Hanaziv	McNally et al. 2018	R	R
ISR_97	ISR		Menardo et al. 2016	R	R

CHN_5_112	CHN		Zeng et al. 2014	R	IR
CHN_5_83	CHN	Shannxi province	Zeng et al. 2014	R	IR
CHN_5_93	CHN		Zeng et al. 2014	R	IR
CHN_51_3	CHN		Zeng et al. 2014	R	IR
CHN_6_21	CHN		Zeng et al. 2014	R	IR
CHN_9_43	CHN		Zeng et al. 2014	R	IR
CHN_HB_22	CHN		Zeng et al. 2014	R	IR
CHN_NJ_16	CHN		Zeng et al. 2014	R	IR
ISR_205	ISR	Kfar-Menahem	McNally et al 2018	R	IR
ISR_209	ISR	K. Revhaya	Menardo et al. 2016	R	IR
ISR_214	ISR	Akko	McNally et al 2018	R	IR
ISR_7	ISR	Hula	Menardo et al. 2016	R	IR
ISR_9	ISR	Hula	McNally et al 2018	R	IR
CHE_97266	CHE		in-house collection	IR	R
ISR_106	ISR	Nahal Oz	McNally et al 2018	IR	R
ISR_107	ISR	Nahal Oz	McNally et al 2018	IR	R
ISR_217	ISR	Kfa Hasidim	Menardo et al. 2016	IR	R
ISR_96	ISR	Negba	McNally et al 2018	IR	R
CHN_13_51	CHN	Guizhou province	Zeng et al. 2014	R	I
CHN_14_32	CHN		Zeng et al. 2014	R	I
CHN_15_9	CHN		Zeng et al. 2014	R	I
CHN_21_1	CHN		Zeng et al. 2014	R	I
CHN_37_38	CHN		Zeng et al. 2014	R	I
CHN_40_2	CHN		Zeng et al. 2014	R	I
CHN_41_5	CHN		Zeng et al. 2014	R	I
ISR_210	ISR	Givat HaMoreh	McNally et al 2018	I	IR
ISR_216	ISR	Ein Shemer	McNally et al 2018	IS	IR
CHN_2_39	CHN		Zeng et al. 2014	R	S
CHE_7004	CHE		Menardo et al. 2016	S	R
CHE_7230	CHE		McNally et al 2018	S	R
CHE_7234	CHE		in-house collection	S	R
CHE_10001	CHE		in-house collection	S	R
CHE_98013	CHE		in-house collection	S	R
CHN_52-27	CHN	Xinjiang	Zeng et al. 2014	S	R
FRA_Syros2000_15	FRA		McNally et al 2018	S	R
ISR_208	ISR	Gilboa	Menardo et al. 2016	S	R
ISR_8	ISR	Hula	Menardo et al. 2016	S	R
JPN_CHIKARA	JPN		McNally et al 2018	S	R
USA_C3-1	USA		McNally et al 2018	S	R
CHN_HB_21	CHN	Hubei province	Zeng et al. 2014	S	IR
CHN_1_47	CHN		Zeng et al. 2014	I	S
CHN_2_5	CHN		Zeng et al. 2014	I	S
CHN_1_19	CHN	Sichuan province	Zeng et al. 2014	S	S
CHN_1_62	CHN		Zeng et al. 2014	S	S
CHN_10_40	CHN		Zeng et al. 2014	S	S
CHN_11_61	CHN		Zeng et al. 2014	S	S
CHN_12_24	CHN		Zeng et al. 2014	S	S

CHN_12_3	CHN		Zeng et al. 2014	S	S
CHN_12_82	CHN		Zeng et al. 2014	S	S
CHN_13_76	CHN		Zeng et al. 2014	S	S
CHN_15_11	CHN		Zeng et al. 2014	S	S
CHN_17_40	CHN	Anhui province	Zeng et al. 2014	S	S
CHN_18_1	CHN		Zeng et al. 2014	S	S
CHN_18_11	CHN		Zeng et al. 2014	S	S
CHN_18_38	CHN		Zeng et al. 2014	S	S
CHN_18_45	CHN		Zeng et al. 2014	S	S
CHN_2_25	CHN	Sichuan province	Zeng et al. 2014	S	S
CHN_2_65	CHN		Zeng et al. 2014	S	S
CHN_24_4	CHN	Jiangsu province	Zeng et al. 2014	S	S
CHN_30_1	CHN	Anhui province	Zeng et al. 2014	S	S
CHN_35_1	CHN		Zeng et al. 2014	S	S
CHN_35_18	CHN		Zeng et al. 2014	S	S
CHN_36_3	CHN		Zeng et al. 2014	S	S
CHN_39_19	CHN		Zeng et al. 2014	S	S
CHN_39_5	CHN		Zeng et al. 2014	S	S
CHN_44_3	CHN	Shandong province	Zeng et al. 2014	S	S
CHN_45_10	CHN	Gansu province	Zeng et al. 2014	S	S
CHN_45_6	CHN	Gansu province	Zeng et al. 2014	S	S
CHN_46_25	CHN	Gansu province	Zeng et al. 2014	S	S
GRB_JIW2	GRB		Wicker et al. 2013	S	S

Supplementary Table 2 | List of EMS-induced Pm4a and Pm4b mutants used in this study. The given name of each mutant (first column) is followed by the donor line, *Fed-Pm4a* or *Fed-Pm4b*, where the EMS treatment was performed. In the column Mutation, the first letter indicates the amino acid in the wild-type followed by the position and the amino acid change in the corresponding mutant. Last column denotes the predicted domain based delimited based on Conserved Domain Database (CDD) from NCBI, where S_TKc (c121453) corresponds to the serine/threonine kinase domain, C2C and C2D (c114603) to C2 domain third and fourth repeat found in Multiple C2 domain and Transmembrane regions Proteins (MCTP). Finally, PRT_C (pfam08372) denotes the plant phosphoribosyltransferase C-terminal domain. The last three columns display the reactions of the EMS-derived mutants after inoculation with *Bgt94202*, *Bgt96224* and *BgtJ1W2*. Values refer to percentage of the surface area of tested leaf segments infected (means of four biological replicates \pm SE).

Mutant name	Source	Mutation	Affected domain	<i>Bgt94202</i>	<i>Bgt96224</i>	<i>BgtJ1W2</i>
pm4b_m7	<i>Fed-Pm4b</i>	S390F	spacer	82.5 \pm 4.3	85.0 \pm 5.0	85.0 \pm 5.0
pm4b_m89	<i>Fed-Pm4b</i>	P497L	C2C	80.0 \pm 0.0	82.5 \pm 4.3	85.0 \pm 5.0
pm4b_m123 ⁶	<i>Fed-Pm4b</i>	G132D	S_TKc	80.0 \pm 0.0	77.5 \pm 8.3	85.0 \pm 5.0
pm4b_m125	<i>Fed-Pm4b</i>	G234D	S_TKc	80.0 \pm 0.0	80.0 \pm 10.0	87.5 \pm 4.3
pm4b_m151 ⁶	<i>Fed-Pm4b</i>	P184L	S_TKc	80.0 \pm 0.0	80.0 \pm 7.1	90.0 \pm 0.0
pm4b_m180	<i>Fed-Pm4b</i>	G665S	PRT_C	70.0 \pm 7.1	80.0 \pm 7.1	85.0 \pm 5.0
pm4b_m207 ⁶	<i>Fed-Pm4b</i>	D170N	S_TKc	72.5 \pm 8.3	80.0 \pm 7.1	85.0 \pm 5.0
pm4b_m244	<i>Fed-Pm4b</i>	Q588*; R737W	PRT_C	72.5 \pm 8.3	80.0 \pm 7.1	87.5 \pm 4.3
pm4b_m256 ⁶	<i>Fed-Pm4b</i>	G659D	PRT_C	75.0 \pm 11.2	85.0 \pm 5.0	85.0 \pm 8.7
pm4b_m324	<i>Fed-Pm4b</i>	T622M	PRT_C	82.5 \pm 8.3	85.0 \pm 5.0	90.0 \pm 0.0
pm4b_m360	<i>Fed-Pm4b</i>	G659D	PRT_C	80.0 \pm 7.1	85.0 \pm 5.0	90.00 \pm 0.0
pm4b_m445	<i>Fed-Pm4b</i>	Q14*	spacer	85.0 \pm 5.0	85.0 \pm 5.0	90.0 \pm 0.0
pm4b_m467	<i>Fed-Pm4b</i>	Y626N	PRT_C	85.0 \pm 5.0	85.0 \pm 5.0	80.0 \pm 0.0
pm4b_m495 ⁶	<i>Fed-Pm4b</i>	Q274*	S_TKc	82.5 \pm 4.3	82.5 \pm 4.3	80.0 \pm 0.0
pm4b_m510	<i>Fed-Pm4b</i>	V477M	C2C	85.0 \pm 5.0	80.0 \pm 7.1	87.5 \pm 4.3
pm4b_m526 ⁶	<i>Fed-Pm4b</i>	R291K	S_TKc	80.0 \pm 7.1	85.0 \pm 5.0	90.0 \pm 0.0
pm4b_m532 ⁶	<i>Fed-Pm4b</i>	G104E	S_TKc	82.5 \pm 8.3	80.0 \pm 7.1	77.5 \pm 4.3
pm4b_m641 ⁶	<i>Fed-Pm4b</i>	G45E	S_TKc	80.0 \pm 7.1	82.5 \pm 8.3	85.0 \pm 5.0
pm4a_m077	<i>Fed-Pm4a</i>	D188N	S_TKc	85.0 \pm 5.0	80.0 \pm 7.1	85.0 \pm 5.0
pm4a_m102	<i>Fed-Pm4a</i>	Q719R	PRT_C	87.5 \pm 4.3	75.0 \pm 5.0	85.0 \pm 5.0
pm4a_m113	<i>Fed-Pm4a</i>	E183K	S_TKc	85.0 \pm 5.0	80.0 \pm 7.1	87.5 \pm 4.3
pm4a_m177	<i>Fed-Pm4a</i>	T204I;P688L	S_TKc	70.0 \pm 0.0	80.0 \pm 7.1	85.0 \pm 5.0
pm4a_m188	<i>Fed-Pm4a</i>	G562D	spacer	70.0 \pm 0.0	82.5 \pm 4.3	85.0 \pm 5.0
pm4a_m226	<i>Fed-Pm4a</i>	W681*	PRT_C	75.0 \pm 5.0	80.0 \pm 7.1	85.0 \pm 5.0
pm4a_m247	<i>Fed-Pm4a</i>	L261F	S_TKc	80.0 \pm 7.1	77.5 \pm 8.3	85.0 \pm 5.0
pm4a_m280	<i>Fed-Pm4a</i>	P617S	PRT_C	72.5 \pm 8.3	77.5 \pm 4.3	85.0 \pm 5.0
pm4a_m293	<i>Fed-Pm4a</i>	G190D	S_TKc	75.0 \pm 5.0	80.0 \pm 7.1	85.0 \pm 5.0
pm4a_m366	<i>Fed-Pm4a</i>	G317S	C2D	80.0 \pm 7.1	80.0 \pm 7.1	85.0 \pm 5.0
pm4a_m398	<i>Fed-Pm4a</i>	E217K	S_TKc	80.0 \pm 7.1	82.5 \pm 4.3	85.0 \pm 5.0
pm4a_m425	<i>Fed-Pm4a</i>	V118I	S_TKc	85.0 \pm 5.0	77.5 \pm 4.3	85.0 \pm 5.0
pm4a_m448	<i>Fed-Pm4a</i>	A100T	S_TKc	80.0 \pm 7.1	77.5 \pm 4.3	85.0 \pm 5.0
pm4a_m507	<i>Fed-Pm4a</i>	P617L	PRT_C	80.0 \pm 7.1	80.0 \pm 7.1	82.5 \pm 4.3

⁶Mutants subjected to chromosome flow sorting and MutChromSeq, and then confirmed by Sanger sequencing

Supplementary Table 3 | Disease reactions of selected T2 families challenged with selected *Bgt* isolates. The first column displays the name of each progeny. Second and third column indicates the presence (+) or absence (-) of the transgenes *Pm4b_V1CDS*- and *Pm4b_V2CDS* (See Methods). The remaining columns show the disease reaction of each T2 line challenged with two *Pm4a/b*-avirulent (*Bgt96224* and *Bgt94202*) and two *Pm4a/b*-virulent (*BgtJIW2* and *Bgt97251*) isolates. Top four rows show the disease reactions of the Fed-*Pm4a* and the Fed-*Pm4b* NILs genotypes, Bobwhite S26, the susceptible background where transgenic complementation assays were performed, and Kanzler, a highly susceptible cultivar to *Bgt*. Five classes of host reactions were considered. R = resistance (0-10% of leaf area covered), IR (10-25% of leaf area covered), I (25-50% of leaf area covered), IS (50-75 % of leaf area covered) and S (>75% of leaf area covered). Evaluation was done 7-9 dpi.

T2_line	Pm4b_V1CDS	Pm4b_V2CDS	<i>Bgt96224</i>	<i>Bgt94202</i>	<i>BgtJIW2</i>	<i>Bgt97251</i>
Fed- <i>Pm4a</i>	-	-	R	R	S	S
Fed- <i>Pm4b</i>	-	-	R	R	S	S
Bobwhite S26	-	-	S	S	S	S
Kanzler	-	-	S	S	S	S
T2#3-2.12_1.1	+	+	R	R	S	IS
T2#3-2.12_1.2	+	+	R	R	S	S
T2#3-2.12_1.4	+	+	R	R	IS	IS
T2#3-2.12_1.5	+	+	IR	R	S	S
T2#3-2.12_1.6	+	+	R	R	IS	IS
T2#3-2.12_1.7	+	+	R	R	IS	IS
T2#3-2.12_1.8	+	+	R	R	IS	S
T2#3-2.12_1.9	+	+	R	R	S	S
T2#3-2.12_1.10	+	+	R	R	S	S
T2#3-2.12_1.11	+	+	R	R	S	S
T2#3-2.12_1.12	+	+	R	R	S	IS
T2#3-2.12_1.13	+	+	R	R	S	S
T2#3-2.12_1.14	+	+	R	R	S	S
T2#3-2.12_1.15	+	+	R	R	S	S
T2#3-2.12_1.16	+	+	R	R	S	S
T2#3-2.13_1.1	-	-	S	S	S	IS
T2#3-2.13_1.2	+	+	IR	IS	S	S
T2#3-2.13_1.3	-	-	S	S	S	S
T2#3-2.13_1.4	+	+	IS	IR	S	S
T2#3-2.13_1.5	-	-	S	S	S	IS
T2#3-2.13_1.6	+	+	R	R	S	S
T2#3-2.13_1.7	+	+	IR	IR	IS	IS
T2#3-2.13_1.8	+	+	R	R	S	S
T2#3-2.13_1.9	+	+	R	R	S	S
T2#3-2.13_1.10	+	+	IR	R	S	S
T2#3-2.13_1.11	+	+	R	R	S	S
T2#3-2.13_1.12	+	+	R	IR	S	S
T2#3-2.13_1.13	+	+	R	IR	S	S
T2#3-2.13_1.14	+	+	R	R	S	S
T2#3-2.13_1.16	+	+	IS	S	S	S
T2#25-1.8_1.1	+	+	IS	S	S	S

T2#25-1.8_1.2	+	+	I	S	S	S
T2#25-1.8_1.3	+	+	R	R	S	S
T2#25-1.8_1.4	+	+	I	IS	S	S
T2#25-1.8_1.5	+	+	R	IR	S	S
T2#25-1.8_1.6	+	+	R	I	S	S
T2#25-1.8_1.8	+	+	R	R	S	IS
T2#25-1.8_1.10	+	+	S	S	S	S
T2#25-1.8_1.11	+	+	R	IR	S	S
T2#25-1.8_1.12	+	+	R	R	S	IS
T2#25-1.8_1.13	+	+	R	R	S	S
T2#25-1.8_1.14	+	+	R	IS	S	S
T2#25-1.8_1.16	-	-	IS	S	S	S
T2#25-1.11_1.1	+	+	I	R	S	S
T2#25-1.11_1.2	+	+	R	R	S	S
T2#25-1.11_1.3	+	+	IS	R	S	S
T2#25-1.11_1.4	+	+	IR	R	S	IS
T2#25-1.11_1.6	+	+	R	IR	IS	S
T2#25-1.11_1.7	+	+	R	R	S	S
T2#25-1.11_1.8_	-	-	S	S	S	S
T2#25-1.11_1.9	+	+	R	R	S	S
T2#25-1.11_1.11	+	+	IR	IR	S	S
T2#25-1.11_1.12	+	+	R	R	S	S
T2#25-1.11_1.13	-	-	IR	IS	S	IS
T2#25-1.11_1.14	-	-	S	S	S	S
T2#25-1.11_1.15	+	+	R	R	IS	IS
T2#25-1.11_1.16	+	+	R	R	IS	IS
T2#52-1.4_1.1	-	-	S	S	S	S
T2#52-1.4_1.2	-	-	S	S	S	S
T2#52-1.4_1.3	-	-	S	S	S	S
T2#52-1.4_1.4	-	-	S	S	S	S
T2#52-1.4_1.5	-	-	I	S	S	S
T2#52-1.4_1.6	-	-	I	S	S	IS
T2#52-1.4_1.7	-	-	IS	S	S	IS
T2#52-1.4_1.8	-	-	IS	S	S	IS
T2#52-1.4_1.9	+	+	R	R	S	S
T2#52-1.4_1.10	+	+	R	R	S	IS
T2#52-1.4_1.11	-	-	I	S	S	S
T2#52-1.4_1.12	+	+	R	R	S	IS
T2#52-1.4_1.13	+	+	R	R	S	S
T2#52-1.4_1.14	+	+	R	R	S	IS
T2#52-1.4_1.15	+	+	R	R	S	S
T2#52-1.4_1.16	+	+	R	R	S	IS
T2#52-3.11_1.2	+	+	R	R	S	IS
T2#52-3.11_1.3	+	+	R	R	S	IS
T2#52-3.11_1.5	+	+	R	R	S	S
T2#52-3.11_1.7	+	+	R	R	S	S
T2#52-3.11_1.8	+	+	R	R	S	S

T2#52-3.11_1.11	+	+	R	R	S	IS
T2#52-3.11_1.12	+	+	R	R	S	S
T2#52-3.11_1.13	+	+	R	R	S	S
T2#52-3.14_1.2	+	+	R	R	S	IS
T2#52-3.14_1.3	+	+	R	R	IS	IS
T2#52-3.14_1.4	+	+	R	R	S	S
T2#52-3.14_1.7	+	+	R	R	IS	S
T2#52-3.14_1.9	+	+	R	R	IS	S
T2#52-3.14_1.12	+	+	R	R	S	S
T2#52-3.14_1.14	+	+	R	R	I	IS
T2#52-3.14_1.16	+	+	R	R	S	IS

Supplementary Table 4 | Disease reactions of selected T1 transgenic lines overexpressing *Pm4b_V1* or *Pm4b_V2* challenged with selected *Bgt* isolates. The first column displays the name of each progeny. Second column displays the *Pm4b* splicing variant transformed: either *Pm4b_V1CDS* or *Pm4b_V2CDS*. The third column, named detection, indicates the presence (+) or absence (-) of the corresponding transgenes: *Pm4b_V1CDS* or *Pm4b_V2CDS*. The remaining columns show the disease reaction of each T1 transgenic line challenged with two *Pm4a/b*-avirulent (*Bgt96224* and *Bgt94202*) and one *Pm4a/b*-virulent (*BgtJIW2*). Top four rows show the disease reactions of the Fed-*Pm4a*, Fed-*Pm4b*, Bobwhite S26, the susceptible background where transgenic complementation assays were performed, and Kanzler, a highly susceptible cultivar to *Bgt*. Five classes of host reactions were considered. R = resistance (0-10% of leaf area covered), IR (10-25% of leaf area covered), I (25-50% of leaf area covered), IS (50-75 % of leaf area covered) and S (>75% of leaf area covered)

Line	Transgene	Detection	<i>Bgt96224</i>	<i>Bgt94202</i>	<i>BgtJIW2</i>
Fed- <i>Pm4a</i>	-		R	R	R
Fed- <i>Pm4b</i>	-		R	R	R
Bobwhite S26	-		S	S	S
Kanzler	-		S	S	S
T1#9_2.1	<i>Pm4b_V1CDS</i>	+	S	S	S
T1#9_2.2	<i>Pm4b_V1CDS</i>	+	S	S	S
T1#9_2.3	<i>Pm4b_V1CDS</i>	+	S	S	S
T1#9_2.4	<i>Pm4b_V1CDS</i>	+	S	S	S
T1#9_2.5	<i>Pm4b_V1CDS</i>	+	S	S	S
T1#9_2.8	<i>Pm4b_V1CDS</i>	+	S	S	S
T1#9_2.9	<i>Pm4b_V1CDS</i>	+	S	S	S
T1#9_2.10	<i>Pm4b_V1CDS</i>	+	S	S	S
T1#9_2.11	<i>Pm4b_V1CDS</i>	+	S	S	S
T1#9_2.12	<i>Pm4b_V1CDS</i>	+	S	S	S
T1#9_2.13	<i>Pm4b_V1CDS</i>	+	S	S	S
T1#9_2.14	<i>Pm4b_V1CDS</i>	-	S	S	S
T1#9_2.15	<i>Pm4b_V1CDS</i>	+	S	S	S
T1#9_2.16	<i>Pm4b_V1CDS</i>	+	S	S	S
T1#12_2.1	<i>Pm4b_V1CDS</i>	+	S	S	S
T1#12_2.2	<i>Pm4b_V1CDS</i>	+	S	S	S
T1#12_2.3	<i>Pm4b_V1CDS</i>	+	S	S	S
T1#12_2.4	<i>Pm4b_V1CDS</i>	+	S	S	S
T1#12_2.5	<i>Pm4b_V1CDS</i>	-	S	S	S
T1#12_2.6	<i>Pm4b_V1CDS</i>	-	S	S	S
T1#12_2.7	<i>Pm4b_V1CDS</i>	+	S	S	S
T1#12_2.8	<i>Pm4b_V1CDS</i>	+	S	S	S
T1#12_2.9	<i>Pm4b_V1CDS</i>	-	S	S	S
T1#12_2.10	<i>Pm4b_V1CDS</i>	+	S	S	S
T1#12_2.11	<i>Pm4b_V1CDS</i>	+	S	S	S
T1#12_2.12	<i>Pm4b_V1CDS</i>	+	S	S	S
T1#12_2.13	<i>Pm4b_V1CDS</i>	+	S	S	S

T1#12_2.14	<i>Pm4b_V1CDS</i>	+	S	S	S
T1#12_2.15	<i>Pm4b_V1CDS</i>	+	S	S	S
T1#12_2.16	<i>Pm4b_V1CDS</i>	-	S	S	S
T1#19_1.1	<i>Pm4b_V1CDS</i>	+	S	S	S
T1#19_1.2	<i>Pm4b_V1CDS</i>	+	S	S	S
T1#19_1.4	<i>Pm4b_V1CDS</i>	+	S	S	S
T1#19_1.5	<i>Pm4b_V1CDS</i>	+	S	S	S
T1#19_1.6.1	<i>Pm4b_V1CDS</i>	-	S	S	S
T1#19_1.6.2	<i>Pm4b_V1CDS</i>	-	S	S	S
T1#19_1.7	<i>Pm4b_V1CDS</i>	-	S	S	S
T1#19_1.9	<i>Pm4b_V1CDS</i>	+	S	S	S
T1#19_1.10	<i>Pm4b_V1CDS</i>	+	S	S	S
T1#19_1.11	<i>Pm4b_V1CDS</i>	+	S	S	S
T1#19_1.12	<i>Pm4b_V1CDS</i>	-	S	S	S
T1#19_1.13	<i>Pm4b_V1CDS</i>	-	S	S	S
T1#19_1.14	<i>Pm4b_V1CDS</i>	-	S	S	S
T1#19_1.15	<i>Pm4b_V1CDS</i>	+	S	S	S
T1#19_1.16	<i>Pm4b_V1CDS</i>	+	S	S	S
T1#6_3.2	<i>Pm4b_V2CDS</i>	-	S	S	S
T1#6_3.3	<i>Pm4b_V2CDS</i>	+	S	S	S
T1#6_3.4	<i>Pm4b_V2CDS</i>	-	S	S	S
T1#6_3.5	<i>Pm4b_V2CDS</i>	+	S	S	S
T1#6_3.6	<i>Pm4b_V2CDS</i>	+	S	S	S
T1#6_3.7	<i>Pm4b_V2CDS</i>	+	S	S	S
T1#6_3.8	<i>Pm4b_V2CDS</i>	-	S	S	S
T1#6_3.11	<i>Pm4b_V2CDS</i>	+	S	S	S
T1#6_3.12	<i>Pm4b_V2CDS</i>	+	S	S	S
T1#6_3.13	<i>Pm4b_V2CDS</i>	+	S	S	S
T1#6_3.14	<i>Pm4b_V2CDS</i>	-	S	S	S
T1#6_3.16	<i>Pm4b_V2CDS</i>	-	S	S	S
T1#24_1.1	<i>Pm4b_V2CDS</i>	+	S	S	S
T1#24_1.2	<i>Pm4b_V2CDS</i>	+	S	S	S
T1#24_1.3	<i>Pm4b_V2CDS</i>	-	S	S	S
T1#24_1.4	<i>Pm4b_V2CDS</i>	+	S	S	S
T1#24_1.5	<i>Pm4b_V2CDS</i>	+	S	S	S
T1#24_1.6	<i>Pm4b_V2CDS</i>	+	S	S	S
T1#24_1.7	<i>Pm4b_V2CDS</i>	+	S	S	S
T1#24_1.8	<i>Pm4b_V2CDS</i>	+	S	S	S
T1#24_1.10	<i>Pm4b_V2CDS</i>	+	S	S	S
T1#24_1.11	<i>Pm4b_V2CDS</i>	+	S	S	S
T1#24_1.12	<i>Pm4b_V2CDS</i>	+	S	S	S
T1#24_1.13	<i>Pm4b_V2CDS</i>	+	S	S	S
T1#24_1.14	<i>Pm4b_V2CDS</i>	+	S	S	S
T1#24_1.15	<i>Pm4b_V2CDS</i>	+	S	S	S

T1#24_1.16	<i>Pm4b_V2CDS</i>	+	S	S	S
T1#29_2.1	<i>Pm4b_V2CDS</i>	-	S	S	S
T1#29_2.2	<i>Pm4b_V2CDS</i>	+	S	S	S
T1#29_2.3	<i>Pm4b_V2CDS</i>	+	S	S	S
T1#29_2.4	<i>Pm4b_V2CDS</i>	+	S	S	S
T1#29_2.5	<i>Pm4b_V2CDS</i>	+	S	S	S
T1#29_2.6	<i>Pm4b_V2CDS</i>	+	S	S	S
T1#29_2.7	<i>Pm4b_V2CDS</i>	+	S	S	S
T1#29_2.8	<i>Pm4b_V2CDS</i>	+	S	S	S
T1#29_2.9	<i>Pm4b_V2CDS</i>	+	S	S	S
T1#29_2.10	<i>Pm4b_V2CDS</i>	+	S	S	S
T1#29_2.12.1	<i>Pm4b_V2CDS</i>	+	S	S	S
T1#29_2.12.2	<i>Pm4b_V2CDS</i>	+	S	S	S
T1#29_2.13	<i>Pm4b_V2CDS</i>	-	S	S	S
T1#29_2.14.1	<i>Pm4b_V2CDS</i>	+	S	S	S
T1#29_2.14.2	<i>Pm4b_V2CDS</i>	+	S	S	S
T1#29_2.15	<i>Pm4b_V2CDS</i>	+	S	S	S
T1#29_2.16	<i>Pm4b_V2CDS</i>	+	S	S	S

Supplementary Table 5 | Disease reactions of wheat cultivars carrying the *Pm4* locus challenged with selected *Bgt* isolates. In the first column, WW refers to Whealbi Wheat lines from Pont et al6. Detailed passport information is available at https://urgi.versailles.inra.fr/download/iwgsc/IWGSC_RefSeq_Annotations/v1.0/iwgsc_refseqv1.0_Whealbi_GWAS.zip. Second column specifies the *Pm4* allele. From third column on, disease reaction of each wheat line to selected *Bgt* isolates, where values refer to percentage of the surface area of tested leaf segments (means of four biological replicates). Note that disease reactions of the Fed-*Pm4a* and the Fed-*Pm4b* NILs genotypes are included in the top to facilitate the comparison of resistance spectra among *Pm4* alleles. In general, *Pm4b*-, *Pm4d*- and *Pm4h*-containing lines exhibit a very similar pattern that Fed-*Pm4a* and the Fed-*Pm4b* NILs, for example susceptible to *BgtJ1W2* and *Bgt97251* but resistant to *Bgt96224*, *Bgt94202*, *Bgt97223* *Bgt97266*. Five classes of host reactions R = resistance (0-10% of leaf area covered), I (10-25% of leaf area covered), IS (25-50% of leaf area covered), IS (50-75 % of leaf area covered) and S (>75% of leaf area covered). Infection test is based on four biological replicates.

Line	<i>Pm4</i> allele	<i>BgtJ1W2</i>	<i>Bgt94202</i>	<i>Bgt96224</i>	<i>Bgt96229</i>	<i>Bgt97028</i>	<i>Bgt97223</i>	<i>Bgt97251</i>	<i>Bgt97266</i>	<i>Bgt98013</i>	<i>Bgt98230</i>	<i>Bgt98250</i>	
Fed- <i>Pm4a</i>	<i>Pm4a</i>	S	R	R	S	S	R	S	R	R	S	S	
Fed- <i>Pm4b</i>	<i>Pm4b</i>	S	R	R	IS	S	R	S	R	R	IS	IS	
WW-001	<i>Pm4b</i>	S	R	R	R	I	R	I	R	S	I	I	
WW-009		S	R	R	S	IS	R	R	R	IR	IS	IS	
WW-012		S	R	R	IS	I	R	R	R	IR	IS	IS	
WW-017		R	R	R	S	R	R	R	R	R	R	R	R
WW-018		R	R	R	R	R	R	R	R	R	R	R	R
WW-019		S	R	R	S	IS	R	IS	R	IS	I	IS	
WW-021		S	R	R	S	IS	R	IS	R	IS	IS	IS	
WW-024		R	R	R	S	R	R	R	R	S	R	R	
WW-048		S	R	R	R	S	R	I	R	S	S	IS	
WW-049		IS	S	IS	S	S	IR	I	R	IS	S	I	
WW-156		R	R	R	IR	IR	R	S	R	S	IS	IR	
WW-161		S	R	R	S	I	R	S	R	S	IS	R	
WW-282		S	R	R	S	IR	R	I	R	S	IS	IS	
WW-286		S	R	R	IS	I	R	IS	R	IS	I	I	
WW-291		S	R	R	S	I	R	IS	R	IS	R	I	
WW-356		S	R	S	S	I	R	S	R	IS	I	S	
WW-399		S	IS	S	S	IS	IS	IS	IS	S	S	S	
WW-451		R	R	R	IR	IR	R	IS	R	I	I	I	
WW-508		IS	R	R	R	I	R	I	R	R	S	I	
WW-003		<i>Pm4d</i>	S	R	R	R	I	R	I	R	I	IS	I
WW-007	IS		R	R	S	R	R	I	R	IS	R	IS	
WW-014	S		R	R	S	I	R	IS	R	IS	IS	I	
WW-037	S		R	R	S	S	R	R	R	I	S	S	
WW-042	S		R	R	R	S	R	R	R	I	S	IS	
WW-157	S		R	R	S	IS	R	IS	R	S	IS	I	
WW-162	S		R	R	R	I	R	I	R	IS	IS	IR	
WW-164	S		R	R	I	IS	R	IS	R	IS	IS	I	
WW-166	S		R	R	R	I	R	S	R	S	IS	I	
WW-085	S		S	S	S	S	S	S	I	S	S	IS	
WW-110	S	S	S	S	S	S	IS	S	S	S	S		
WW-143	S	S	IS	IS	IS	S	S	S	S	S	IR		
WW-149	S	S	IS	IS	S	S	S	S	IS	S	R		
WW-243	R	R	R	R	R	IR	R	R	R	R	R		
WW-262	IS	I	I	IS	R	IR	IS	R	I	I	I		
WW-265	I	IR	IR	IR	IR	IR	I	I	IR	IR	IR		
WW-335	S	IS	I	S	S	S	IS	I	I	S	IS		
WW-336	R	IS	S	IS	IS	I	S	R	I	S	I		
WW-341	S	S	IS	IS	S	S	S	S	S	IS	IS		
WW-445	S	S	IS	IR	R	S	S	S	IS	IS	I		
WW-093	<i>Pm4g</i>	S	IS	IS	S	S	S	S	S	S	S	S	
WW-213		IS	S	R	I	IR	R	R	R	R	R	R	
WW-470		S	S	S	S	I	IS	S	I	IS	S	I	
WW-474	<i>Pm4h</i>	S	R	R	I	R	IR	S	R	I	R	R	

Supplementary Table 6 | List of *Pm4* homologues found in different species within the Triticeae tribe The first column displays the given name used in Supplementary Fig. 4. If annotated in the corresponding reference assembly (last column), the real name of each *Pm4* homologue is given in the second column. Third column specifies the species where is found the *Pm4* homologue, followed by the chromosome and its length and the hit positions corresponding to the beginning and end of the gene. chr: chromosome. Note that if a homologue does not have assigned a chromosome is due to the fact that that homologue was located in the “unknown” (Un) chromosome. If this was the case, the given name includes “Un”.

Given name	Real name	Species	chr	chr length	blast_hit_1	blast_hit_2	Assembly mapping
HORVU2Hr1G126810	HORVU2Hr1G126810	<i>Hordeum vulgare</i>	2H	686565487	675091299	675096975	Barley HC Proteins May2016 ⁷
AET2Gv21296200	AET2Gv21296200	<i>Aegilops tauschii</i>	2	658177745	648456981	648448441	ASM34733v1 → Aet_v4.0
AET2Gv21296800	AET2Gv21296800	<i>Aegilops tauschii</i>	2	658177745	648669491	648660155	ASM34733v1 → Aet_v4.0
AET2Gv21297100	AET2Gv21297100	<i>Aegilops tauschii</i>	2	658177745	649380150	649375185	ASM34733v1 → Aet_v4.0
Pm4_Scer_2R-H1	gene not annotated	<i>Secale cereale</i>	2R	946003182	942144497	942135749	Scer_Lo7_v1p1p0
Pm4_Scer_2R-H2	gene not annotated	<i>Secale cereale</i>	2R	946003182	942196000	942188331	Scer_Lo7_v1p1p1
Pm4_Scer_2R-H3	SECCE2Rv1G0142720.1	<i>Secale cereale</i>	2R	946003182	942510789	942518886	Scer_Lo7_v1p1p1
Pm4_DW_2B-H1	gene not annotated	<i>Triticum turgidum durum</i>	2B	803510855	783236667	783242710	Tdur_Svevo_v2
Pm4_DW_Un-H1	gene not annotated	<i>Triticum turgidum durum</i>	-	-	-	-	
Pm4_DW_Un-H2	gene not annotated	<i>Triticum turgidum durum</i>	-	-	-	-	Tdur_Svevo_v2
Pm4_Tu-H1	gene not annotated	<i>Triticum urartu</i>	-	-	-	-	Tura
Pm4_WEW_2A-H1	gene not annotated	<i>Triticum turgidum dicoccoides</i>	2A	788103699	772507911	772501710	Ttur_Zavitan_v2
Pm4_WEW_2A-H2	TRITDC2AG081930	<i>Triticum turgidum dicoccoides</i>	2A	788103699	772732306	772727283	Ttur_Zavitan_v2
Pm4_WEW_2A-H3	gene not annotated	<i>Triticum turgidum dicoccoides</i>	2A	788103699	772765384	772758678	Ttur_Zavitan_v2
Pm4_WEW_2B-H1	TRITDC2BG090970	<i>Triticum turgidum dicoccoides</i>	2B	816754914	801015698	801021217	Ttur_Zavitan_v2
Pm4_WEW_2B-H2	TRITD2Bv1G265730	<i>Triticum turgidum dicoccoides</i>	2B	816754914	802467722	802462401	Ttur_Zavitan_v2
TraesCS2A01G558500	TraesCS2A01G558500	<i>Triticum aestivum</i>	2A	796414552	761903162	761896325	Taes_HC_2017_proteins ⁸
TraesCS2B01G621800	TraesCS2B01G621800	<i>Triticum aestivum</i>	2A	817281873	795988821	795978311	Taes_HC_2017_proteins

Supplementary Table 7 | Primers used in this study

Primer	Sequence	Description	Function
GH438 (TI GH dT25VN)	CTATCAGCAACCATTGAGTCACGTCCTCAAAGATGCTCAdT25VN		5' RACE
GH439 (U-GH)	CTATCAGCAACCATTGAGTCACG		3' RACE
GH377	AGAGTGCAGAGACTTCAATCCA		3' RACE
GH432	GCACGTTCCCACTCACGATTGCAATTGCT		5' RACE
GH398	CCTTCACACGGCAAATCTGAA	Fw long-range	Full-length amp. <i>Pm4b_V1</i> transcript
GH399	GATGTGCACCAACTAACT	Rv long-range	Full-length amp. <i>Pm4b_V1</i> transcript
GH400	ATCAGAGTCTCTATCGCCCT	Fw nested	Full-length amp. <i>Pm4b_V1</i> transcript
GH401	CACCAACACTAACTGAAAGGAG	Rv nested	Full-length amp. <i>Pm4b_V1</i> transcript
GH382	GTTCCCACTCACGATTGTC	Sequencing	Seq of full-length <i>Pm4b_V1/V2</i> transcript
GH385	TCGACGATAACATGGAACCCAA	Sequencing	Seq of full-length <i>Pm4b_V1/V2</i> transcript
GH387	CACCATTGGAAGGATGAGCTG	Sequencing	Seq of full-length <i>Pm4b_V1/V2</i> transcript
GH397	TAAAGATACAGATGGGCGGC	Sequencing	Seq of full-length <i>Pm4b_V1</i> transcript
JS233	ACTTTGCAATTAGGCGGTTG	Sequencing	Seq of full-length <i>Pm4b_V1/V2</i> transcript
JS293	AGTCACCACCAACATGAAGTC	Sequencing	Seq of full-length <i>Pm4b_V1</i> transcript
GH398	CCTTCACACGGCAAATCTGAA	Fw long-range	Full-length amp. <i>Pm4b_V2</i> transcript
GH407	AGTAATAACTCTACGCAACATGAAG	Rv long-range/semi-nested	Full-length amp. <i>Pm4b_V2</i> transcript
GH400	ATCAGAGTCTCTATCGCCCT	Fw semi-nested	Full-length amp. <i>Pm4b_V2</i> transcript
JS280	CGCACATAGACATGACGCTG	Sequencing	Seq of full-length <i>Pm4b_V2</i> transcript
JS292	TGCATTCTGGACCCTGACTC	Sequencing	Seq of full-length <i>Pm4b_V2</i> transcript
JS298	TGGTCTCTAGCGTCATGGTC	Sequencing	Seq of full-length <i>Pm4b_V2</i> transcript
JS540	GACCATGACGCTAGAGACCA	Sequencing	Seq of full-length <i>Pm4b_V2</i> transcript
JS717	AGGTGGACATCTAGGCGCT	Forward	Haplotype marker
JS718	GATCTGGGTACCACAGCACCG	Reverse	Haplotype marker
JS256	GCTGAGTGATTTAATTTGTTCCGG	Fw long-range	Amp. Exon1-5 gDNA
JS257	AGAAAAAGGCAACTATAGCCCAT	Rv long-range/nested	Amp. Exon1-5 gDNA
JS251	TCTGACAAGTATATGTAGCAACCC	Fw nested	Amp. Exon1-5 gDNA
GH382	GTTCCCACTCACGATTGTC	Sequencing	Seq Exon1-5 gDNA
GH384	AAGCAGCTAGTTGGCTCATA	Sequencing	Seq Exon1-5 gDNA
GH385	TCGACGATAACATGGAACCCAA	Sequencing	Seq Exon1-5 gDNA
JS255	GTAGCAACCCAAATTAAGGAAGAA	Sequencing	Seq Exon1-5 gDNA
JS278	ACTAACCAGTACTCTGCC	Fw long-range/nested	Amp. Exon6-7 gDNA
JS261	CTTGCCTGGAGAAAGGAACAA	Rv long-range	Amp. Exon6-7 gDNA
GH407	AGTAATAACTCTACGCAACATGAAG	Fw nested	Amp. Exon6-7 gDNA
JS280	CGCACATAGACATGACGCTG	Sequencing	Seq Exon 6-7 gDNA
JS292	TGCATTCTGGACCCTGACTC	Sequencing	Seq Exon 6-7 gDNA
GH387	CACCATTGGAAGGATGAGCTG	Sequencing	Seq Exon 6-7 gDNA
GH397	TAAAGATACAGATGGGCGGC	sequencing	Seq Exon 6-7 gDNA
GH402	ACCACATTTACAGAGAGCTA	Sequencing	Seq Exon 6-7 gDNA
GH414	TAGTGTGGAGAGATCACAACGA	Fw; Exon5-6; 179-bp	qRT-PCR <i>Pm4</i> expression
GH415	CTGAGGTAGAGGAGGCAACTT	Rv; Exon5-6; 179-bp	qRT-PCR <i>Pm4</i> expression
GH377	AGAGTGCAGAGACTTCAATCCA	Fw; Exon5-7; 159-bp	qRT-PCR <i>Pm4</i> expression
GH417	TTCTTCGTACCCAGCAGGTC	Rv; Exon5-7; 159-bp	qRT-PCR <i>Pm4</i> expression
JS483	CACCATGGAACACAAAAGTACCACAC	Universal forward	TOPO cloning <i>Pm4b_V1/2</i>
JS486	TCAGGTCAGCAGGTGGTACT	Rv; stop codon	TOPO cloning <i>Pm4b_V1</i>
JS487	GGTCAGCAGGTGGTACTCC	Rv; no stop codon	TOPO cloning <i>Pm4b_V1</i>
JS484	TCACAGGAGCAGTCCC	Rv; stop codon	TOPO cloning <i>Pm4b_V2</i>
JS485	CAGGAGCAGTCCC	Rv; no stop codon	TOPO cloning <i>Pm4b_V2</i>
JS274	TAAATTGGCGCGCCCATGGAACACAAAAGTACCACA	Universal forward (<i>Asc I</i>)	Biostic bombardment
JS275	CTCTCTTAATTAATTTACAGGAGCAGTCCC	Rv (<i>Pac I</i>)	Biostic bombardment <i>Pm4b_V2</i> CDS
JS276	TCTCTTAATTAATTTACAGGTCAGCAGGTGGTAC	Rv (<i>Pac I</i>)	Biostic bombardment <i>Pm4b_V1</i> CDS
JS295	CATCTGAGCCTTGAGACGGA	Fw sitting on Exon 6	Detection of transgene <i>Pm4b_V1</i> CDS
JS297	GAGGAAATGAAACTGCGCCT	Fw sitting on Exon 7	Detection of transgene <i>Pm4b_V2</i> CDS
HZ010	ATGTATAATTGCGGGACTCT	Universal Rv (nos terminator)	Detection of transgene <i>Pm4b_V1/2</i> CDS
JS189	GCTTCGCAAGAGCGCCAT	Fw <i>Pm4b_V1_target_1</i> (Exon 6)	VIGS of <i>Pm4b_V1</i>
JS190	CCTTGCCATCTGTGGTCTC	Rv <i>Pm4b_V1_target_1</i> (Exon 6)	VIGS of <i>Pm4b_V1</i>
JS498	GGCAGAAAGTGCCTCCTCTA	Fw <i>Pm4b_V2_target_1</i> (Exon 7)	VIGS of <i>Pm4b_V2</i>
JS499	GTTGTAGCGTGTGCTGGTGG	Rv <i>Pm4b_V2_target_1</i> (Exon 7)	VIGS of <i>Pm4b_V2</i>
JS589	GAACACAAAAGTACCACAC	N-terminal Flag tagging <i>Pm4b_V1</i>	Epitope tagging
JS590	CTTGTCGTCATCGTCTGTAGTCCATGGTGAAGGG	N-terminal Flag tagging <i>Pm4b_V1</i>	Epitope tagging
JS601	GATTATGCTGAACACAAAAGTACT	N-terminal HA-tagging <i>Pm4b_V1</i>	Epitope tagging
JS602	TGGAACATCGTATGGATACATGGT	N-terminal HA-tagging <i>Pm4b_V1</i>	Epitope tagging
JS593	GATGACGACAAGTGAAGGGTGGGCGCGCC	C-terminal Flag tagging <i>Pm4b_V2</i>	Epitope tagging
JS594	GTCCCTGTAGTCGGTCAGCAGGTGGTACTCCG	C-terminal Flag tagging <i>Pm4b_V2</i>	Epitope tagging

JS488	TTCCAGATTATGCTTAAAAGGGTGGGCGCGCCG	C-terminal Flag tagging Pm4b_V2	Epitope tagging
JS489	CATCGTATGGATACAGGAGCACGTCCCC	C-terminal Flag tagging Pm4b_V2	Epitope tagging

Supplementary Table 8 | Target-specific amplification efficiencies of the splicing variants *Pm4b_V1* and *Pm4b_V2* and the reference genes used in this study.

gene / Target	gene ID	position	primer	amplicon length bp	efficiency (E) slope r2 of calibration curve	reference
Pm4_V1		Exon 5-6	F: TAGGTTGGAGAGATCACAAACGA (GH414) R: CTGAGGTAGAGGAGGCAACTT (GH415)	179	E: 97.6 % slope: -3.381 r2: 0.999	this work
Pm4_V2		Exon 5-7	F: AGAGTGCAGAGACTTCAATCCA (GH377) R: TTCTTCGTACCCAGCAGGTC (GH417)	159	E: 93.1 % slope: -3.500 r2: 0.991	this work
ADP	TraesCS3B01G368600, TraesCS3D01G330500 (TA.2291)	Exon 2	F: TCTCATGGTTGGTCTCGATG (GH094) R: GGATGGTGGTGACGATCTCT (GH095)	80	E: 98.2 % slope: -3.365 r2: 0.999	Giménez et al ⁹
ZFL	TraesCS3D01G432800, TraesCS3A01G440000	Exon 1	F: CAGGCATCTCACTGGAGACT (GH105) R: TGGCATCTCTTTGCTTCTG (GH106)	79	E: 96.7 % slope: -3.403 r2: 0.989	this work